ISSN 1881-7831 Online ISSN 1881-784X

DD&T

Drug Discoveries & Therapeutics

Volume 14, Number 6
December 2020

IRCA BSSA

IACMHR

www.ddtjournal.com

DD&T
Drug Discoveries & Therapeutics

IRCA BSSA
IACMHR

ISSN: 1881-7831
Online ISSN: 1881-784X
CODEN: DDTRBX
Issues/Year: 6
Language: English
Publisher: IACMHR Co., Ltd.

Drug Discoveries & Therapeutics is one of a series of peer-reviewed journals of the International Research and Cooperation Association for Bio & Socio-Sciences Advancement (IRCA-BSSA) Group. It is published bimonthly by the International Advancement Center for Medicine & Health Research Co., Ltd. (IACMHR Co., Ltd.) and supported by the IRCA-BSSA.

Drug Discoveries & Therapeutics publishes contributions in all fields of pharmaceutical and therapeutic research such as medicinal chemistry, pharmacology, pharmaceutical analysis, pharmaceutics, pharmaceutical administration, and experimental and clinical studies of effects, mechanisms, or uses of various treatments. Studies in drug-related fields such as biology, biochemistry, physiology, microbiology, and immunology are also within the scope of this journal.

Drug Discoveries & Therapeutics publishes Original Articles, Brief Reports, Reviews, Policy Forum articles, Case Reports, News, and Letters on all aspects of the field of pharmaceutical research. All contributions should seek to promote international collaboration in pharmaceutical science.

Editorial Board

Editorial and Head Office:

Pearl City Koishikawa 603,
2-4-5 Kasuga, Bunkyo-ku,
Tokyo 112-0003, Japan
E-mail: office@ddtjournal.com

Drug Discoveries & Therapeutics

Editorial and Head Office

Pearl City Koishikawa 603, 2-4-5 Kasuga, Bunkyo-ku,
Tokyo 112-0003, Japan

E-mail: office@ddtjournal.com
URL: www.ddtjournal.com

Editorial Board Members

CONTENTS *Volume 14, Number 6, 2020*

Review

Original Article

Brief Report

Review

DOI: 10.5582/ddt.2020.03106

Does coronaviruses induce neurodegenerative diseases? A systematic review on the neurotropism and neuroinvasion of SARS-CoV-2

Ines ElBini Dhouib[1,2,*]

[1] Institut Pasteur de Tunis, Laboratoire des Biomolécules, Venins et Applications Théranostiques, Tunis, Tunisia;
[2] Université de Tunis El Manar, Tunis, Tunisia.

SUMMARY The novel coronavirus, severe acute respiratory syndrome coronavirus 2 (SARS-CoV-2) was identified in 2019 in Wuhan, China. Clinically, respiratory tract symptoms as well as other organs disorders are observed in patients positively diagnosed coronavirus disease 2019 (COVID-19). In addition, neurological symptoms, mainly anosmia, ageusia and headache were observed in many patients. Once in the central nervous system (CNS), the SARS-CoV-2 can reside either in a quiescent latent state, or eventually in actively state leading to severe acute encephalitis, characterized by neuroinflammation and prolonged neuroimmune activation. SRAS-CoV-2 requires angiotensin-converting enzyme 2 (ACE2) as a cell entry receptor. The expression of this receptor in endothelial cells of blood-brain barrier (BBB) shows that SRAS-CoV-2 may have higher neuroinvasive potential compared to known coronaviruses. This review summarizes available information regarding the impact of SRAS-CoV-2 in the brain and tended to identify its potential pathways of neuroinvasion. We offer also an understanding of the long-term impact of latently form of SARS-CoV-2 on the development of neurodegenerative disorders. As a conclusion, the persistent infection of SRAS-CoV-2 in the brain could be involved on human neurodegenerative diseases that evolve a gradual process, perhapes, over several decades.

Keywords SRAS-CoV-2, neurotropism, neuroinvasion, neurodegenerative diseases

1. Introduction

Coronaviruses (CoVs) are positive-sense RNA viruses that belong to the Coronvirinae subfamily, in the Coronaviridae family of the Nidovirales order (*1*). This family is classified into four subgroups alpha, beta, gamma, and delta. Alpha- and beta-coronaviruses infect only mammals, usually causing respiratory symptoms in humans and gastroenteritis in animals (*2*). All CoVs caused diseases to humans have had animal origins such as bats (*3*). Currently, there are seven CoVs that can infect humans: HCoV-229E, HCoV-NL63, HCoV-HKU1, HCoV-OC43, MERS-CoV, SARS-CoV-1 and SARS-CoV-2 (*4*). Four of these CoVs: HCoV-NL63, HCoV-229E, HCoV-OC43 and HKU1 have usually caused influenza symptoms and the last three CoVs have caused pandemics in the past two decades (*5,6*), while HCoV-229E and HCoV-OC43, besides SARS-CoV-1 have been shown to infect neurons (*6*).

SARS-CoV-2, which shares highly homological sequence with SARS-CoV-1, is responsible for the current COVID-19 outbreak with more than 70 million patients diagnosed and over 1,612,000 deaths. These statistics exceed the total of SARS-CoV-1 and MERS-CoV in 2002 and 2012, respectively (*5*).

CoVs are named for the crown-like spikes on their surface. To gain access to host cells, CoVs rely on spike proteins (S), which are membrane-anchored trimers containing a receptor-binding S1 segment and a membrane-fusion S2 segment (*7*). The S1 contains a receptor-binding domain (RBD) that binds to a host cell receptor. SARS-CoV-2 are also covered by spike proteins that contain a variable RBD. RBD binds to angiotensin-converting enzyme-2 (ACE2) receptor expressed in all tissues with greatest activity in the ileum and kidney followed by heart, brain, lung, vasculature, stomach and liver (*7,8*).

The binding of the S to the ACE2 receptor is correlated with viral infectivity in the targeted tissue and governs clinical outcomes (*9*). For example, binding of the SARS-CoV-2 to the ACE2 receptor in the type II pneumocytes in the lungs, triggers a cascade of inflammation in the lower respiratory tract (*5*). In fact, 98% of COVID-19 patients developed clinical pneumonia with hypoxic respiratory failure in the first wave of the pandemic (*1,5*). Consequently,

clinicians concluded that this infection alters not only the respiratory function but also the cardiovascular homeostasis (*10*).

Despite the short duration of the current pandemic outbreak, several neurological and neuroradiological phenotypes have been reported including headache, anosmia and ageusia (*11,12*), followed by muscle soreness, then altered consciousness. Given the lack of data regarding the neurotropism of SRAS-CoV-2, we will try to gain more insight into its characteristics based on those of other CoVs. Indeed, in light of the structural similarity between SARS-CoV-2 and others betacoronaviruses, it is highly suspected that all CoVs have similar neuroinvasive and neurotropic properties. Indeed, SARS-CoV-1 and SARS-CoV-2 have comparable binding affinities achieved by balancing energetics and dynamics (*13,14*).

Though the understanding of the pathogenetic mechanisms underlying the neuroinvasion will be revealed in time, there is an urgent need to answer the questions of whether SARS-CoV-2 is neurotropic and whether it contributes to post infectious neurodegenerative diseases.

2. Neurological manifestations

Information about neurological manifestations in COVID-19 patients is still scanty. However, it is now well-known that SRAS-CoV-2 may invade the brain inducing neurological diseases. Such neuroinvasive property of CoVs has been well documented almost for SARS-CoV-1, MERS-CoV, HCoV-229E, HCoV-OC43, mouse hepatitis virus (MHV), and porcine hemagglutinating encephalomyelitis coronavirus (HEV) (*15*).

The first study about neurological disease following SRAS-CoV-2 virus infection was reported during March 2020. Indeed, researchers from Beijing Ditan Hospital, China, described and confirmed patient with COVID-19, whose cerebrospinal fluid (CSF) was tested positive for SRAS-CoV-2, by gene sequencing (*16*). Another study evaluated 214 patients diagnosed with COVID-19 from China of which 36% had neurological manifestations, including acute cerebrovascular disease and impaired consciousness (*17*). A recent study from France reported neurologic issues in 58 of 64 patients with COVID-19, including encephalopathy, prominent agitation and confusion (*18*). The most common neurologic symptoms in COVID-19 clinical cases are headache, anosmia, and ageusia. Interestingly, these three neurological manifestations occurred in early stage of the disease and therefore could be considered as a predictor of clinical impairment. Besides, other neurological findings include stroke, impairment of consciousness, and encephalopathy are showed. All these informations advocate a possible neuroinvasion and neurotropism of SARS-CoV-2.

3. Neuroinvasion of SARS-CoV-2

The following section tempt to elucidate two features: (*i*) how certain patients develop neurological disease after SARS-CoV-2 infection? and (*ii*) whether the virus acts directly or indirectly towards neurons?

As for the route of SARS-CoV-2 entering the CNS, the hematogenous one's appears to be likely the pathway for virus to reach the brain, although the existence of BBB. In addition, neuronal pathway is also reported to be an important vehicle for neurotropic viruses to enter the brain. SARS-CoV-2 can across the cribriform plate of the ethmoid bone in proximity to the olfactory bulb (*11,19,20*). In fact, SARS-CoV-2 may first invade peripheral nerve terminals, and then gain access to the CNS *via* a synapse-connected route in a way of retrograde or anterograde transport. Also, leukocyte migration across the BBB could be a plausible route of viral neuroinvasion (*21*). In the following part, we will documented the putative routes for SARS-CoV-2 neuroinvasion that are summarized in Figure 1.

3.1. Infection *via* blood-brain barrier spread

The blood-brain barrier is a highly selective barrier critical for CNS homeostasis. BBB controls peripheral blood-brain exchange and prevents toxins and pathogens from access to the CNS. The functional and structural integrity of the BBB mainly relies on specific features of the brain microvascular endothelial cells (BMECs) lining the brain capillaries. These cells are tightly connected by an assembly of adherens and tight-junction complexes (*22*). Despite the complex structure of BBB, consisting in astrocytes, pericytes and endothelial cells, neuroviruses have evolved to disrupt and evade it (*23*). Two possible mechanisms for SARS-CoV-2 spread across the BBB are hypothesized: (*i*) the first one is through infection of BMECs and (*ii*) the second mechanism by leukocytes infection that pass through the BBB. Therefore, the possible hallmark of SRAS-CoV-2 neuropathogenesis is the disruption of the BBB.

SRAS-CoV-2 viruses may compromise also the integrity of BBB by either infecting or inducing cellular damage to the neurovascular unit or by eliciting innate and adaptive immune responses leading to neuroinflammation (*24*). BBB invasion by SRAS-CoV-2 correlates with virus-induced disruption of tight junctions on BMECs, leading to BBB dysfunction and enhanced permeability. Indeed, BMECs have already been reported as potential cell targets for CoVs viruses such as MHV (*25*) since they express ACE2 receptor (*26*). S protein of SRAS-CoV-2 can interact with ACE2 on the BMEC cell surface and can infect endothelial cells, facilitating the entry of virus into the CNS, may be without disturbing the BBB. Although BBB disruption can be observed later, accompanied by the degradation of tight junctions proteins and an increase in MMPs (*25*). This hypothesis

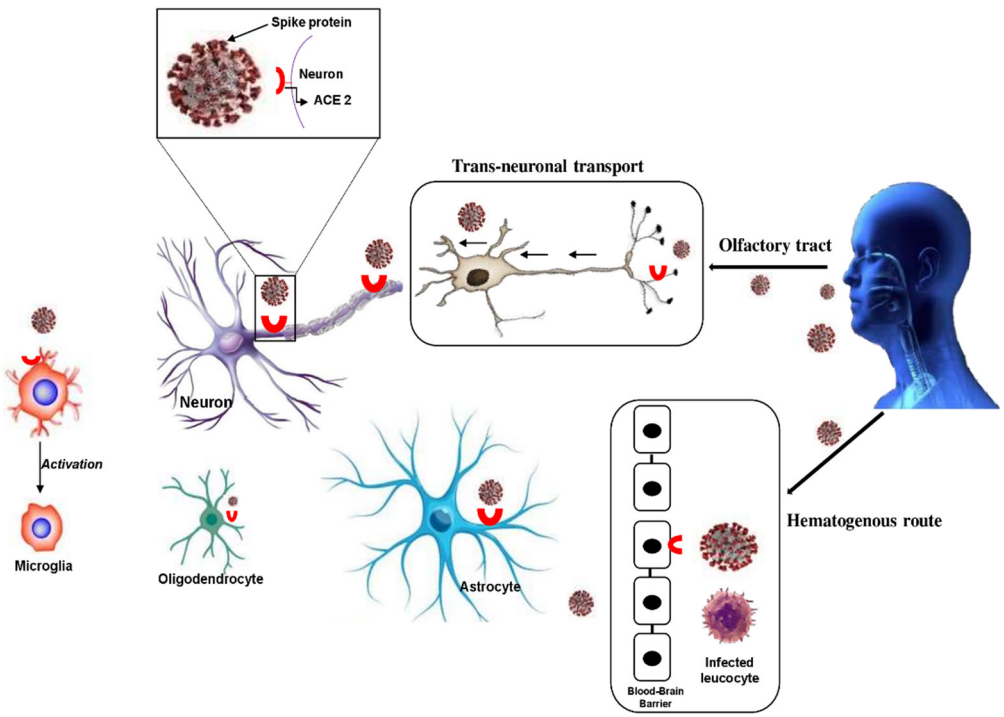

Figure 1. Putative routes for SARS-CoV-2 neuroinvasion. The most specific routes where SARS-CoV-2 enters the brain are: (*i*) Hematogenous route *via* blood-brain barrier (BBB), SARS-CoV-2 induces direct infection of the neurovascular unit in the BBB. So, infected migrating leukocyte cross BBB freed to infect local neuronal cells. (*ii*) Trans-neuronal route: SARS-CoV-2 could enter the nervous system through peripheral nerve fibers including the olfactory receptors, the pulmonary network and the enteric nervous system. ACE2: angiotensin-converting enzyme 2.

can be confirmed by data regarding viral replication of SRAS-CoV-2 in BMECs. In the other hand, reduced expression of tight junctions proteins is a characteristic feature of BBB disruption by neurotropic viruses such as Japanese encephalitis virus (JEV) (*27*), West Nile virus (WNV) (*28*), and human immunodeficiency virus type 1 (HIV-1) (*29*). In fact, these viruses induced a downregulating transcription level of tight junctions mRNA (*30*).

Disruption of tight-junction complexes is often associated with enhanced generation of reactive oxygen species (ROS). Viral infection in target cells can induce mitochondrial damage or NADPH oxidase activation, resulting in high ROS generation (*31*) engendering detrimental effects (*32*). Indeed, ROS can target all biological molecules, including lipid, protein, and nucleic acid, resulting in the release of various cytokines and proteases that damage vasculature in BBB (*31*). In addition, astrocytes are also prone to oxidative stress (*33*). This is confirmed by Masanetz and Lehmann showing that, exposure to viral proteins such as HIV-1 increase astrocyte sensitivity to redox insults (*34*).

In the other hand, SARS-CoV-1 has been shown to infect lymphocytes, granulocytes and monocytes, which all express ACE2 (*35,36*). Infected leukocytes thwart the BBB *via* diapedesis like the "Trojan horse"mechanism (*37,38*). However, it has been demonstrated that T lymphocytes allow SARS-CoV-2 infection but do not support viral replication (*19,26*).

Accordingly, the systemic inflammation, that characterizes COVID-19, increases the permeability of the BBB, thereby allowing infected immune cells, cytokines, and possibly virus might pass into the CNS and interact with ACE2 on neurons and glia (*39*). Thus, BBB plays a key role in the pathogenesis of neurotropic viruses by controlling the access of immune cells or viruses into the CNS. Once the virus gains access to neuronal tissue, it could begin a cycle of viral budding and further damage neuronal tissue.

3.2. Infection *via* viral trans-neuronal spread

According to clinical studies, CoVs neuroinvasion could plausibly be achieved by (*i*) transsynaptic transfer across infected neurons and (*ii*) entry *via* the olfactory nerve.

The olfactory system, a well-known route of entry for human viruses into the CNS, is connected to the limbic structures of the brain, providing a possible path for viruses to infect the CNS. In the litterature, a number of neurotropic viruses including Theiler's murine encephalomyelitis virus, and WNV are known to rapidly disseminate throughout the CNS by olfactory transmission in animal models (*28,40*).

In the few recent report, the nasal cavity is the main gate for SARS-CoV-2 entrance (*19,21*). Notably, the olfactory epithelium (OE) is a suitable source of biological samples for early SARS-CoV-2 detection. OE is a continuously regenerating tissue containing both

neuronal and non-neuronal cells. Therefore, olfactory tract becomes an important channel for SARS-CoV-2 transmission to the brain.

In the other hand, CoV has been shown to spread retrograde *via* transsynaptic transfer using an endocytosis or exocytosis mechanism and a fast axonal transport mechanism of vesicle transport to vehicle virus to neuronal cell bodies (*19*). For instance, HIV and HCoV-OC43 have all been shown to use retrograde fast axonal transport to infect the neurons (*41*). Herein, neuronal expression of ACE2 facilitate SARS-CoV-2 infection through the uptake into dendrites and soma (*21*). Once in CSF, the virus could reach most of the brain areas including the brainstem where cardiorespiratory controlling nuclei are located (*42,43*). Moreover, there is an ACE2 activity in the rostral ventrolateral medulla region in the brainstem. As previously shown, SRAS-CoV-1 and MERS-CoV can invade brainstem *via* a synapse-connected route from the lungs (*21,44,45*). Thus, neuroinvasion of SARS-CoV-2 in the brainstem may be one reason for the acute respiratory failure (*46,47*).

4. Neurotropism of SARS-CoV-2 and inflammation

It is not yet confirmed whether SARS-CoV-2 induced inflammation in the animal or human brain; however, it is well established in the literature that other CoVs target the brain and cause inflammation and encephalomyelitis. For example, human HCoV-OC43 has been associated with encephalitis in children (*48*). In addition, SARS-CoV-1 RNA has been detected in the CSF of a patient with SARS (*49*). Further studies showed that human HCoV-OC43 as well as animal CoVs reach the CNS and cause encephalitis (*50*). However, there remains the question of how the tropism of SRAS-CoV-2 can mediate the acute inflammation in the brain. We can response to this question based on the scientific data reporting that once in the brain, SRAS-CoV-2 replicates on endothelial cells on the BBB receptor and on neuron before targeting astrocytes, oligodendrocytes, and microglia. In addition, it is recently showed that ACE2 is expressed in neurons, astrocytes, and oligodendrocytes (*19*) (Figure 2). Interestingly, ACE2 was shown to be highly concentrated in the substantia nigra, ventricles, middle temporal gyrus, and posterior cingulate cortex (*39*).

When SRAS-CoV-2 reach the brain, the innate immune system serves as the first line of host defense against infection. It detects viral infection through the recognition of pathogen-associated molecular patterns by pathogen-recognition receptors (PRRs) including Toll-Like Receptors (TLRs). Following infection, neurovirulent CoVs manifests significant upregulation of inflammatory cytokines, chemokines, and MMPs, all of which serve to initiate a cell anti-viral response (*51-53*). Other cells including neutrophils and macrophages are the primary innate immune cells recruited into the CNS immediately following CoVs infection (*54,55*). Herein, SRAS-CoV-2 induced TNF-α, IL-6, CCL2, and CXCL10 production; possibly with the inhibition of protective IFN-β production by BMECs (*56*).

In the other hand, TLRs contributes in providing the host against CoVs infection (*57*). Indeed, it has been demonstrated that TLR3 and TLR7 signaling restricted neurotropic infection of WNV in neurons (*58,59*). Thus, TLR3 and TLR7 enhanced BBB permeability after viral neuroinvasion. Equally important is the recent

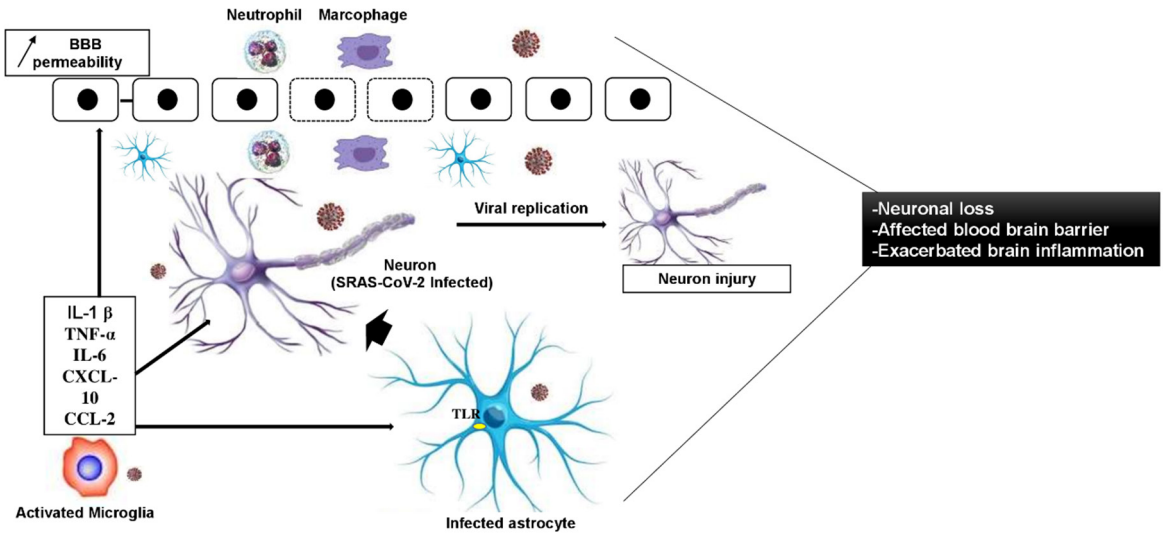

Figure 2. Schematic representation of the acute inflammation during SRAS-CoV-2 infection. Once neurons are infected, the virus begins multiplying and replicating, which causes the first round of neuronal injury accompanied by the production of cytokines or chemokines. These cytokines/chemokines activate microglia and astrocytes, which in turn stimulates more production of proinflammatory cytokines/chemokines and contributes to further neuronal injury. Also, cytokines and chemokines can activate immune cells inside the brain that initiate and/or potentiate BBB dysfunction and alter the architecture of tight junctions on BBB. Furthermore, transendothelial migration of leukocytes (macrophage and neutrophil) causes acute neuronal tissue damage. BBB: blood brain barrier; TLR: Toll-Like Receptors.

demonstration that the activation of TLR-2 and TLR-4 was reported during MHV infection of astrocytes, with subsequent IFN type-I expression and up-regulation of IL-6 cytokine, which was dependent of viral replication (*60*). Indeed, MHV-A59 and SARS-CoV-2 have multiple similarities such as a proinflammatory cytokine reaction involving IL-6 (*60,61*).

On another side, if the innate immune system fails to confine SRAS-CoV-2, the adaptive one will be activated as it is slow, systemic, and virus-specific, leading to stimulation of the immunological memory. The adaptive immune response includes usually cell-mediated immunity and humoral immunity and involves the action of $CD4^+$ T helper cells, $CD8^+$ cytotoxic T cells and B cells. Herein, SRAS-CoV-2 infection might be removed by the action of T cells of the adaptive immune response and virus-specific antibodies. Nevertheless, viral infections may spread to all CNS tissues if the virus escapes from the immune system, causing increased virus replication or overreactive innate immune responses. Subsequently, activation of glial cells by SRAS-CoV-2 viruses results in the production of multiple inflammatory chemokines and cytokines. In fact, CoV strains such as MHV were shown to activate astrocyte that can be a source of CCL5 and CXCL10 (*62,63*).

Noteworthy, activated microglial cells can be the major source of TNF-α, which can be deleterious to neurons (*64*). Thus, the elevated levels of the proinflammatory cytokines IL-6, IL-15, IL-1β and TNF-α in the CNS could induce irreversible neuronal damage (*64*). Additionally, previous studies showed that when CoVs attacked glial cells, a large amount of inflammatory factors such as IL-12, IL-16, IL-17, and IL-18 were released (*60*). Also, the elevated levels of the chemokine CCL2 in the infected CNS by SRAS-CoV-2 could establish an inflammatory and immunosuppressive environment (*65*). Therefore, inflammatory factors can be one of the pathophysiological processes of brain damage.

As shown in Figure 3A, the storm of cytokines that is up-regulated following SRAS-CoV-2 infection consists of proinflammatory cytokines, which would normally be associated with the recruitment of inflammatory cells, including lymphocytes and macrophages, to the site of infection.

In summary, infected neurons by SRAS-CoV-2 viruses may produce chemokines that can also induce the activation of glial cells, which in turn produce a preponderance of inflammatory chemokines and cytokines (Figure 3A). These inflammatory mediators can break down the BBB by reducing the integrity of the tight junctions between BMECs. Inflammatory mediators can further compromise the BBB and inceased infiltration of inflammatory cells from the periphery to the CNS. Increased inflammatory infiltrates can lead to further neuroinflammation and neuronal injury (Figure 3B). Moreover, levels of some cytokines have been reported to be elevated for months to years following the recovery after SARS-CoV-1 infection (*66*), leading to a post-infectious proinflammatory state that may contribute to a possible long-term neuroinflammation. Nevertheless, advanced investigations are warranted to determine the pathways by which the post-infected brain could contribute to the onset of neuron demyelination or neurodegeneration.

5. Persistent infection of SARS-CoV-2 associated with neurodegeneration

In the following section, we documentated if infection with SRAS-CoV-2 can result in long-term neural damage in both symptomatic and asymptomatic individuals? The first scenario, assumes that neural cells could serve as latent reservoirs for the SRAS-CoV-2. The second one supposes a possible long-term neuroinflammation in the brain. In general, these two possibilities can activate the pathways of apoptosis and oxidative stress leading to neurodegeneration.

In experimental data, viral dissemination in animal brain tissue was shown to be accompanied by vascular endothelium dysfunction, which has been reported to contribute to cognitive impairment (*67*). In addition, susceptible rodent after direct inoculation of HCV-OC43 and SARS-CoV-1 developed acute encephalitis with viral RNA present for several months causing neuronal degeneration (*68*) and ultimately apoptosis (*69*). In fact, Jacomy and his collaborators postulated apoptosis, after CoV infection, as the mechanism involved in neuronal loss observed in the CA1 and CA3 layers of the mice hippocampus (*70*). Also, Chen and Lane assigned apoptosis as a mechanism by which MHV induced neuronal death in mice brain (*71*). Based on these reported results, we suppose that caspases may be the principal executors of apoptotic neuronal cell death as shown in Figure 3C. In fact, caspase-3 has been severally identified as a key mediator of the apoptotic process in neurons (*72*). Noteworthy, alterations in signaling pathways related to apoptosis have been described to be implicated in Alzheimer's disease (AD) (*73*) and Parkinson's disease (PD) (*74*). Hence, SRAS-CoV-2 modulation of neuronal apoptosis both, during latent infections could eventually relate to alterations of neuronal processes leading to neuron degeneration and brain damage.

Oxidative stress is another mechanism by which SRAS-CoV-2 latency infection induces neurodegeneration (Figures 3B and 3C). Viral infection in target cells can induce mitochondrial damage resulting in high ROS generation (*75*). In addition, disruption of tight junction complexes *via* MMPs activation is often associated with enhanced ROS generation (*76*). Notably, recent studies indicate that oxidative stress is associated with neurodegenerative diseases, such as AD (*77*), PD (*74*) and multiple sclerosis (MS) (*78*). For instance,

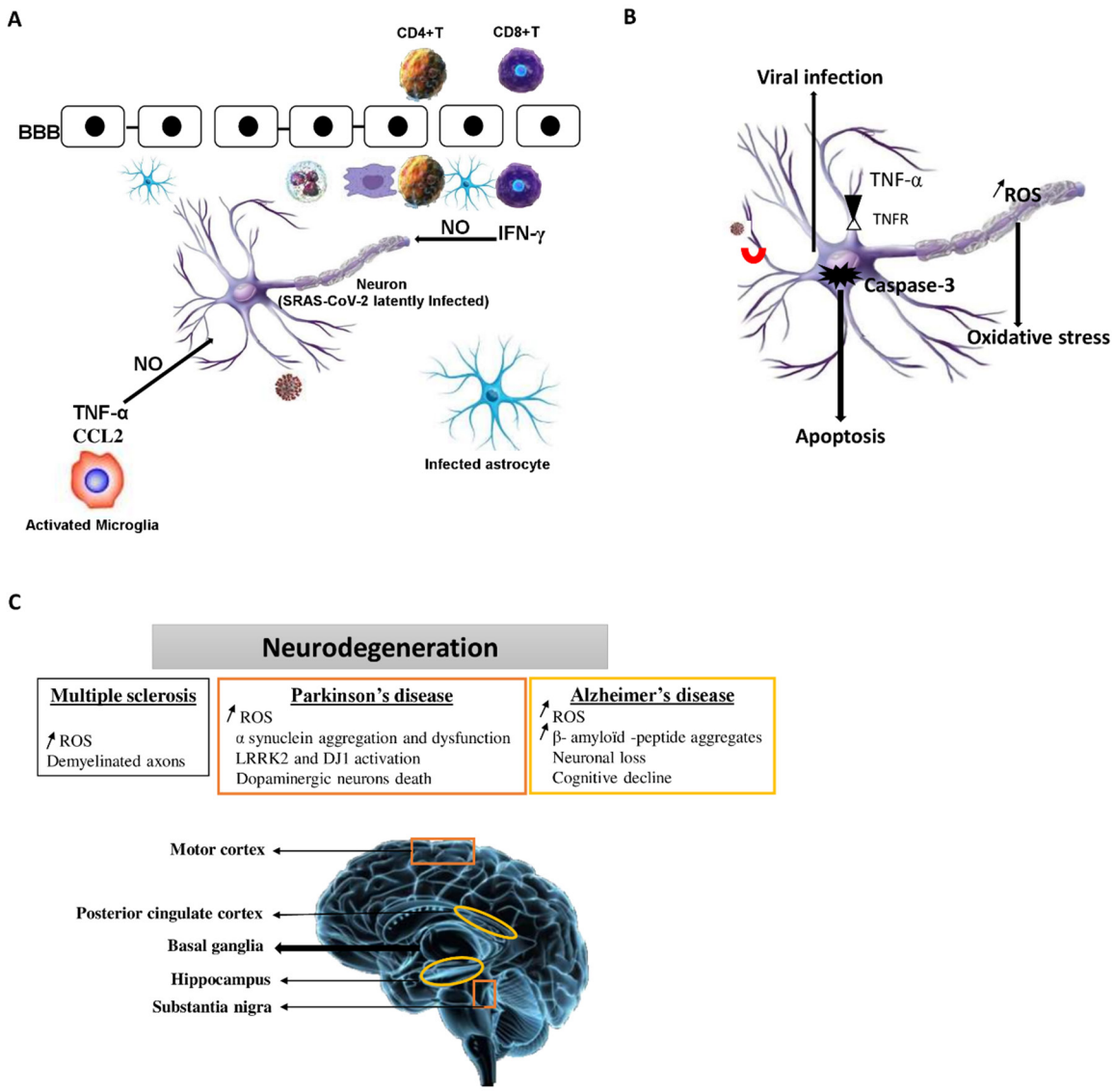

Figure 3. Proposed model of the neurotropism of latent form of SRAS-CoV-2 and its interrelationships with neurodegenerative disorders. (A) SRAS-CoV-2 latent brain infection: SRAS-CoV-2 latent form is characterized by the infiltration of $CD8^+$ and $CD4^+$ T cells. Importantly, these T cells are localized near latently infected neurons. In addition, $CD8^+$ T cells can secrete IFN-γ. As a consequence of immune cell infiltration into the brain during persistent SRAS-CoV-2 infection of the brain, cytokines such as TNF-α and IL-1β can affect the BBB, which can exacerbate brain inflammation. **(B)** Synergistic effects between TNF-α and IFN-γ can lead to induced oxidative stress and increased nitric oxide-induced neurodegeneration and demyelination in the brain. In addition, SRAS-CoV-2 modulates cellular processes; latently form of virus hampers events leading to apoptosis at different stages of signaling cascades. **(C)** The boxes show the cellular processes or pathologies that occur in Alzheimer's disease (orange box) or Parkinson's disease (yellow box) or multiple sclerosis (black box) associated with apoptosis, oxidative stress and neuronal injury. Neurodegenerative disease pathologies are expressed in multiple regions of the human and rodent brain, including the motor cortex, posterior cingulate cortex, ventricles and substantia nigra. BBB: blood brain barrier, ROS: reactive oxygen species, ACE2: angiotensin-converting enzyme 2, NO: nitric oxide, TNFR: TNFα receptor.

AD patients overall display increased ROS levels, while a reduced antioxidant capacity (*79*). Importantly, ROS generation is associated with amyloid beta (Aβ)-protein aggregates, which are known to promote synaptic dysfunction (*80*). Also, elevated levels of ROS production associated to demyelination and axonal damage, have been reported in MS (*81*).

5.1. SARS-CoV-2 post-infection associated with multiple sclerosis

Coronaviruses have long been mentioned as potential candidate viruses that could cause or enhance MS disease (*82-85*). Recently, clinical case studies evaluated the prevalence of SRAS-CoV-2 in patients with relapsing-remitting MS (RRMS) comparing it with that of healthy controls (*5,86*). The discovery of CoVs genetic material in the tissue and fluid samples of MS patients has given space for this plausible hypothesis. Indeed, HCV-229E was isolated from the CSF of patient during a first episode of MS (*87*). Before that, HCoV had been isolated from the brain of a patient with MS (*88*). In addition, several experimental models have used CoVs to explore the environmental component triggering the autoimmune

changes in MS (*25,89-90*). For instance, mice infected by MHV3 surviving the initial infection, develop an immune mediated demyelinating disease (*25,91*). Analysis of the spinal cords of infected mice confirms that the loss of myelin integrity is associated with the continued presence of both viral antigen and inflammatory immune cells (*92*), oxidative injury (*93*) and the loss of myeline synthesis (*94,95*). Moroever, in their studies, Savarin *et al*. have reported curtail percentages of $CD4^+$ T cells in the blood of MS patients, which could be associated with impaired responses against CoVs infection (*96,97*). It is possible that defective T cell control due to CoVs infection and exhaustion of T cells in patients with MS may lead to CoVs reactivation in these patients. However, further studies are needed to confirm this hypothesis

5.2. SARS-CoV-2 postinfection associated with Alzheimer's disease

Data in epidemiology and postmortem AD brains have suggested that viral infections may contribute to the onset of AD. For example, CoVs genetic material has been detected in brain samples and found to co-localize with Aβ protein (*98*). Importantly, SRAS-CoV-2 can induce the accumulation of Aβ protein.

In experimental models, HCoV-OC43 induced not only the neuropathogenesis in mice (*70*), but also, an upregulation of a lipocalin apo D protein (*99*). In addition, MHV induced neuroinflammation, exacerbated tau levels, and compromised cognitive function in aged transgenic 3xTg-AD mice (*100*). The inflammation-mediated exacerbation of tau pathological features leads to impairment in cognitive function that is effectively blocked by inhibiting glycogen synthase kinase (GSK)-3β in CA1 neurons of the hippocampus (*100*). Notably, the regions of the CNS damaged during SRAS-CoV-2 are related to the limbic system, composed by subcortical structures and the cerebral cortex that are associated with memory and cognitive processes (Figure 3C). Taken together, these findings suggest that latently form of SRAS-CoV-2 in the brain may induce increased deposition of Aβ in this tissue and accelerating disease development in predisposed patients.

5.3. SARS-CoV-2 postinfection associated with Parkinson's disease

In patients suffering from severe forms of COVID-19, the hypothesis of a systemic failure of the dopamine synthetic pathway should be taken into account and further explored. In fact, the basal ganglia and dopamine-rich brain regions seem to be a vulnerable target to SRAS-CoV-2 (Figure 3C). Consequently, chronic neuroinflammation leads to basal ganglia dysfunction, BBB permeability alteration, and neurodegeneration.

As previously shown, intraperitoneally inoculation of HCoV-OC43 induced microglia activation and neuroinflammation in mice (*101*); followed by encephalitis, neuronal degeneration, and decrease of locomotor activity (*70,101*).

In humans, HCV-OC43 and HCV-229E have been found in the CSF of PD patients (*102*). Of note, intranasal/intraocular inoculation led to detect CoV RNA in the brain, while post-mortem analyses indicated the presence of brain pathology, including inflammation and white matter edema in the basal ganglia (*102*).

In the other hand, neurotropic viruses have been shown to affect the levels of PD-associated proteins, including DJ1 and Leucine rich repeat kinase 2 (LRRK2) (*103*). DJ1 is a gene linked to early onset PD and a key regulator of dopamine and ROS balance in neuronal cells (*74*). Indeed, pathologic LRRK2 and DJ1 activation was found to be an important mediator of neuroinflammation and neuronal damage in *in vitro* and *in vivo* models of neurotropic virus (*103,104*). In addition, Ijomone *et al*. proposed that viral agents from SRAS-CoV-2 can, through microglial activation and oxidative stress, induce the aggregation and oligomerization of α-synuclein in substantia nigra region (*72*).

6. Discussion

This review reported considerable evidences that latent form of SRAS-CoV-2 are associated to adverse outcomes in the brain and induced neurodegenerative's disease. Herein, we highlight the neuroinvasive property of SRAS-CoV-2 and their effect on the brain. Although the exact mechanism of neuroinvasion is still unclear, some penetration routes, such hematogenous route and trans-synaptic transmission, have been suggested. Similarly reported by Zubair *et al*., which also examined the neuropathogenesis and neurologic manifestations of the CoVs in the age of COVID-19 (*19*). Equally important is the demonstration that the long-term effects of COVID-19 seems to be implicated as putative etiologic agents of neurodegenerative diseases (*24,55*).

Moreover, the expression of ACE2 receptors in neurons, astrocytes, and oligodendrocytes contributes to the neurotropism of SRAS-CoV-2 (*19*). Consequently, the persistent infection of SRAS-CoV-2 in the brain could be involved on human neurodegenerative diseases that evolves a gradual process, perhapes, over several decades. Of note, detection of SARS-CoV-1 RNA in the CSF of a patient with SARS has been reported after ten years of infection (*49*).

Considerably, there is an urgent need for longitudinal studies to determine whether the COVID-19 pandemic will lead to enhanced incidence of neurodegenerative disorders in infected individuals. Further studies are needed to confirm these speculations. Therefore, we suggest that a designed cohort study can provide powerful results. In addition, further experiments using in experimental and postmortem studies could provide more informations on the neural alteration and

neurodegeneration after SARS-CoV-2 infection.

Unfortunately, our review is limited to studies published between December 2019 and August 2020, we may have missed some experimental reports of SRAS-CoV-2 virus in association with neurodegenerative's disease. In addition, through our research strategy we focused upon studies that contained both a neuroinvasion and neurotropism of virus, as well as a poor description of neurologic manifestations because, there are currently a small number of published case reports and clinical studies. Third, a diligent documentation of anti-virus therapies is recommended to establish novel therapeutics to target the virus. Currently, there are no specific antiviral agents or vaccines for SRAS-CoV-2 virus. However, some compounds active against SRAS-CoV-2 virus have been reported, including both direct-acting and host-targeting antivirals such as aminoquinolines (*105,106*) and melatonin (*107*); however, most of these compounds have yet to find their way into experimental models and clinical trials. For that, a profound understanding of the tropism and pathogenesis of this virus is imperative for the development of therapeutic design.

Finally, we suggest, through this review, to provide CSF, in part, to better understand the neurotropism of SARS-CoV-2 and to evaluate whether direct (*via* direct infection) or indirect (*via* secondary effects relating to enhanced inflammatory/proinflammatory signaling) impact on the CNS. This goal must be reached using a multidisciplinary approach including brain imaging and tests of brain tissue.

7. Conclusion

This review has highlighted a series of possible additional pathophysiological mechanisms based on some literature data, which elucidate the association between the neurotropism of SRAS-CoV-2 and the development of neurodegenerative's disease. Data from all the above-mentioned studies confirm the neuroinvasive and the neurotropism properties of SRAS-CoV-2 and his effects on the brain. Although the exact mechanism of neuroinvasion is still unclear, two penetration routes (hematogenous route *via* BBB structure and trans-synaptic transmission) of the virus to reach the brain, have been suggested. In fact, virus can modulate numerous key cellular processes in neuron and glia, such as apoptosis and cellular oxidation. Taken together, we suggest that neuron infection with SRAS-CoV-2 can lead to brain damage. These hypothesis call for further studies that evaluate the interrelationship between SRAS-CoV-2 and neurodegeneration. Therefore, we suggest that a designed cohort study can provide powerful results for this possible relationship. In the same way, future challenges in experiments models (*in vitro* and *in vivo*) could shed more light on the possible neural injuries after SARS-CoV-2 infection.

Acknowledgements

I gratefully acknowledge Pr. Najet Srairi-Abid (Laboratoire des Biomolécules, Venins et Applications Théranostiques, Institut Pasteur de Tunis) for the scientific discussion and for revising the English writing of this review.

Funding: None.

Conflict of Interest: The author has no conflicts of interest to disclose.

References

1. Rabi FA, Al Zoubi MS, Kasasbeh GA, Salameh DM, Al-Nasser AD. SARS-CoV-2 and coronavirus disease 2019: What we know so far. Pathogens. 2020; 9:231.
2. Cui J, Li F, Shi ZL. Origin and evolution of pathogenic coronaviruses. Nat Rev Microbiol. 2019; 17:181-192.
3. Fan Y, Zhao K, Shi ZL, Zhou P. Bat coronaviruses in China. Viruses. 2019; 11:210.
4. Zhu N, Zhang D, Wang W, *et al*. A novel coronavirus from patients with pneumonia in China, 2019. N Engl J Med. 2020; 382:727-733.
5. Huang C, Wang Y, Li X, *et al*. Clinical features of patients infected with 2019 novel coronavirus in Wuhan, China. Lancet. 2020; 395:497-506.
6. Zhang H. Early lessons from the frontline of the 2019-nCoV outbreak. Lancet. 2020; 395:687.
7. Ksiazek TG, Erdman D, Goldsmith CS, *et al*. A novel coronavirus associated with severe acute respiratory syndrome. N Engl J Med. 2003; 348:1953-1966.
8. Zhang H, Penninger JM, Li Y, Zhong N, Slutsky AS. Angiotensin-converting enzyme 2 (ACE2) as a SARS-CoV-2 receptor: molecular mechanisms and potential therapeutic target. Intensive Care Med. 2020; 46:586-590.
9. Mossel EC, Huang C, Narayanan K, Makino S, Tesh RB, Peters CJ. Exogenous ACE2 expression allows refractory cell lines to support severe acute respiratory syndrome coronavirus replication. J Virol. 2005; 79:3846-3850.
10. South AM, Diz DI, Chappell MC. COVID-19, ACE2, and the cardiovascular consequences. Am J Physiol Heart Circ Physiol. 2020; 318:H1084-H1090.
11. Li Z, Huang Y, Guo X. The brain, another potential target organ, needs early protection from SARS-CoV-2 neuroinvasion. Sci China Life Sci. 2020; 63:771-773.
12. Yin R, Feng W, Wang T, Chen G, Wu T, Chen D, Lv T, Xiang D. Concomitant neurological symptoms observed in a patient diagnosed with coronavirus disease 2019. J Med Virol. 2020; 92:1782-1784.
13. Brielle ES, Schneidman-Duhovny D, Linial M. The SARS-CoV-2 exerts a distinctive strategy for interacting with the ACE2 human receptor. Viruses. 2020; 12:497.
14. Othman H, Bouslama Z, Brandenburg JT, da Rocha J, Hamdi Y, Ghedira K, Srairi-Abid N, Hazelhurst S. Interaction of the spike protein RBD from SARS-CoV-2 with ACE2: Similarity with SARS-CoV, hot-spot analysis and effect of the receptor polymorphism. Biochem Biophys Res Commun. 2020; 527:702-708.
15. Li Y, Fu L, Gonzales DM, Lavi E. Coronavirus neurovirulence correlates with the ability of the virus to induce proinflammatory cytokine signals from astrocytes

and microglia. J Virol. 2004; 78:3398-3406.
16. Sun T, Guan J. Novel coronavirus and the central nervous system. Eur J Neurol. 2020; 27:e52.
17. Mao L, Jin H, Wang M, Hu Y, Chen S, He Q, Chang J, Hong C, Zhou Y, Wang D, Miao X, Li Y, Hu B. Neurologic manifestations of hospitalized patients with coronavirus disease 2019 in Wuhan, China. JAMA Neurol. 2020; 77:683-690.
18. Helms J, Kremer S, Merdji H, Clere-Jehl R, Schenck M, Kummerlen C, Collange O, Boulay C, Fafi-Kremer S, Ohana M, Anheim M, Meziani F. Neurologic features in severe SARS-CoV-2 infection. N Engl J Med. 2020; 382:2268-2270.
19. Zubair AS, McAlpine LS, Gardin T, Farhadian S, Kuruvilla DE, Spudich S. Neuropathogenesis and neurologic manifestations of the coronaviruses in the age of coronavirus disease 2019: A review. JAMA Neurol. 2020; 77:1018-1027.
20. Ransohoff RM, Engelhardt B. The anatomical and cellular basis of immune surveillance in the central nervous system. Nat Rev Immunol. 2012; 12:623-635.
21. Briguglio M, Bona A, Porta M, Dell'Osso B, Pregliasco FE, Banfi G. Disentangling the hypothesis of host dysosmia and SARS-CoV-2: The bait symptom that hides neglected neurophysiological routes. Front Physiol. 2020; 11:671.
22. Spindler KR, Hsu TH. Viral disruption of the blood-brain barrier. Trends Microbiol. 2012; 20:282-290.
23. Kobiler D, Lustig S, Gozes Y, Ben-Nathan D, Akov Y. Sodium dodecylsulphate induces a breach in the blood-brain barrier and enables a West Nile virus variant to penetrate into mouse brain. Brain Res. 1989; 496:314-316.
24. Cain MD, Salimi H, Diamond MS, Klein RS. Mechanisms of pathogen invasion into the central nervous system. Neuron. 2019; 103:771-783.
25. Bleau C, Filliol A, Samson M, Lamontagne L. Brain invasion by mouse hepatitis virus depends on impairment of tight junctions and β interferon production in brain microvascular endothelial cells. J Virol. 2015; 89:9896-908.
26. Wang J, Chen S, Bihl J. Exosome-mediated transfer of ACE2 (angiotensin-converting enzyme 2) from endothelial progenitor cells promotes survival and function of endothelial cell. Oxid Med Cell Longev. 2020; 2020:4213541.
27. Diagana M, Preux PM, Dumas M. Japanese encephalitis revisited. J Neurol Sci. 2007; 262:165-170.
28. Lim SM, Koraka P, Osterhaus AD, Martina BE. West Nile virus: immunity and pathogenesis. Viruses. 2011; 3:811-828.
29. McArthur J, Smith B. Neurologic complications and considerations in HIV-infected persons. Curr Infect Dis Rep. 2013; 15:61-66.
30. Al-Obaidi MMJ, Bahadoran A, Wang SM, Manikam R, Raju CS, Sekaran SD. Disruption of the blood brain barrier is vital property of neurotropic viral infection of the central nervous system. Acta Virol. 2018; 62:16-27.
31. Lehner C, Gehwolf R, Tempfer H, Krizbai I, Hennig B, Bauer HC, Bauer H. Oxidative stress and blood-brain barrier dysfunction under particular consideration of matrix metalloproteinases. Antioxid Redox Signal. 2011; 15:1305-1323.
32. Elbini Dhouib I, Jallouli M, Annabi A, Gharbi N, Elfazaa S, Lasram MM. A mini-review on N-acetylcysteine: An old drug with new approaches. Life Sci. 2016; 151:359-363.
33. Keck F, Brooks-Faulconer T, Lark T, Ravishankar P, Bailey C, Salvador-Morales C, Narayanan A. Altered mitochondrial dynamics as a consequence of Venezuelan equine encephalitis virus infection. Virulence. 2017; 8:1849-1866.
34. Masanetz S, Lehmann MH. HIV-1 Nef increases astrocyte sensitivity towards exogenous hydrogen peroxide. Virol J. 2011; 8:35.
35. Gu J, Gong E, Zhang B, *et al*. Multiple organ infection and the pathogenesis of SARS. J Exp Med. 2005; 202:415-424.
36. Spiegel M, Schneider K, Weber F, Weidmann M, Hufert FT. Interaction of severe acute respiratory syndrome-associated coronavirus with dendritic cells. J Gen Virol. 2006; 87:1953-1960.
37. Fletcher NF, Meeker RB, Hudson LC, Callanan JJ. The neuropathogenesis of feline immunodeficiency virus infection: barriers to overcome. Vet J. 2011; 188:260-269.
38. Desforges M, Le Coupanec A, Brison E, Meessen-Pinard M, Talbot PJ. Neuroinvasive and neurotropic human respiratory coronaviruses: potential neurovirulent agents in humans. Adv Exp Med Biol. 2014; 807:75-96.
39. Baig AM, Khaleeq A, Ali U, Syeda H. Evidence of the COVID-19 virus targeting the CNS: tissue distribution, host-virus interaction, and proposed neurotropic mechanisms. ACS Chem Neurosci. 2020; 11:995-998.
40. Wada Y, Fujinami RS. Viral infection and dissemination through the olfactory pathway and the limbic system by Theiler's virus. Am J Pathol. 1993; 143:221-229.
41. Berth SH, Leopold PL, Morfini GN. Virus-induced neuronal dysfunction and degeneration. Front Biosci (Landmark Ed). 2009; 14:5239-5259.
42. Netland J, Meyerholz DK, Moore S, Cassell M, Perlman S. Severe acute respiratory syndrome coronavirus infection causes neuronal death in the absence of encephalitis in mice transgenic for human ACE2. J Virol. 2008; 82:7264-7275.
43. Harberts E, Yao K, Wohler JE, Maric D, Ohayon J, Henkin R, Jacobson S. Human herpesvirus-6 entry into the central nervous system through the olfactory pathway. Proc Natl Acad Sci U S A. 2011; 108:13734-13739.
44. Jean A, Quach C, Yung A, Semret M. Severity and outcome associated with human coronavirus OC43 infections among children. Pediatr Infect Dis J. 2013; 32:325-329.
45. Dubé M, Le Coupanec A, Wong AHM, Rini JM, Desforges M, Talbot PJ. Axonal transport enables neuron-to-neuron propagation of human coronavirus OC43. J Virol. 2018; 92:e00404-18.
46. Cure E, Cumhur Cure M. Comment on "Should COVID-19 concern nephrologists? why and to what extent? The emerging impasse of angiotensin blockade". Nephron. 2020; 144:251-252.
47. Dixon L, Varley J, Gontsarova A, Mallon D, Tona F, Muir D, Luqmani A, Jenkins IH, Nicholas R, Jones B, Everitt A. COVID-19-related acute necrotizing encephalopathy with brain stem involvement in a patient with aplastic anemia. Neurol Neuroimmunol Neuroinflamm. 2020; 7:e789.
48. Morfopoulou S, Brown JR, Davies EG, Anderson G, Virasami A, Qasim W, Chong WK, Hubank M, Plagnol V, Desforges M, Jacques TS, Talbot PJ, Breuer J. Human coronavirus OC43 associated with fatal encephalitis. N Engl J Med. 2016; 375:497-498.
49. Hung EC, Chim SS, Chan PK, Tong YK, Ng EK, Chiu RW, Leung CB, Sung JJ, Tam JS, Lo YM. Detection of

SARS coronavirus RNA in the cerebrospinal fluid of a patient with severe acute respiratory syndrome. Clin Chem. 2003; 49:2108-2109.
50. Paniz-Mondolfi A, Bryce C, Grimes Z, Gordon RE, Reidy J, Lednicky J, Sordillo EM, Fowkes M. Central nervous system involvement by severe acute respiratory syndrome coronavirus-2 (SARS-CoV-2). J Med Virol. 2020; 92:699-702.
51. Parra B, Hinton DR, Lin MT, Cua DJ, Stohlman SA. Kinetics of cytokine mRNA expression in the central nervous system following lethal and nonlethal coronavirus-induced acute encephalomyelitis. Virology. 1997; 233:260-270.
52. Rempel JD, Quina LA, Blakely-Gonzales PK, Buchmeier MJ, Gruol DL. Viral induction of central nervous system innate immune responses. J Virol. 2005; 79:4369-4381.
53. Savarin C, Stohlman SA, Rietsch AM, Butchi N, Ransohoff RM, Bergmann CC. MMP9 deficiency does not decrease blood-brain barrier disruption, but increases astrocyte MMP3 expression during viral encephalomyelitis. Glia. 2011; 59:1770-1781.
54. Templeton SP, Kim TS, O'Malley K, Perlman S. Maturation and localization of macrophages and microglia during infection with a neurotropic murine coronavirus. Brain Pathol. 2008; 18:40-51.
55. Hosking MP, Lane TE. The biology of persistent infection: Inflammation and demyelination following murine coronavirus infection of the central nervous system. Curr Immunol Rev. 2009; 5:267-276.
56. Hwanga M, Bergmann CC. Alpha/beta interferon (IFN-α/β) signaling in astrocytes mediates protection against viral encephalomyelitis and regulates IFN-γ-dependent responses. J Virol. 2018; 92:e01901-17.
57. Xagorari A, Chlichlia K. Toll-like receptors and viruses: induction of innate antiviral immune responses. Open Microbiol J. 2008; 2:49-59.
58. Daffis S, Suthar MS, Gale M, Diamond MS Jr. Measure and countermeasure: type I IFN (IFN-α/β) antiviral response against West Nile virus. J Innate Immun. 2009; 435-445.
59. Town T, Bai F, Wang T, Kaplan A T, Qian F, Montgomery RR, Anderson JF, Flavell RA, Fikrig E. Toll-like receptor 7 mitigates lethal West Nile encephalitis *via* interleukin 23-dependent immune cell infiltration and homing. Immunity. 2009; 30:242-253.
60. Lavi E, Cong L. Type I astrocytes and microglia induce a cytokine response in an encephalitic murine coronavirus infection. Exp Mol Pathol. 2020; 115:104474.
61. Mehta P. COVID-19: consider cytokine storm syndromes and immunosuppression. Lancet. 2020; 395:1033-1034.
62. Skinner D, Marro BS, Lane TE. Chemokine CXCL10 and coronavirus-induced neurologic disease. Viral Immunol. 2019; 32:25-37.
63. Wang X, Xu W, Hu G, Xia S, Sun Z, Liu Z, Xie Y, Zhang R, Jiang S, Lu L. SARS-CoV-2 infects T lymphocytes through its spike protein-mediated membrane fusion. Cell Mol Immunol. 2020.
64. Li Y, Fu L, Gonzales DM, Lavi E. Coronavirus neurovirulence correlates with the ability of the virus to induce proinflammatory cytokine signals from astrocytes and microglia. J Virol. 2004; 78:3398-3406.
65. Trujillo JA, Fleming EL, Perlman S. Transgenic CCL2 expression in the central nervous system results in a dysregulated immune response and enhanced lethality after coronavirus infection. J Virol. 2013; 87:2376-2389.
66. Ng OW, Chia A, Tan AT, Jadi RS, Leong HN, Bertoletti A, Tana YJ. Memory T cell responses targeting the SARS coronavirus persist up to 11 years post-infection. Vaccine. 2016; 34:2008-2014.
67. Toth P, Tarantini S, Csiszar A, Ungvari Z. Functional vascular contributions to cognitive impairment and dementia: mechanisms and consequences of cerebral autoregulatory dysfunction, endothelial impairment, and neurovascular uncoupling in aging. Am J Physiol-Heart Circulatory Physiol. 2017; 312:H1-H20.
68. Arbour N, Talbot PJ. Persistent infection of neural cell lines by human coronaviruses. Adv Exp Med Biol. 1998; 440:575-581.
69. Netland J, Meyerholz DK, Moore S, Cassell M, Perlman S. Severe acute respiratory syndrome coronavirus infection causes neuronal death in the absence of encephalitis in mice transgenic for human ACE2. J Virol. 2008; 82:7264-7275.
70. Jacomy H, Fragoso G, Almazan G, Mushynski W E, Talbot PJ. Human coronavirus OC43 infection induces chronic encephalitis leading to disabilities in BALB/C mice. Virol. 2006; 349:335-346.
71. Chen BP, Lane TE. Lack of nitric oxide synthase type 2 (NOS2) results in reduced neuronal apoptosis and mortality following mouse hepatitis virus infection of the central nervous system. J Neurovirol. 2002; 8:58-63.
72. Ijomone OM, Olatunji SY, Owolabi JO, Naicker T, Aschner M. Nickel-induced neurodegeneration in the hippocampus, striatum and cortex: an ultrastructural insight, and the role of caspase-3 and α-synuclein. J Trace Elem Med Biol. 2018; 50:16-23.
73. Obulesu M, Lakshmi MJ. Apoptosis in Alzheimer's disease: an understanding of the physiology, pathology and therapeutic avenues. Neurochem Res. 2014; 39:2301-2312.
74. Lev N, Melamed E, Offen D. Apoptosis and Parkinson's disease. Prog Neuropsychopharmacol Biol Psychiatry. 2003; 27:245-250.
75. Cavezzi A, Troiani E, Corrao S. COVID-19: hemoglobin, iron, and hypoxia beyond inflammation. A narrative review. Clin Pract. 2020; 10:1271.
76. Schuh C, Wimmer I, Hametner S, Haider L, Van Dam AM, Liblau RS, Smith KJ, Probert L, Binder CJ, Bauer J, Bradl M, Mahad D, Lassmann H. Oxidative tissue injury in multiple sclerosis is only partly reflected in experimental disease models. Acta Neuropathol. 2014; 128:247-266.
77. Umeno A, Biju V, Yoshida Y. *In vivo* ROS production and use of oxidative stress-derived biomarkers to detect the onset of diseases such as Alzheimer's disease, Parkinson's disease, and diabetes. Free Radic Res. 2017; 51:413-427.
78. Feitosa CM, da Silva Oliveira GL, do Nascimento Cavalcante A, Morais Chaves SK, Rai M. Determination of parameters of oxidative stress *in vitro* models of neurodegenerative diseases - A review. Curr Clin Pharmacol. 2018; 13:100-109.
79. Wojsiat J, Zoltowska KM, Laskowska-Kaszub K, Wojda U. Oxidant/antioxidant imbalance in Alzheimer's disease: Therapeutic and diagnostic prospects. Oxid Med Cell Longev. 2018; 13:1-16.
80. Hilt S, Altman R, Kálai T, Maezawa I, Gong Q, Wachsmann-Hogiu S, Jin LW, Voss JC, Bifunctional A. Anti-amyloid blocks oxidative stress and the accumulation of intraneuronal amyloid-β. Molecules. 2018; 23:2010.

81. Choi BY, Kim JH, Kho AR, Kim IY, Lee SH, Lee BE, Choi E, Sohn M, Stevenson M, Chung TN, Kauppinen TM, Suh SW. Inhibition of NADPH oxidase activation reduces EAE-induced white matter damage in mice. J Neuroinflammation. 205; 12:104.
82. Murray RS, Brown B, Brian D, Cabirac GF. Detection of coronavirus RNA and antigen in multiple sclerosis brain. Ann Neurol. 1992; 31:525-533.
83. Fazakerley JK, Walker R. Virus demyelination. J Neurovirol. 2003; 9:148-164.
84. Biswas K, Chatterjee D, Addya S, Khan RS, Kenyon LC, Choe A, Cohrs RJ, Shindler KS, Das Sarmaa J. Demyelinating strain of mouse hepatitis virus infection bridging innate and adaptive immune response in the induction of demyelination. Clin Immunol. 2016; 170:9-19.
85. Perlman S, Zhao J. Roles of regulatory T cells and IL-10 in virus-induced demyelination. J Neuroimmunol. 2017; 308:6-11.
86. Borrielloa G, Ianniello A. COVID-19 occurring during Natalizumab treatment: a case report in a patient with extended interval dosing approach. Mult Scler Relat Disord. 2020; 41:102165.
87. Boucher A, Desforges M, Duquette P, Talbot PJ. Long-term human coronavirus-myelin cross-reactive T-cell clones derived from multiple sclerosis patients. Clin Immunol. 2007; 123:258-267.
88. Stewart JN, Mounir S, Talbot PJ. Human coronavirus gene expression in the brains of multiple sclerosis patients. Virol. 1992; 1191:502-505.
89. Theil DJ, Tsunoda I, Rodriguez F, Whitton JL, Fujinami RS. Viruses can silently prime for and trigger central nervous system autoimmune disease. J Neurovirology. 2001; 7:220-227.
90. Mohindru M, Kang B, Kim BS. Functional maturation of proteolipid protein139–151-specific Th1 cells in the central nervous system in experimental autoimmune encephalomyelitis. J Neuroimmunol. 2004; 155:127-135.
91. Martin JP, Chen W, Koehren F, Pereira CA. The virulence of mouse hepatitis virus 3, as evidenced by permissivity of cultured hepatic cells toward escape mutants. Res Virol. 1994; 145:297-302.
92. Owens GP, Gilden D, Burgoon MP, Yu X, Bennett JL. Viruses and multiple sclerosis. Neuroscientist. 2011; 17:659-676.
93. Schuh C, Wimmer I, Hametner S, Haider L, Van Dam AM, Liblau RS, Smith KJ, Probert L, Binder CJ, Bauer J, Bradl M, Mahad D, Lassmann H. Oxidative tissue injury in multiple sclerosis is only partly reflected in experimental disease models. Acta Neuropathol. 2014; 128:247-266.
94. Wu GF, Dandekar AA, Pewe L, Perlman S. CD4 and CD8 T cells have redundant but not identical roles in virus-induced demyelination. J Immunol. 2000; 165:2278-2286.
95. Libbey JE, Lane TE, Fujinami RS. Axonal pathology and demyelination in viral models of multiple sclerosis. Discov Med. 2014; 18:79-89.
96. Savarin C, Bergmann CC, Hinton DR, Stohlman SA. Differential regulation of self-reactive CD4+ T cells in cervical lymph nodes and central nervous system during viral encephalomyelitis. Front Immunol. 2016; 7:370.
97. Savarin C, Bergmann CC. Viral-induced suppression of self-reactive T cells: Lessons from neurotropic coronavirus-induced demyelination. J Neuroimmunol. 2017; 308:12-16.
98. Arbour N, Day R, Newcombe J, Talbot PJ. Neuroinvasion by human respiratory coronaviruses. J Virol. 2000; 74:8913-8921.
99. Do Carmo S, Jacomy H, Talbot PJ, Rassart E. Neuroprotective effect of apolipoprotein D against human coronavirus OC43-induced encephalitis in mice. J Neurosci. 2008; 28:10330-10338.
100. Sy M, Kitazawa M, Medeiros R, Whitman L, Cheng D, Lane TE, LaFerla FM. Inflammation induced by infection potentiates Tau pathological features in transgenic mice. Am J Pathol. 2011; 178:2811-2822.
101. Jacomy H, Talbot PJ. Vacuolating encephalitis in mice infected by human coronavirus OC43. Virol. 2003; 315:20-33.
102. Dehner LF, Spitz M, Pereira JS. Parkinsonismin HIV infected patients during antiretroviral therapy – data from a Brazilian tertiary hospital. Braz J Infect Dis. 2016; 20:499-501.
103. Limphaibool N, Iwanowski P, Holstad M J V, Kobylarek D, Kozubski W. Infectious etiologies of parkinsonism: Pathomechanisms and clinical implications. Front Neurol. 2019; 10:652.
104. Patil VM, Singhal S, Masand N. A systematic review on use of aminoquinolines for the therapeutic management of COVID-19: Efficacy, safety and clinical trials. Life Sci. 2020; 254:117775.
105. Sun JK, Chen YT, Fan XD, Wang XY, Han QY, Liu ZW. Advances in the use of chloroquine and hydroxychloroquine for the treatment of COVID-19. Postgrad Med. 2020; 132:604-613.
106. Zhang R, Wang X, Ni L, Di X, Ma B, Niu S, Liu C, Reiter RJ. COVID-19: Melatonin as a potential adjuvant treatment. Life Sci. 2020; 250:117583.

Received November 18, 2020; Revised December 18, 2020; Accepted December 28, 2020.

Address correspondence to:
Ines ElBini Dhouib, Laboratoire des Biomolécules, Venins et Applications Théranostiques, 1002, Tunis, Tunisia.
E-mail: ines.bini@pasteur.tn

Released online in J-STAGE as advance publication December 31, 2020.

Review

DOI: 10.5582/ddt.2020.03097

Analytical methods for the determination of remdesivir as a promising antiviral candidate drug for the COVID-19 pandemic

Yaser Pashaei

Young Researchers and Elite Club, Tehran Medical Sciences, Islamic Azad University, Tehran, Iran.

SUMMARY Coronavirus disease 2019 (COVID-19), which is caused by severe acute respiratory syndrome coronavirus 2 (SARS-CoV-2), is undoubtedly the most challenging pandemic in the current century. A total of 73,953,702 confirmed cases of COVID-19 and 1,644,416 deaths were reported globally up to December 17, 2020. Therefore, in the absence of a safe and effective vaccine, it is urgent to identify a novel antiviral drug to effectively treat patients with COVID-19. On October 22, the U.S. Food and Drug Administration approved remdesivir, a nucleotide analog prodrug with broad antiviral activity, for adults and children (12 years of age and older and weighing at least 40 kg) who need to be admitted to hospital for covid-19 treatment. In order to monitor the optimization of patient clinical response profile, as well as address the challenges associated with remdesivir metabolism, highly sensitive, selective and accurate analytical methods are necessary. This review clearly covers all the analytical methods developed for the identification and quantitative determination of remdesivir and its metabolites in biological matrices, which helps the researchers in developing new methods for the analysis of remdesivir by considering the pros and cons of the previously reported methods.

Keywords Remdesivir, antiviral, COVID-19, SARS-CoV-2, analytical methods

1. Introduction

Coronaviruses are large, enveloped, positive-strand RNA viruses that can cause diseases ranging from the common cold to severe acute respiratory syndrome (SARS). The virus causing coronavirus disease 2019 (COVID-19) is a novel β-coronavirus which is now named as SARS-CoV-2 (*1*). This virus has four essential structural proteins including the small envelope (E) glycoprotein, membrane (M) protein, nucleocapsid (N) protein, and spike (S) glycoprotein, and also three accessory (non-structural) proteins including papain-like protease (PLpro) and 3Chemotrypsin-like protease (3CLpro, also known as the main protease-Mpro), which are responsible for cleavage of viral polypeptide into functional units; and RNA-dependent RNA polymerase (RdRp), which is critical for viral replication and transcription (*2*). SARS-CoV-2 penetrates the host cell *via* the binding of its S-protein with the angiotensin converting enzyme II (ACE-2) receptor, which is found in virtually all human organs in varying degrees (*3*). In general, S protein, PLpro, 3CLpro, RdRp and ACE-2 are the most attractive targets for the development of new antiviral drugs against COVID-19 (*4*).

Although this disease is asymptomatic to mild in most people (approximately 80%), in the most severe cases, it can lead to pneumonia, acute respiratory distress syndrome, sepsis and septic shock, multi-organ failure, and even death (*5*). Despite global containment measures to fight the current pandemic, the incidence of COVID-19 has continued to rise, with over 73.9 million confirmed-cases and over 1.6 million deaths worldwide as of 17 December 2020 (*6*). COVID-19 poses a serious threat to global public health and a broadly effective therapeutic strategy could provide a key means of overcoming this crisis (*7*). Unfortunately, there is currently no known effective treatment for COVID-19. Thus, drug repurposing (*i.e.*, testing the efficacy of existing drugs used previously to treat other diseases) is a basic goal in order to develop a fast therapeutic approach for patients with COVID-19 (*8*).

One of these drugs is remdesivir, an RdRP inhibitor, which shows a broad spectrum of antiviral activity against many RNA viruses like Ebola virus, Marburg, MERS-CoV, SARS-CoV, respiratory syncytial virus and Nipah virus *in vivo* and *in vitro* studies, and thus it is being studied for post-infection treatment for COVID-19 (*9-12*). Human studies of the pharmacokinetic-pharmacodynamics relationship of remdesivir and

its metabolite appeared necessary in the context of COVID-19. Despite these study needs, to the best of our knowledge, only four studies have been reported for the analysis of remdesivir and its metabolites in biological samples. Therefore, there is an urgent need to improve the robustness of the available analytical methods and to establish new standardized methods, which must be fast, more sensitive, more accurate and more specific, to determine remdesivir and its metabolites in biological matrices (*e.g.*, urine, serum, plasma, intracellular matrix, tissues).

On the other hand, the maximum information (physical and chemical properties) about the drug is important and necessary to dispose of a starting point to develop the analytical method. For instance, the structures (Figure 1), acid/basic activity and hydrophobicity are useful to elucidate the composition of the mobile phase (*13*). These parameters are listed in Table 1. To the best of our knowledge, up until now, no systematic report summarizing the analytical methods applied to remdesivir analysis has been achieved in the literature. This review article highlights the analytical methods used for the quantification and identification of remdesivir in biological matrices.

2. Remdesivir

Remdesivir (Veklury®; GS-5734) is a novel antiviral drug developed by Gilead Sciences, originally for the treatment of Ebola virus disease and Marburg virus infections (*14*). Remdesivir, 2-ethylbutyl (2S)-2-[[[(2R,3S,4R,5R)-5-(4-aminopyrrolo [2,1-f][1,2,4] triazin-7-yl)-5-cyano-3,4-dihydroxyoxolan-2-yl] methoxy-phenoxyphosphoryl]amino]propanoate (Figure 1A), is a single diastereomer monophosphoramidate prodrug of a nucleoside analog that perturbs viral replication. It is a white to off-white or yellow non hygroscopic solid, practically insoluble in water and soluble in ethanol (*15*). The physicochemical properties of remdesivir are summarized in Table 1.

2.1. Remdesivir mechanism of action

Remdesivir has a complex activation pathway (see Figure 1 for further details). Briefly, upon diffusion of remdesivir (Figure 1A) into the respiratory epithelial cell, it is first metabolized into an intermediate alanine metabolite (GS-704277; Figure 1B), which is further processed into nucleoside monophosphate derivative (GS-441524; Figure 1C), the major circulating metabolite of remdesivir, *via* a phosphoramidase-type enzyme. Ultimately, GS-441524 is rapidly converted by intracellular kinases to the pharmacologically active nucleoside triphosphate analog (GS-443902; Figure 1D), a final product of remdesivir activation, which has a prolonged intracellular half-life ($T_{½}$ ~40 hours). Overall, remdesivir inhibits the RdRp activity of SARS-CoV-2 *via* non-obligate termination of RNA chains, after being activated to a triphosphate (*16,17*).

2.2. Efficacy of remdesivir against SARS-COV-2

Antiviral actions of remdesivir against SARS-CoV-2 have been evaluated in both cultured cells and animal models. Pruijssers *et al.* (*18*) reported that remdesivir potently inhibited SARS-CoV-2 replication in human lung cells and primary human airway epithelial cultures with a half maximal effective (EC_{50}) concentration of 0.01 µM. Remdesivir was also found to have an EC_{50} of 0.77 µM against SARS-CoV-2 in Vero E6 cells (*19*). Moreover, *in vivo* studies in a rhesus macaque model infected with SARS-CoV-2 was found to prevent

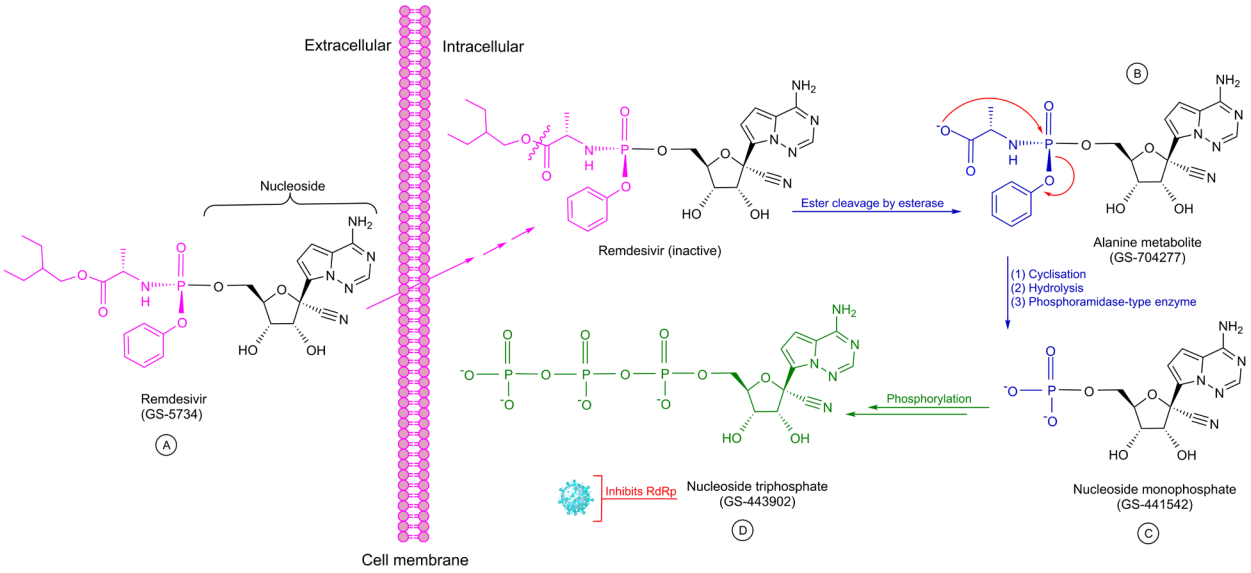

Figure 1. Remdesivir and its intracellular conversion.

Table 1. Salient features of the studied drug

Generic Name/Trade Name	Remdesivir (GS-5734)/Veklury
Drug Class	Antiviral (Small Molecule)
Therapeutic Area	Coronavirus Infections
Molecular Formula	$C_{27}H_{35}N_6O_8P$
Molecular Weight	602.59 g/moL
Exact Mass	602.22539 Da
Water Solubility	0.339 mg/L
pKa (strongest acidic/basic)	10.23/0.65
Log Po/w	2.01
Charge at pH 7	0
Route	Intravenous (*i.v.*)
Dose	200 mg *i.v.* loading dose over 30 min on day 1, then 100 mg *i.v.* daily over 30 min on days 5 to 10
C_{max} (ng/mL) (*i.v.* 100 mg once daily)	2229 and 145 (GS-441524)
EC_{50}	ND
AUC_{tau} (ng/hour/mL) (*i.v.* 100 mg once daily)	1585 and 2229 (GS-441524)
C_{trough} (ng/mL)	ND (24-hr post dose) and 69.2 (GS-441524)
Bioavailability (%)	0
T_{max} (hour)	0.67-0.68 and 1.51-2.00 (GS-441524)
$T_{1/2}$ (hour)	~1 and ~27 (GS-441524)
Toxicity	ND
Protein Binding (%)	88-93.6% and 2% (GS-441524)
Metabolic pathway(s)	CES1 (80%), Cathepsin A (10%), CYP3A (10%)
Major route of elimination	Metabolism (for remdesivir) and Glomerular filtration and active tubular secretion (for GS-441524)
Extraction	Urine: 10% and 49% (GS-441524) Feces: ND and 0.5% (GS-441524)

ND: not detected; C_{max}: maximum plasma concentration; EC_{50}: half maximal effective concentration; $T_{1/2}$: plasma half-life; Tmax: time post-dose of maximum plasma concentration; AUC: the integrated area under the plasma concentration-time curve.

disease progression with remdesivir (*20*). These initial studies demonstrate that remdesivir is potently active against SARS-CoV-2 virus infection *in vitro* and *in vivo*, supporting its further clinical testing for treatment of COVID-19.

There are several randomized control trials currently being conducted to assess the efficacy and safety of this drug in patients with COVID-19 (*https://clinicaltrials.gov*). Some evidence suggests that compassionate use of remdesivir may cause some clinical improvement in patients with mild or moderate, or severe COVID-19 disease (*21-24*). But, before making any conclusive statement about the efficacy of remdesivir for COVID-19 treatment, more randomized, placebo-controlled clinical trials and other scientific validation need to be performed.

2.3. Remdesivir pharmacokinetics

Table 1 summarizes the data on the pharmacokinetic properties of remdesivir for SARS-CoV-2. Remdesivir is administered *via* an intravenous (*i.v.*) infusion, in a total volume of up to 250 mL 0.9% saline over 30 to 120 min, with a loading dose of 200 mg once daily in patients ≥ 12 years old and weighing ≥ 40 kg, followed by a maintenance dose of 100 mg once daily for 5 to10 days (*25*). This dose is also being evaluated in multicenter randomized trials. Remdesivir is not recommended for patients with an estimated glomerular filtration rate of ≤ 30 mL/min, or for patients with an alanine aminotransferase level ≥ 5 times the upper limit of normal (*26*). The most common adverse effects include gastrointestinal distress, elevated transaminase and bilirubin levels, and infusion site reactions (*27*).

Due to poor hepatic stability, remdesivir should not be given orally as bioavailability is expected to be low. Remdesivir is unstable in plasma and is widely distributed in many tissues, including the kidney, kidney medulla, and liver, but does not cross the blood-brain barrier (*28*). After *i.v.* administration, maximum plasma concentrations (C_{max}) of remdesivir and its main metabolite (GS-441524) were 2,229 ng/mL and 145 ng/mL, respectively. Plasma $T_{½}$ of remdesivir and GS-441524 were 1 and 27 hours, respectively. Remdesivir is widely bound to human plasma proteins (88-93.6%). By contrast, metabolites GS-704277 and GS-441524 exhibit low plasma protein binding (< 2% bound). Remdesivir is a substrate for CYP2C8 (minor), CYP2D6 (minor), and CYP3A4 (minor), and is a substrate for organic anion transporting polypeptides 1B1 and P-glycoprotein transporters (minor). The majority of the remdesivir dose recovered in urine is GS-441524 (49%), while 10% is recovered as the unmetabolized parent compound (*24,29*).

3. Therapeutic drug monitoring

Therapeutic drug monitoring (TDM), which is defined as

a valuable tool to individualize and optimize drug dosage in order to obtain drug concentrations associated with the highest therapeutic efficacy with a reduced risk of concentration-dependent adverse effects, is already well-established in many different infectious diseases (*30,31*) and may be useful in the issue of COVID-19 therapy (*32*). This approach involves determining drug concentration in a human biological matrix (*e.g.*, serum, plasma, or whole blood) and interpreting these concentrations in terms of relevant clinical parameters.

In general, determination of drug concentration is an inherent part of preclinical and clinical investigation of new therapeutic agents because no pharmacokinetic studies can be carried out without it. It is necessary to investigate drug-effect or drug-toxicity relationship and can be also used to understand drug mechanism of action (*33*). Therefore, both for pharmacokinetic-pharmacodynamic studies and for possible future TDM, there is an imperative and urgent need to develop a highly sensitive, rapid, and high-throughput analytical method for the quantitative determination of remdesivir and/or its metabolite (GS-441524) in biological matrices. Despite these study needs, to our knowledge, only a few methods have been reported for the qualitative and quantitative analysis of remdesivir and its metabolites (*34-37*). The instrumental and analytical properties of each reported method are described in detail and tabulated for easy access (see Table 2 for further details).

4. Analytical methods

In 2016, Warren *et al.* (*9*) developed a liquid chromatography-tandem mass spectrometry (LC-MS/MS) for the pharmacokinetic study of remdesivir in uninfected male rhesus monkeys (*Macaca mulatta*). The MS instrument was operated in positive ion electrospray ionization (ESI) mode with multiple reaction monitoring (MRM). Remdesivir was formulated in solution at 5 mg/mL with 12% sulfobutylether-β-cyclodextrin in water, pH 3.5-4.0, and 2 mL/kg was administered by slow bolus (~ 1 min) for a final dose of 10 mg/kg. An aliquot of plasma sample was spiked with 20 nM 5-(2-aminopropyl)indole solution as internal standard (IS), extracted with 90% methanol and acetonitrile mixture (1:1, v:v) and 10% water, evaporated to dryness at 40°C under a gentle stream of nitrogen, reconstituted in a mixture containing 1% acetonitrile and 99% water with 0.01% formic acid, and assayed. A Phenomenex Synergi Hydro-RP 30A (75 × 2.0 mm, 4.0 µm) column was used as a stationary phase, and mobile phase was chosen as a binary mobile phase gradient (A: 0.2% formic acid in 99% water and 1% acetonitrile and B: 0.2% formic acid in 95% acetonitrile and 5% water) at flow rate of 0.26 mL/min. Unfortunately, the details of the validation process are not described.

In 2020, Alvarez *et al.* (*34*) determined remdesivir and its metabolite GS-441524 in human plasma using an LC-MS/MS method with the help of a simple protein precipitation (PP) step using a mixture of methanol and Zinc sulphate ($ZnSO_4$, 1 M). $ZnSO_4$ reduces protein stability by altering the isoelectric points and by replacing protons on proteins, thereby lowering of the solution's pH. Therefore, the use of $ZnSO_4$ makes the PP thoroughly and enhances the detection sensitivity of remdesivir at low concentration. When $ZnSO_4$ is used as the sole reagent for extraction, a lot of inorganic salts move into the supernatant to contaminate the MS sources. The addition of methanol or acetone/methanol mixture to the precipitation step successfully prevents water and water-soluble salt into the supernatant, making the reconstituted samples definitely cleaner (*13*). In this work the authors used deuterated remdesivir-13C6 as an IS. The system was operated in positive (+) ESI mode, and the following MRM transitions were used: 603.3→200.0 and 603.3→229.0 for remdesivir, 292.2→173.1 and 292.2→147.1 for GS-441524, and 609.3→206.0 for IS. The authors used a Kinetex® Polar C18 column (100 × 2.1 mm I.D., 2.6 µm) to separate analytes. The elution was performed with a gradient of 10 mM sodium formate buffer in 0.1% formic acid (A) and acetonitrile (B) starting from 0% of (B) to 100% in 2 min, at flow rate of 0.50 mL/min, and the total run time was 5 min per sample. The method linearity was over the range of 1-5,000 ng/mL for remdesivir and 5-2,500 ng/mL for GS-441524, with limit of detection (LOD), as the lower concentration with a signal/noise (S/N) ratio higher than three, of 0.3 and 2 ng/mL and lower limit of quantitation (LLOQ) of 1 and 5 ng/mL, for remdesivir and GS-441524, respectively. The major advantages of the method were the requirement for small plasma volume and simple sample preparation procedure, while the main limitation of study was slightly higher LLOQ value obtained for GS-441524 (5 ng/mL). After the optimization and validation according to European Medicines Agency guidelines, the method was successfully applied to a pharmacokinetic study in a COVID-19 patient after a single dose of remdesivir (200 mg *i.v.*).

Humeniuk *et al.* (*35*) also used an LC-ESI(+)-MS/MS method to determine plasma remdesivir concentrations. Quantification was performed using MRM of the transitions m/z 603.3→402.2 and m/z 606.3→402.2 for remdesivir and an isotopically-labeled IS (GS-829143), m/z 441.1→150.1 and m/z 444.1→150.1 for metabolite GS-704277 and an isotopically-labeled IS (GS-829466), m/z 292.2→202.2 and m/z 295.2→205.2 for metabolite GS-441524 and an isotopically-labeled IS (GS-828840), respectively. The method was linear over the range of 4-4,000 ng/mL for remdesivir, 2-2,000 ng/mL for GS-704277 and 2-2,000 ng/mL for GS-441524, respectively. Interassay precision, based on coefficient of variation for remdesivir, GS-704277 and GS-441524, ranged

from 2.1% to 5.3%, and accuracy, based on interassay percent relative error for remdesivir, GS-704277 and GS-441524, ranged from – 9.8% to 9.5%. This study has some drawbacks, such as the lack of analysis of selectivity, sensitivity, robustness, and stability. However, these parameters are reported as fundamental performance characteristics for a method to be considered as validated.

Recently, Avataneo *et al.* (*36*) described a simple, rapid and sensitive UHPLC-ESI(+)-MS/MS, an fast technique (total run time < 2.5 min) which has the advantage of high sensitivity and high sample throughput over conventional LC-MS systems, method for the quantification of remdesivir and its main metabolite, GS-441524, in spiked human plasma. The MRM transitions were set at 603.15>200 (m/z), 292>163 (m/z) and 313.2>78.05 (m/z) for remdesivir, GS-441524 and 6,7-dimethyl-2,3-di(2-pyridyl) quinoxaline (as IS), respectively. After a PP procedure with a mixture of methanol:acetonitrile (50:50, v/v), the chromatographic separation of the analytes was achieved on an Acquity® HSS T3 column (50 × 2.1 mm I.D., 1.8 µm) with gradient elution of the mobile phase (A: water/formic acid 0.05% and B: acetonitrile/ formic acid 0.05%) at flow rate of 0.40 mL/min. Retention times were 0.98, 1.67 and 1.72 min for GS-441524, remdesivir and IS, respectively. The LLOQ value for both the analytes was 0.98 ng/mL while the LOD values (S/N > 3) were 0.24 ng/mL for remdesivir and 0.98 ng/mL for GS-441524. The recoveries ranged from 87-118% (remdesivir) and 81-102% (GS-441524). The established method was shown to be accurate, precise, sensitive, and linear. However, it is still necessary to develop a more sensitive method to measure the concentrations of remdesivir in human plasma for advanced pharmacokinetic profiles in low dose remdesivir. According to the authors, this method could be a useful tool for studying remdesivir and GS-441524 clinical pharmacokinetics, particularly during the current COVID-19 outbreak.

The same UHPLC system was then employed by Tempestilli *et al.* (*37*) for the pharmacokinetic evaluation of remdesivir and GS-441524 in two critically ill patients who recovered from COVID-19. They used a PP technique (600 µL of methanol/ acetonitrile, 50:50, v/v) for pretreatment and cleanup of plasma samples. Using this method remdesivir and GS-441524 were simultaneously measured with a LOQ of 5.86 ng/mL for remdesivir and 1.96 ng/mL for GS-441524. Since most studies, including *in vivo* pharmacokinetics, have a large number of samples to analyze, run time per sample can be very important. The main advantage of the developed methods is the lack of a laborious sample preparation step, which results in a shortening of the analysis time. Although recoveries obtained by LC-MS/MS (*34,35*) and UPLC-MS/MS (*36,37*) were similar, UHPLC gave significantly better precision. The details of these methods are summarized in Table 2.

5. Conclusions and future perspectives

COVID-19, a highly infectious respiratory disease, is undoubtedly the most challenging pandemic in the current century. It has been shown that remdesivir is highly effective in stopping the replication mechanism of the coronavirus that causes COVID-19. This review provides for the first time a simplified and thorough evaluation of the analytical methods for the analysis of remdesivir from 2000 up to 2020.

A survey of the literature reveals that only LC-MS methods have been introduced for remdesivir determination in biological samples, which increases analysis costs to a considerable extent. To date, all the studies reported in literature have been performed in biological fluids, particularly in plasma samples. The sample clean-up procedure is a mandatory step in the whole analytical process, due to the low concentration of remdesivir and interference of complex matrix in biological samples. Surprisingly, all the authors have used conventional PP technique for the extraction of remdesivir and its metabolites. PP is a rapid, low cost and convenient extraction technique; however, it is nonselective and does not remove many of the matrix interferences. In addition, PP is not as rugged and reproducible sample perpetration procedure with LC-MS quantification due to the strong and inconsistent matrix effect. On the other hand, it is difficult to choose the ideal precipitating agents to remove interfering proteins from biological samples. Hence, to overcome such drawbacks, it is recommended that future trends should focus on the development of modern and more effective sample preparation techniques.

Qualitative and quantitative determination plays an important role in ensuring the safety and efficacy of drugs in different matrices. To the best of our knowledge, no stability indicating method has been reported for the estimation of remdesivir impurities and degradation products present in pharmaceutical formulation. Thus, it is felt necessary to carry out forced degradation studies as per International Conference on Harmonization guidelines and design a selective and validated stability-indicating HPLC method. According to the literature data, it can be concluded that both LC-MS/MS and UPLC-MS/MS methods provide acceptable analytical performance for remdesivir measurement but UPLC exhibited shorter analysis time, higher efficiency with better resolution and better precision. In all cases, the MS instrument was operated in the positive polarity. Furthermore, the protonated molecular ion $[M+H]^+$ was chosen as a precursor ion for quantitation in all developed methods. Based on the cited literature, ESI is the most widely used ion source in the analysis of remdesivir and its metabolites in biological matrices by means of LC-

Table 2. Summary of liquid chromatographic methods for the analysis of remdesivir and its metabolites

Analyte(s)	Chromatographic conditions	Validation parameters	Key assay findings	*Ref.*
Remdesivir and its metabolite GS-441524	System: LC-MS/MS, using a TSQ Endura triple-quadrupole mass spectrometer (Thermo Fisher) equipped with an ESI source set in a positive mode with ion spray potential at +3.5 kV. Mass spectrometric detection: MRM transitions were set according to the following m/z values: 603.3→200.0 (35%) and 603.3→229.0 (23%) for remdesivir, 292.2→173.1 (24%) and 292.2→147.1 (29%) for GS-441524, and 609.3→206.0 for (33%) remdesivir-$_{13}C^6$. Matrix: human plasma. Column: Kinetex® 2.6 Polar C18 100A LC (100×2.1 mm, 3 µm), preheated at 30 °C. Mobile phase: 10 mM sodium formate buffer in 0.1% formic acid (A) and acetonitrile (B) starting from 0% of (B) to 100% in 2 min. Sample volume: 50 µL. Extraction: a one-step protein precipitation (PP): 50 µL of samples were precipitated with 75 µL methanol containing IS and 5 µL of $ZnSO_4$ 1M. After vortex mix for 15 s, samples were left at +4°C for 10 min, and then centrifuged. Supernatants were collected and injected to system. Internal standard: remdesivir-$_{13}C^6$ (20 µL). Injection volume: 20 µL. Flow rate: 0.5 mL min^{-1}. Total run time: 5 min Retention time: 1.9, 2.41 and 2.42 min for GS-441524, remdesivir and IS, respectively.	Regression type: linear fit with weighting factor (1/x). Linearity: 1-5,000 ng/mL for remdesivir and 5-2,500 ng/mL for GS-441524, with coefficient of determination r^2 = 0.998 and r^2 = 0.997, respectively. Precision and Accuracy: inter- and intra-day precision (%CV) ranged from 2.6-5.6 and 2.5-7.3%. Inter- and intra-day accuracy (as percent of the nominal value) was 89.6–100.4 and 88.9-108.9%. Limit of detection (LOD): 0.3 and 2 ng/mL (S/N>3) for remdesivir and GS-441524, respectively. Lower limit of quantification (LLOQ): 1 and 5 ng/mL for remdesivir and GS-441524, respectively. Selectivity: no interference was observed from the six different blank matrices on the retention times and ion channel of both compounds and IS. Carry-over: a replicate of blank sample was analyzed immediately after the highest CS, and there was no significant carry-over. Matrix effect: for remdesivir, GS and IS, matrix factor was similar, ranging from 72 to 84%.A slight matrix effect was observed, compensated by IS. Stability: remdesivir and GS-441524 were stable in whole blood stored at +4°C for 24 h but not at ambient temperature. Stability for remdesivir was adequate in NaF-plasma when frozen at −20°C. On Li-heparin-plasma, a 50-60% decrease was observed even if plasma was frozen at −20°C. GS is stable in both plasma when frozen at −20°C. After two frozen/thaw cycles, GS appeared to increase in Li-heparin-plasma. Remdesivir was stable at 8°C for 4 h and 48 h when kept in the autosampler.	► A simple, rapid and accurate LC method, according to the European Medicines Agency (EMA) guidelines, was developed and fully validated for the measurement of plasma concentrations of remdesivir and its active metabolite, GS-441524. ► Higher stability of remdesivir and metabolite was observed on NaF-plasma tubes. ► This method was successfully applied to a pharmacokinetic study in a patient suffering from COVID-19.	*34*
Remdesivir, GS-704277 and GS-441524	System: LC system with ABSciex 4000 Q-trap MS/MS with an ESI source in positive mode. Mass spectrometric detection: as follows: m/z 603.3→402.2 and m/z 606.3→402.2 for remdesivir and GS-829143 (as an isotopically-labeled IS), m/z 441.1→150.1 and m/z 444.1→150.1 for GS-704277 and GS-829466 (as an isotopically-labeled IS), m/z 292.2→202.2 and m/z 295.2→205.2 for GS-441524 and GS-828840 (as an isotopically-labeled IS), in MRM mode. Matrix: human plasma.	Calibration range: 4-4,000 ng/mL for remdesivir, 2-2,000 ng/mL for GS-704277 and 2-2,000 ng/mL for GS-441524, respectively. Precision and Accuracy: interassay precision (%CV) for remdesivir, GS-704277 and GS-441524 ranged from 2.1% to 5.3%, and accuracy, based on interassay percent relative error for remdesivir, GS-704277 and GS-441524, ranged from −9.8% to 9.5%.	► This study reports results of first-in-human single- and multiple-dose studies conducted to evaluate safety and pharmacokinetics of solution and lyophilized formulations of remdesivir in healthy volunteers. ► Overall, remdesivir exhibited favorable safety and pharmacokinetic profiles that supported once-daily dosing.	*35*

Table 2. Summary of liquid chromatographic methods for the analysis of remdesivir and its metabolites (continued)

Analyte(s)	Chromatographic conditions	Validation parameters	Key assay findings	*Ref.*
Remdesivir and its metabolite GS-441524	System: Perkin Elmer LX-50VR UHPLC system coupled with a Triple Quadrupole QSight 220®, equipped with an ESI source in positive mode. Mass spectrometric detection: MRM traces (m/z) were quantified as: 603.15→200 for remdesivir, 292→163 for metabolite GS-441524 and 313.2→78.05 for 6,7-dimethyl-2,3-di(2-pyridyl) quinoxaline (QX; as IS). Matrix: human plasma. Column: Acquity® HSS T3 C18 (2.1 × 50 mm, 1.8 µm; Waters Corp), The column temperature was 40°C. Mobile phase: water/formic acid 0.05% (A) and acetonitrile/formic acid 0.05% (B) with linear gradient elution. Sample volume: 50 µL. Extraction: several-step PP technique; plasma samples were precipitated with 600 µL of methanol/acetonitrile (50:50 v/v) containing IS. After being vortexed for 30 s, 300 µL of the supernatant reconstituted in 600 µL of pure water, and then injected into system. Internal standard: QX. Injection volume: 8 µL. Flow rate: 0.4 mL min^{-1}. Total run time: 2.5 min. Retention time: 0.98, 1.67 and 1.72 min for GS-441524, remdesivir and IS, respectively.	Regression type: linear fit with weighting factor (1/x). Precision and Accuracy: intra–day and inter–day precision (RSD%) were in the range from 1-10% and 6-12% (for remdesivir), 6-9% and 3-14% (for GS), respectively. Accuracy was 87-118% and 81-102%% for remdesivir and GS. Recovery: mean recovery was 71% with %RSD = 6% for remdesivir and 102% with %RSD = 7% for GS. Extraction: mean extraction was 67% with %RSD = 9% for remdesivir and 105% with %RSD = 10% for GS. LOD: (S/N >3) 0.24 ng/mL for remdesivir and 0.98 ng/mL for GS. LLOQ: 0.98 ng/mL for both the analytes. Specificity and Selectivity: blank plasma, alone and spiked with antiretroviral drugs, presented no interfering peaks at the analyte retention times. Matrix effect: 6% with %RSD = 4% for remdesivir and −2% with %RSD = 12% for GS. Stability: both remdesivir and GS remained stable in QCs conserved at −80°C for over 4 months. Remdesivir, when dissolved in plasma, was found to be unstable at ambient temperature and 4°C, even for 24 h; in contrast, in extracted plasma samples, remdesivir was stable for up to 7 days in the autosampler (10°C).	► Validation data showed that the assay for remdesivir is sensitive, selective, fast, and reproducible. ► This method represents a useful tool for studying remdesivir and GS-441524 clinical pharmacokinetics, particularly during the current COVID-19 outbreak.	*36*

MS(/MS) methods. These methods provide a powerful analytical tool for clinical therapeutic monitoring of remdesivir. However, MS apparatuses are usually quite expensive, and this cost may be prohibitive to clinical laboratories. As a result, despite many advantages of MS detection, the application of separation methods based on MS can be problematic in clinical practice.

Unlike complicated analytical techniques, miniaturized analytical systems offer a low-cost, fast, easy-to-use, and on-site analysis method to explore the full potential of TDM. Also, on-site TDM has the potential to improve patient outcomes and extremely reduce health-care costs. Therefore, it is recommended that future trends should focus on the design and development of a highly sensitive, portable and miniaturized biosensor for monitoring of remdesivir. At last, it is hoped that this study provides new ideas and prospective for researchers involved in the development of new analytical methods, formulations, and quality and medical control of remdesivir.

Funding: None.

Conflict of Interest: The author has no conflicts of interest to disclose.

References

1. Zhu N, Zhang D, Wang W, *et al.* A novel coronavirus from patients with pneumonia in China, 2019. N Engl J Med. 2020; 382:727-733.
2. Indwiani Astuti Y. Severe acute respiratory syndrome coronavirus 2 (SARS-CoV-2): An overview of viral structure and host response. Diabetes Metab Syndr. 2020; 14:407-412.
3. Zhang H, Penninger JM, Li Y, Zhong N, Slutsky AS. Angiotensin-converting enzyme 2 (ACE2) as a SARS-CoV-2 receptor: molecular mechanisms and potential therapeutic target. Intensive Care Med. 2020; 46:586-590.
4. Liu C, Zhou Q, Li Y, Garner LV, Watkins SP, Carter LJ, Smoot J, Gregg AC, Daniels AD, Jervey S, Albaiu D. Research and development on therapeutic agents and vaccines for COVID-19 and related human coronavirus diseases. ACS Cent Sci. 2020; 6:315-331.
5. Chen N, Zhou M, Dong X, Qu J, Gong F, Han Y, Qiu Y, Wang J, Liu Y, Wei Y, Xia J, Yu T, Zhang X, Zhang L. Epidemiological and clinical characteristics of 99 cases of 2019 novel coronavirus pneumonia in Wuhan, China: a descriptive study. Lancet. 2020; 395:507-513.
6. Johns Hopkins University and Medicine. Coronavirus Resource Center. *https://coronavirus.jhu.edu/map.html* (accessed December 17, 2020).
7. Jamrozik E, Selgelid MJ. COVID-19 human challenge studies: ethical issues. Lancet Infect Dis. 2020; 20:198-203.
8. Fragkou PC, Belhadi D, Peiffer-Smadja N, Moschopoulos CD, Lescure FX, Janocha H, Karofylakis E, Yazdanpanah Y, Mentré F, Skevaki C, Laouénan C, Tsiodras S. Review of trials currently testing treatment and prevention of COVID-19. Clin Microbiol Infect. 2020; 26:988-998.
9. Warren TK, Jordan R, Lo MK, *et al.* Therapeutic efficacy of the small molecule GS-5734 against Ebola virus in rhesus monkeys. Nature. 2016; 531:381-385.
10. Sheahan TP, Sims AC, Graham RL, *et al.* Broad-spectrum antiviral GS-5734 inhibits both epidemic and zoonotic coronaviruses. Sci Transl Med. 2017; 9:3653-3663.
11. Lo MK, Jordan R, Arvey A, *et al.* GS-5734 and its parent nucleoside analog inhibit Filo-, Pneumo-, and Paramyxoviruses. Sci Rep. 2017; 7:43395.
12. Chang WT, Liu PY, Gao ZH, Lee SW, Lee WK, Wu SN. Evidence for the effectiveness of remdesivir (GS-5734), a nucleoside-analog antiviral drug in the inhibition of IK (M) or IK (DR) and in the stimulation of IMEP. Front Pharmacol. 2020; 11:1091.
13. Pashaei Y, Mehrabi M, Shekarchi M. A review on various analytical methods for determination of anthracyclines and their metabolites as anti-cancer chemotherapy drugs in different matrices over the last four decades. Trends Analyt Chem. 2020; 130:115991.
14. Eastman RT, Roth JS, Brimacombe KR, Simeonov A, Shen M, Patnaik S, Hall MD. Remdesivir: A review of its discovery and development leading to emergency use authorization for treatment of COVID-19. ACS Cent Sci. 2020; 6:672-683.
15. DrugBank. Remdesivir. *https://www.drugbank.ca/drugs/DB14761* (accessed December 15, 2020).
16. Jorgensen SC, Kebriaei R, Dresser LD. Remdesivir: Review of pharmacology, pre-clinical data and emerging clinical experience for COVID-19. Pharmacotherapy. 2020; 40:660-671.
17. Amirian ES, Levy JK. Current knowledge about the antivirals remdesivir (GS-5734) and GS-441524 as therapeutic options for coronaviruses. One Health. 2020; 9:100128.
18. Pruijssers AJ, George AS, Schäfer A, *et al.* Remdesivir inhibits SARS-CoV-2 in human lung cells and chimeric SARS-CoV expressing the SARS-CoV-2 RNA polymerase in mice. Cell Rep. 2020; 32:107940.
19. Wang M, Cao R, Zhang L, *et al.* Remdesivir and chloroquine effectively inhibit the recently emerged novel coronavirus (2019-nCoV) *in vitro*. Cell Res. 2020; 30:269-271.
20. Williamson BN, Feldmann F, Schwarz B, *et al.* Clinical benefit of remdesivir in rhesus macaques infected with SARS-CoV-2. Nature. 2020; 585:273-276.
21. Shih WJ, Shen X, Zhang P, Xie T. Remdesivir is effective for moderately severe patients: A re-Analysis of the first double-blind, placebo-controlled, randomized trial on remdesivir for treatment of severe COVID-19 patients conducted in Wuhan City. Open Access J Clin Trials. 2020; 12:15-21.
22. Wang Y, Zhang D, Du G, *et al.* Remdesivir in adults with severe COVID-19: a randomised, double-blind, placebo-controlled, multicentre trial. Lancet. 2020; 395:1569-1578.
23. Grein J, Ohmagari N, Shin D, *et al.* Compassionate use of remdesivir for patients with severe Covid-19. N Engl J Med. 2020; 382:2327-2336.
24. Beigel JH, Tomashek KM, Dodd LE, *et al.* Remdesivir for the treatment of Covid-19-final report. N Engl J Med. 2020; 383:1813-1826.
25. Marjani M, Tabarsi P, Moniri A, *et al.* NRITLD protocol for the management of patients with COVID-19 admitted to hospitals. Tanaffos. 2020; 19:91-99.
26. Adamsick ML, Gandhi RG, Bidell MR, Elshaboury RH, Bhattacharyya RP, Kim AY, Nigwekar S, Rhee EP,

Sise ME. Remdesivir in patients with acute or chronic kidney disease and COVID-19. J Am Soc Nephrol. 2020; 31:1384-1386.
27. Mehta N, Mazer-Amirshahi M, Alkindi N, Pourmand A. Pharmacotherapy in COVID-19; A narrative review for emergency providers. Am J Emerg Med. 2020; 38:1488-1493.
28. Sahakijpijarn S, Moon C, Koleng JJ, Christensen DJ, Williams III RO. Development of remdesivir as a dry powder for inhalation by thin film freezing. Pharmaceutics. 2020; 12:1002.
29. US Food and Drug Administration. Fact sheet for health care providers emergency use authorization of remdesivir. *https://www.fda.gov/media/137566/download* (accessed October 28, 2020).
30. Punyawudho B, Singkham N, Thammajaruk N, Dalodom T, Kerr SJ, Burger DM, Ruxrungtham K. Therapeutic drug monitoring of antiretroviral drugs in HIV-infected patients. Expert Rev Clin Pharmacol. 2016; 9:1583-1595.
31. Conti M, Cavedagna TM, Ramazzotti E, Mancini R, Calza L, Rinaldi M, Badia L, Guardigni V, Viale P, Verucchi G. Multiplexed therapeutic drug monitoring (TDM) of antiviral drugs by LC-MS/MS. Clin Mass Spectrom. 2018; 7:6-17.
32. Asadi-Pooya AA, Attar A, Moghadami M, Karimzadeh I. Management of COVID-19 in people with epilepsy: drug considerations. Neurol Sci. 2020; 41:2005-2011.
33. Buclin T, Thoma Y, Widmer N, André P, Guidi M, Csajka C, Decosterd LA. The steps to therapeutic drug monitoring: A structured approach illustrated with imatinib. Front Pharmacol. 2020; 11:177.
34. Alvarez JC, Moine P, Etting I, Annane D, Larabi IA. Quantification of plasma remdesivir and its metabolite GS-441524 using liquid chromatography coupled to tandem mass spectrometry. Application to a Covid-19 treated patient. Clin Chem Lab Med. 2020; 58:1461-1468.
35. Humeniuk R, Mathias A, Cao H, Osinusi A, Shen G, Chng E, Ling J, Vu A, German P. Safety, tolerability, and pharmacokinetics of remdesivir, an antiviral for treatment of COVID-19, in healthy subjects. Clin Transl Sci. 2020; 13:896-906.
36. Avataneo V, de Nicolò A, Cusato J, Antonucci M, Manca A, Palermiti A, Waitt C, Walimbwa S, Lamorde M, di Perri G, D'Avolio A. Development and validation of a UHPLC-MS/MS method for quantification of the prodrug remdesivir and its metabolite GS-441524: a tool for clinical pharmacokinetics of SARS-CoV-2/COVID-19 and Ebola virus disease. J Antimicrob Chemother. 2020; 75:1772-1777.
37. Tempestilli M, Caputi P, Avataneo V, Notari S, Forini O, Scorzolini L, Marchioni L, Ascoli Bartoli T, Castilletti C, Lalle E, Capobianchi MR, Nicastri E, D'Avolio A, Ippolito G, Agrati C. Pharmacokinetics of remdesivir and GS-441524 in two critically ill patients who recovered from COVID-19. J Antimicrob Chemother. 2020; 75:2977-2980.

Received October 21, 2020; Revised December 18, 2020; Accepted December 26, 2020.

**Address correspondence to:*
Yaser Pashaei, Young Researchers and Elite Club, Tehran Medical Sciences, Islamic Azad University, Tehran, Iran.
E-mail: yaser.pashaei@yahoo.com

Released online in J-STAGE as advance publication December 30, 2020.

Mini-Review

DOI: 10.5582/ddt.2020.03083

Approach to acute febrile illness during the COVID-19 pandemic

Manasvini Bhatt[1], Manish Soneja[1], Nitin Gupta[2,*]

[1] Department of Medicine, All India Institute of Medical Sciences, New Delhi, India;
[2] Department of Infectious Diseases, Kasturba Medical College, Manipal Academy of Higher Education, Manipal, Karnataka, India.

SUMMARY Coronavirus disease 2019 (COVID-19) is a febrile respiratory illness that has spread rampantly across the globe and has emerged as one of the biggest pandemics of all time. Besides the direct effects of COVID-19 on mortality, collateral impacts on diagnosis and management of acute febrile illnesses (AFI) is a matter of great concern. The overlap in presentation, shunting of available resources and infection control precautions in patients with suspected COVID-19 result in a significant delay in diagnoses and management of AFI. This review highlights the challenges in the management of acute febrile illness during COVID pandemic and possible solutions for the same.

Keywords Dengue, scrub typhus, leptospirosis, chikungunya, malaria

1. Introduction

Coronavirus disease 2019 (COVID-19) is caused by a virus named Severe Acute Respiratory Syndrome Coronavirus 2 (SARS-CoV-2). The disease was first reported in December of 2019 and has evolved into a pandemic with more than 75 million cases as on December 20, 2020. The number of reported deaths due to COVID-19 is more than 1.6 million (*1*). However, there are no official reports on the number of deaths in non-COVID patients who suffered as collateral damage of COVID-19. One such group of patients who are speculated to be affected is patients with acute febrile illnesses (AFI) who may present with similar manifestations as COVID-19 but remain undiagnosed. AFI is an umbrella term used for infectious febrile illness of short duration (< 14 days) in tropical and sub-tropical countries (*2*). The most common AFIs include dengue, chikungunya, malaria, enteric fever, scrub typhus, leptospirosis, Zika virus, and Kyasanur forest disease (KFD) (*3*). The aim of this review is to discuss the interplay between COVID-19 and AFIs.

2. Epidemiology

Acute febrile illness is one of the most common causes of admission in the monsoon/post-monsoon season in both the public and private sectors. With the increase in the human population and overcrowding, the prevalence of AFIs has been increasing throughout the world. Due to the lockdown instituted in several geographical regions, interventions such as seasonal chemotherapy prophylaxis, insecticidal measures, and environmental surveillance may take a hit, thereby increasing the incidence further.

These AFIs are either mosquito-borne (dengue, chikungunya, malaria, Zika) with a higher number of reported cases in the monsoon season or are tick (KFD)/ louse-borne (scrub typhus) with predominant activity in the post-monsoon season. Waterborne illnesses such as leptospirosis and enteric fever can be seen throughout the year, but a spike is noticed in their reports in the monsoon season. Mosquito-borne AFIs like dengue, malaria, chikungunya, and Zika have wide geographic distribution spanning the continents of Asia, Africa, and South Americas. In a recent review of literature, 262 dengue outbreaks were identified throughout the world from 1990-2015, with the highest number of them reported from India (58/262) (*4*). Malaria affects more than 90 countries and territories in the tropical and subtropical regions with Africa. According to the World Malaria Report 2017, in the year 2016, more than half of the population (698 million) was at risk of malaria (*5*). India accounted for 6% of all malaria cases in the world, 6% of the deaths, and 51% of the global *Plasmodium vivax* cases. The report estimates the total cases in India at 1.31 million (0.94-1.83 million) and deaths at 23,990 (1,600-46,500) (*6*). Following the initial outbreak at Tanganyika in the year 1952, Chikungunya epidemics have been reported from several parts of the world including Africa, Asia, and elsewhere. As of September 2015, 1.7 million cases and 240 deaths were reported from 45 of the 53 countries or territories reporting to the Pan American Health Organization (*7*). The three major outbreaks of Zika virus disease occurred in the Yap Islands (2007), French Polynesia (2013-14), and South

Americas (2015-16) after years of sporadic reports from Africa. The first proven cases of ZIKV from India were reported in the year 2017. This was followed by major outbreaks in the states of Rajasthan and Madhya Pradesh in 2018 (*8,9*).

Tick/louse-borne AFIs like scrub typhus and KFD have a more defined geographical distribution. Scrub typhus, a rickettsial infection caused by *Orientia tsutsugamushi*, is supposed to be endemic in major parts of Asia and Australia. It accounts for up to 23% of all febrile episodes, with an estimated 1 million cases occurring annually in endemic areas (*9*). The KFD virus is transmitted by the bites of infected *Haemaphysalis spinigera* ticks. This is predominantly reported from five states in Southern India (Karnataka, Kerala, Goa, Maharashtra, and Tamil Nadu) (*10*).

Water-related diseases like leptospirosis and enteric fever have a world-wide distribution. Leptospirosis infection occurs from exposure to water contaminated with animal urine, while enteric fever is associated with the intake of contaminated food or water. As a part of a multi-centric study from India, of 3,682 patients with acute febrile illness, 469 (12.7%) were found to have a leptospiral infection (*11*). The global annual burden of typhoid was estimated at approximately 12 million cases for 2010, with a case fatality rate of 1% (*12*).

3. Clinical manifestations

The most common clinical manifestations of patients with mild COVID 19 are fever and upper respiratory tract symptoms. There are a significant fraction of patients with COVID-19 who present with fever but without upper respiratory tract symptoms. In patients with moderate/severe disease, there is concomitant respiratory distress and hypoxemia (*13*). Similar to the manifestations of COVID-19, patients with acute febrile illness present with fever with accompanying symptoms (Table 1) (*14*). Respiratory involvement as a consequence of increased vascular permeability or direct involvement as a part of multi-organ dysfunction is seen in many of the febrile illnesses (*15*). Consequently, the distinction between COVID-19 and AFI on clinical grounds alone is difficult. Some of the AFIs like dengue fever present commonly with a rash, but these rashes are often difficult to appreciate in dark-skinned individuals residing in the tropics. Besides, a similar rash has been described in a small percentage of patients with COVID-19. Characteristic eschar in scrub typhus help in differentiating from COVID in some cases, but its frequency is variable and may go unnoticed in many cases unless looked for carefully (*16*). Conjunctival suffusion and jaundice are characteristic of leptospirosis and are not commonly reported with COVID-19. However, a larger proportion of patients with leptospirosis do not have either of these signs (*17*). The presence of arthralgia is common to both AFIs (Chikungunya, Zika virus disease) and COVID-19. However, the presence of small joint arthritis is not commonly reported in COVID-19, which may help in diagnosing chikungunya.

4. Laboratory manifestations

The laboratory manifestations of COVID-19 and AFIs have been summarized in Table 2. Similar to patients with COVID-19, AFIs such as dengue, chikungunya, and KFD also present with leucopenia. Leucocytosis seen in some cases of scrub typhus or leptospirosis is rare in COVID-19. Thrombocytopenia (dengue, chikungunya, scrub typhus, leptospirosis, enteric fever, KFD) is, however, more common in most acute febrile illnesses when compared to COVID-19. Elevated transaminases (scrub typhus, enteric fever, dengue) are common to several AFI and COVID-19, but hyperbilirubinemia seen in leptospirosis is uncommon in COVID-19. Acute kidney injury in leptospirosis or scrub typhus can also be seen with severe COVID-19. Raised inflammatory markers such as C-reactive protein (scrub typhus, leptospirosis) is common to both AFI and moderate/severe COVID-19.

5. Diagnosis

Healthcare workers in resource-limited settings often diagnose patients presumptively on the basis of clinical features and region-specific prevalence of the pathogens.

Table 1. Clinical manifestations of COVID-19 and acute febrile illnesses

Disease	Fever	Cough	Rash	GI Symptoms	Jaundice	Conjunctival suffusion	Lymph adenopathy	Hepato splenomegaly
COVID-19 (*23*)	Y	Y	N	N	N	N	N	N
Dengue (*24*)	Y	?Y	Y	Y	-	Y	?Y	
Malaria (*15*)	Y		N	?Y	Y	-	-	?Y
Chikungunya (*25*)	Y		Y	N	-	-	?Y	-
Scrub typhus (*26*)	Y	?Y	?Y	N	?Y	?Y	?Y	Y
Leptospirosis (*27*)	Y	?Y		?Y	Y	Y	-	-
Enteric fever (*28*)	Y	Y		Y		-	-	Y
KFD (*29-31*)	Y	Y		?Y	N	Y	-	-
Zika (32-33)	Y		Y	?Y	N	Y	-	-

Abbreviations- Y, feature commonly present; ?Y, present but not very common; N, not commonly present.

Table 2. Laboratory manifestations of COVID-19 and acute febrile illnesses

Disease	Anemia	Leukopenia	Leukocytosis	Thrombocytopenia	Deranged LFT	Raised Creatinine	Raised CRP	Coagulopathy
COVID-19 (*23,34*)	N	?Y	N	N	N	N	?Y	Y
Dengue (*24,35*)	N	Y	N	Y	Y	N	-	Y
Malaria (*15,36*)	Y	N	N	Y	Y	Y	-	Y
Chikungunya (*25*)	N	Y	N	Y	-	N	-	-
Scrub typhus (*25,34-36,40*)	?Y	N	Y	Y	Y	?Y	Y	?Y
Leptospirosis (*27,41*)	?Y	N	Y	Y	Y	Y	Y	-
Enteric fever (*42*)	?Y	?Y	Y	Y	?Y		-	-
KFD (*29-31*)	N	Y	-	Y	Y	-	-	-
Zika (*33*)	-	Y	-	?Y	-	-	-	-

Abbreviations- Y, feature commonly present; ?Y, present but not very common; N, not commonly present.

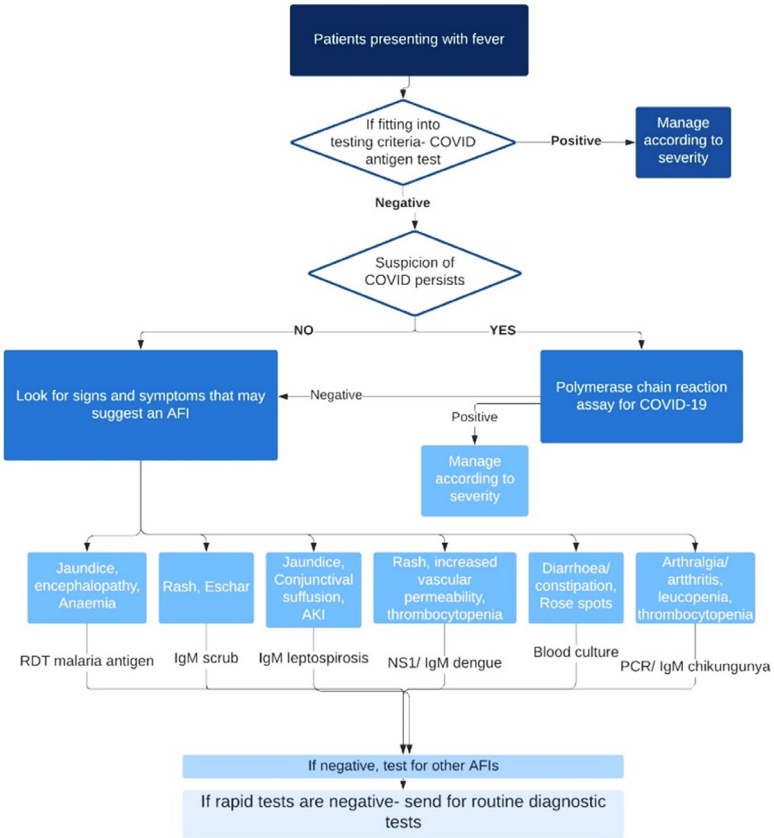

Figure 1. Proposed algorithm for the approach to Acute febrile illness during COVID time. Abbreviations: AFI- Acute febrile illness, AKI- Acute kidney injury, RDT- Rapid diagnostic test, PCR- Polymerase chain reaction assay.

However, the accurate determination of the aetiology of AFI requires laboratory tests, as many of the AFIs have similar clinical presentations. The overlap of the clinical spectrum of acute febrile illnesses with COVID 19 has further added fuel to the fire by presenting as a diagnostic and management conundrum for the health care system in resource-limited settings. Besides, due to the infection control precautions that are mandated in most hospitals, tests for acute febrile illnesses are often not sent until the COVID tests return negative. Depending on the turn-around time of COVID-19 tests, the diagnosis of AFI is often delayed. Also, due to unreal concerns of infection from the blood of suspected patients, peripheral smear and quantitative buffy coat are discontinued in many hospitals resulting in significant difficulty in diagnosing malaria. It has to be also kept in mind that some of the serological tests for AFI are not perfect and may yield false-positive results. As a result, a patient with COVID-19 may be falsely diagnosed with AFI, and infection control precautions may be discontinued. This can lead to unnecessary exposure to healthcare professionals. A report from Singapore highlighted patients with false-positive rapid serological testing for dengue, who later confirmed to

have severe acute respiratory syndrome coronavirus 2 (SARS-CoV-2) infection- the causative virus of COVID-19 (*18,19*). A similar report published by Ullah *et al.* described a patient with COVID 19 presenting with arthralgia and a false positive chikungunya test (*20*). Also, considering the current endemicity of both groups of illnesses, coinfections cannot be ruled out. During the pandemic, the routine non-COVID diagnostics have been severely compromised due to the shunting of resources (manpower and materials) in the COVID area. In such a scenario, the use of rapid diagnostic testing for the diagnosis of COVID-19 and AFIs will be beneficial in early diagnosis and prompt initiation of treatment (*21*). However, it must be kept in mind that rapid diagnostic tests suffer from poor sensitivity. In the presence of high clinical suspicion, they should be confirmed by routine gold standard diagnostics. An integrated algorithm has been proposed for the management of a patient with suspected AFI. (Figure 1) (*22-42*).

6. Treatment

The rapidly evolving use of experimental COVID-19 therapies is gaining importance globally. While most of these therapies are initiated without proof of their efficacy in COVID-19, they may have potential clinical harms. Biologicals like anakinra and tocilizumab may suppress the cytokine storm, a potential defence mechanism against febrile illnesses. Pharmacokinetic and pharmacodynamic interactions involving the HIV protease inhibitor lopinavir/ritonavir may affect the absorption, distribution, and metabolism of other systemic therapy administered to the patient. The rampant off-label use of chloroquine derivatives for COVID 19 prophylaxis may increase resistance in malaria in endemic regions. The use of agents like doxycycline and azithromycin as empiric therapy can decrease the sensitivity of molecular diagnostics by many folds (*43*).

7. Conclusion

It is of prime importance that the infrastructure and manpower at the healthcare facilities should be expanded to avoid neglect of endemic acute febrile diseases. The primary care physicians should be sensitized about the importance of suspecting AFIs in COVID-19 suspects. There is a need for formulating integrated clinical algorithms for the management of AFIs, keeping into account the epidemiology and seasonal prevalence of febrile diseases.

Funding: None.

Conflict of Interest: The authors have no conflicts of interest to disclose.

References

1. Dong E, Du H, Gardner L. An interactive web-based dashboard to track COVID-19 in real time. Lancet Inf Dis. 2020; 20:533-534.
2. Mørch K, Manoharan A, Chandy S, *et al.* Acute undifferentiated fever in India: a multicentre study of aetiology and diagnostic accuracy. BMC Infect Dis. 2017; 17:665.
3. Shrestha P, Roberts T, Homsana A, Myat TO, Crump JA, Lubell Y, Newton PN. Febrile illness in Asia: gaps in epidemiology, diagnosis and management for informing health policy. Clin Microbiol Infect. 2018; 24:815-826.
4. WHO Global Strategy for dengue prevention and control, 2012-2020. Available from: *https://www.who.int/denguecontrol/9789241504034/en/* (accessed September 1, 2020).
5. Nghochuzie NN, Olwal CO, Udoakang AJ, Amenga-Etego LN, Amambua-Ngwa A. Pausing the fight against malaria to combat the COVID-19 pandemic in Africa: Is the future of malaria bleak? Front Microbiol. 2020; 11:1476.
6. Malaria in India. Malaria Site. 2015. Available from: *https://www.malariasite.com/malaria-india/* (accessed August 29, 2020).
7. Petersen LR, Powers AM. Chikungunya: epidemiology. F1000Res. 2016; 5:F1000 Faculty Rev-82.
8. Gupta N, Kodan P, Baruah K, Soneja M, Biswas A. Zika virus in India: past, present and future. QJM. 2019:hcz273.
9. Biswas A, Kodan P, Gupta N, *et al.* Zika outbreak in India in 2018. J Travel Med. 2020; 27:taaa001.
10. Mourya DT, Yadav PD, Patil DY. Expediency of dengue illness classification: the Sri Lankan perspective highly infectious tick-borne viral diseases: Kyasanur forest disease and Crimean-Congo haemorrhagic fever in India. WHO South East Asia J Public Health. 2014; 3:8-21.
11. Sehgal SC, Sugunan AP, Vijayachari P. Leptospirosis disease burden estimation and surveillance networking in India. Southeast Asian J Trop Med Public Health. 2003; 34 (Suppl 2):170-177.
12. John J, Van Aart CJ, Grassly NC. The burden of typhoid and paratyphoid in India: Systematic review and meta-analysis. PLoS Negl Trop Dis. 2016; 10:e0004616.
13. Guan WJ, Ni ZY, Hu Y, *et al.* Clinical characteristics of coronavirus disease 2019 in China. N Engl J Med. 2020; 382:1708-1720.
14. Chanda-Kapata P, Kapata N, Zumla A. COVID-19 and malaria: A symptom screening challenge for malaria endemic countries. Int J Infect Dis. 2020; 94:151-153.
15. Echeverri M, Tobón A, Alvarez G, Carmona J, Blair S. Clinical and laboratory findings of *Plasmodium vivax* malaria in Colombia, 2001. Rev Inst Med Trop Sao Paulo. 2003; 45:29-34.
16. Le Van N, Pham Van C, Nguyen Dang M, Dao Van T, Le T Do Q, Vu Hoang H, Tran Viet T, Nhu Do B. Clinical features, laboratory characteristics and prognostic factors of severity in patients with Rickettsiaceae at two military hospitals, Northern Vietnam. Infect Drug Resist. 2020; 13:2129-2138.
17. Sambasiva RR, Naveen G, PB, Agarwal SK. Leptospirosis in India and the rest of the world. Braz J Infect Dis. 2003; 7:178-193.
18. Yan G, Lee CK, Lam LTM, *et al.* Covert COVID-19 and false-positive dengue serology in Singapore. Lancet Infect Dis. 2020; 20:536.
19. Lorenz C, Azevedo TS, Chiaravalloti-Neto F. COVID-19

and dengue fever: A dangerous combination for the health system in Brazil. Travel Med Infect Dis. 2020; 35:101659.
20. Ullah W, Tran A, Roomi S, Saeed R, Sarwar U. COVID-19 masquerading as Chikungunya fever. Am J Infect Dis. 2020:73-76.
21. Gupta N, Nischal N. Management of acute febrile diseases in limited resource settings: a case-based approach. Infez Med. 2020; 28:11-16.
22. Lim JH, Baek EJ. A case of false-negative malaria rapid diagnostic test induced by treatment with doxycycline. Laboratory Medicine Online. 2019; 9:194-196.
23. Rodriguez-Morales AJ, Cardona-Ospina JA, Gutiérrez-Ocampo E, *et al.* Clinical, laboratory and imaging features of COVID-19: A systematic review and meta-analysis. Travel Med Infect Dis. 2020; 34:101623.
24. Daumas RP, Passos SR, Oliveira RV, Nogueira RM, Georg I, Marzochi KB, Brasil P. Clinical and laboratory features that discriminate dengue from other febrile illnesses: a diagnostic accuracy study in Rio de Janeiro, Brazil. BMC Infect Dis. 2013; 13:77.
25. Lakshmi V, Neeraja M, Subbalaxmi MV, Parida MM, Dash PK, Santhosh SR, Rao PV. Clinical features and molecular diagnosis of Chikungunya fever from South India. Clin Infect Dis. 2008; 46:1436-1442.
26. Kumar R, Thakur S, Bhawani R, Kanga A, Ranjan A. Clinical profile and complications of scrub typhus: hospital-based study in sub-himalayan region. J Assoc Physicians India. 2016; 64:30-34.
27. Becirovic A, Numanovic F, Dzafic F, Piljic D. Analysis of clinical and laboratory characteristics of patients with leptospirosis in five-year period. Mater Sociomed. 2020; 32:15-19.
28. Azmatullah A, Qamar FN, Thaver D, Zaidi AK, Bhutta ZA. Systematic review of the global epidemiology, clinical and laboratory profile of enteric fever. J Glob Health. 2015; 5:020407.
29. Webb HE, Rao RL. Kyasanur forest disease: a general clinical study in which some cases with neurological complications were observed. Trans R Soc Trop Med Hyg. 1961; 55:284-298.
30. Gupta N, Varma M, Saravu K. Difference in clinical presentation between the first and second phases of Kyasanur Forest disease: an experience from a teaching hospital in South India. Infez Med. 2020; 28:597-602.
31. Gupta N, Wilson W, Neumayr A, Saravu K. Kyasanur Forest disease: State-of-the-art review. QJM. 2020:hcaa310.
32. Azeredo EL, Dos Santos FB, Barbosa LS, Souza TM, Badolato-Corrêa J, Sánchez-Arcila JC, Nunes PC, de-Oliveira-Pinto LM, de Filippis AM, Dal Fabbro M, Romanholi IH. Clinical and laboratory profile of zika and dengue infected patients: lessons learned from the co-circulation of dengue, zika and chikungunya in Brazil. PLoS curr. 2018; 10.
33. Wilder-Smith A, Chang CR, Leong WY. Zika in travellers 1947-2017: a systematic review. J Travel Med. 2018; 25.
34. Wright FL, Vogler TO, Moore EE, Moore HB, Wohlauer MV, Urban S, Nydam TL, Moore PK, McIntyre RC Jr. Fibrinolysis shutdown correlation with thromboembolic events in severe COVID-19 infection. J Am Coll Surg. 2020; 231:193-203.
35. Kannan A, Narayanan KS, Sasikumar S, Philipose J, Surendran SA. Coagulopathy in dengue fever patients. Int J Res Med Sci. 2014; 2:1070-1072.
36. Conroy AL, Hawkes M, Elphinstone RE, Morgan C, Hermann L, Barker KR, Namasopo S, Opoka RO, John CC, Liles WC, Kain KC. Acute kidney injury is common in pediatric severe malaria and is associated with increased mortality. Open Forum Infect Dis. 2016; 3:ofw046.
37. Thakur CK, Chaudhry R, Gupta N, Vinayaraj EV, Singh V, Das BK, Jadon RS, Wig N, Lodha R, Kabra SK, Dey AB. Scrub typhus in patients with acute febrile illness: a 5-year study from India. QJM. 2020; 113:404-410.
38. Narayanasamy DK, Arun Babu T, Vijayadevagaran V, Kittu D, Ananthakrishnan S. Predictors of severity in pediatric scrub typhus. Indian J Pediatr. 2018; 85:613-617.
39. Premraj SS, Mayilananthi K, Krishnan D, Padmanabhan K, Rajasekaran D. Clinical profile and risk factors associated with severe scrub typhus infection among non-ICU patients in semi-urban south India. J Vector Borne Dis. 2018; 55:47-51.
40. Park SW, Lee CS, Kim JH, *et al.* Severe fever with thrombocytopenia syndrome: comparison with scrub typhus and clinical diagnostic prediction. BMC Infect Dis. 2019; 19:174.
41. Furlanello T, Reale I. Leptospirosis and immune-mediated hemolytic anemia: A lethal association. Vet Res Forum. 2019; 10:261-265.
42. Khosla SN, Lochan R. Renal dysfunction in enteric fever. J Assoc Physicians India. 1991; 39:382-384.
43. Gupta N, Chaudhry R, Kabra SK, *et al.* Comparative evaluation of serological and molecular methods for the diagnosis of scrub typhus in Indian settings. Jpn J Infect Dis. 2017; 70:221-222.

Received September 6, 2020; Revised December 21, 2020; Accepted December 24, 2020.

**Address correspondence to:*
Nitin Gupta, Department of Infectious diseases, Kasturba Medical College, Manipal Academy of Higher Education, Manipal, Karnataka-576104, India.
E-mail: nityanitingupta@gmail.com

Released online in J-STAGE as advance publication December 30, 2020.

Original Article

DOI: 10.5582/ddt.2020.03099

Development of an *in vivo*-mimic silkworm infection model with *Mycobacterium avium* complex

Akiho Yagi[1], Hiroyuki Yamazaki[1], Takeshi Terahara[2], Taehui Yang[2], Hiroshi Hamamoto[3], Chiaki Imada[2], Hiroshi Tomoda[4], Ryuji Uchida[1,*]

[1] Department of Natural Product Chemistry, Faculty of Pharmaceutical Sciences, Tohoku Medical and Pharmaceutical University, Sendai, Miyagi, Japan;
[2] Graduate School of Marine Science and Technology, Tokyo University of Marine Science and Technology, Tokyo, Japan;
[3] Institute of Medical Mycology, Teikyo University, Tokyo, Japan;
[4] Microbial Chemistry and Medical Research Laboratories, Graduate School of Pharmaceutical Sciences, Kitasato University, Tokyo, Japan.

SUMMARY *In vivo*-mimic silkworm infection models with *Mycobacterium avium* and *Mycobacterium intracellulare* were newly established to evaluate the therapeutic effects of anti-*M. avium* complex (MAC) antibiotics. Silkworms raised at 37°C died within 72 hours of an injection of *M. avium* or *M. intracellulare* (2.5×10^7 colony-forming unit (CFU)/larva·g) into the hemolymph. Clinical anti-mycobacterial (tuberculosis) antibiotics were evaluated under these conditions. Clarithromycin, kanamycin, streptomycin, amikacin, and ciprofloxacin exerted therapeutic effects in a dose-dependent manner, which was consistent with those in the mouse model. Furthermore, three effective actinomycete culture broths were selected in the screening program of our microbial broth library using the silkworm model, and four active metabolites, ohmyungsamycins A and B (**1** and **2**), chartreusin (**3**), and griseoviridin (**4**), were identified. Among these compounds, **1** showed the lowest 50% effective dose (ED_{50}) value (8.5 μg/larva·g), while **3** had the best ED_{50}/minimum inhibitory concentration (MIC) ratio (7.4). These results indicate that silkworm models are a useful tool for identifying anti-MAC antibiotics candidates with veritable therapeutic effects.

Keywords silkworm infection model, antibiotics, *Mycobacterium avium* complex (MAC), nontuberculosis mycobacteria (NTM), natural product, microbial origin

1. Introduction

Mycobacterium avium complex (MAC) infection is mainly caused by *M. avium* and *M. intracellulare*, which are nontuberculosis mycobacteria (NTM), and is a nontuberculous mycobacterial pulmonary and intractable disorder, the incidence of which has been increasing more than that of tuberculosis in developed countries (*1,2*). Although the majority of individuals infected with MAC bacteria are asymptomatic, patients with compromised immune functions due to cancer or HIV/AIDS or those with lung disease, such as chronic obstructive pulmonary disease or cystic fibrosis, are at the highest risk of developing MAC infection. Pulmonary MAC infection progresses slowly, worsens over time, and may persist for weeks or months, and its symptoms are similar to those of tuberculosis, such as weight loss, fever, fatigue, and night sweats (*1*). Limited drugs are currently available for use in clinical practice, and the treatment approach employs the combination of first-line clarithromycin with rifampicin and ethambutol. However, this treatment is not sufficiently effective, and the emergence of bacterial resistance is a major issue because it necessitates treatment for more than one year (*3*). Although amikacin liposome inhalation suspension (ALIS) was newly approved for the treatment of MAC infection in 2018 (*4*), the development of new candidates for MAC infection with novel skeletal structures and different mechanisms of action to existing drugs is urgently needed.

In the screening of potential antibiotics against various pathogenic microorganisms from natural resources, we have conducted *in vivo*-mimic infection assays using silkworms at the early stage of drug development (*5-10*). This assay system concept is straightforward: candidate compounds or test samples are injected into pathogenic microorganism-infected silkworm larvae, and the survival rate over a few days is then monitored to assess the therapeutic effects of the sample. Furthermore, the silkworm model may be

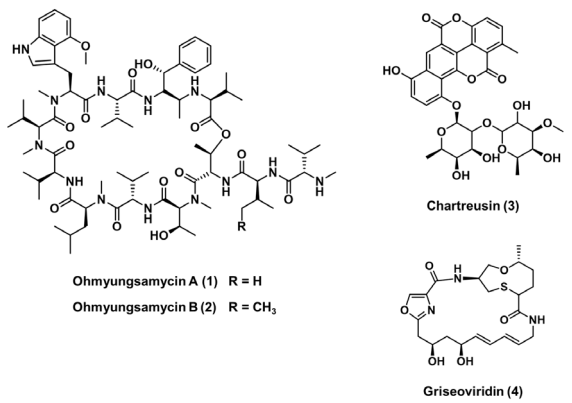

Figure 1. Structures of compounds 1-4.

evaluated more rapidly and efficiently than a mouse model. We previously established a silkworm model with *M. smegmatis* and *Mycobacteroides* (*My.*) *abscessus* for the screening anti-tuberculosis and anti-NTM agents, respectively (*11,12*), and found that lariatins (*13*), calpinactam (*14*), lysocin E (*5*), propeptin (*15*), and nosiheptide (*16*) exerted therapeutic effects in the silkworm model.

We herein successfully established a silkworm model with *M. avium* and *M. intracellulare*, which had not been achieved in previous studies, and clinical anti-tuberculosis and anti-MAC drugs were evaluated using this model. The screening study from our microbial broth library resulted in the identification of four microbial metabolites, ohmyungsamycins A (**1**) and B (**2**) (*17,18*), chartreusin (**3**) (*19*), and griseoviridin (**4**) (*20*), from the culture broths of actinomycete strains (Figure 1). We described the establishment of the silkworm model with *M. avium* and *M. intracellulare* and the *in vivo* therapeutic effects of anti-mycobacterial agents and **1**-**4**.

2. Materials and Methods

2.1. Materials

Kanamycin, streptomycin, amikacin, ciprofloxacin, and rifampicin were purchased from FUJIFILM Wako Pure Chemical Industries (Osaka, Japan). Clarithromycin, ethambutol, isoniazid, and pyrazinamide were purchased from Tokyo Chemical Industries (Tokyo, Japan). Unless otherwise stated, all other reagents were reagent-grade commercial products. Middlebrook 7H9 broth (Becton, Dickinson and Company, NJ, USA) was blended with 0.05% Tween 80 (Tokyo Chemical Industries) and 10% ADC enrichment [5% bovine serum albumin (FUJIFILM Wako Pure Chemical Industries), 2% glucose (FUJIFILM Wako Pure Chemical Industries), and 0.85% NaCl (FUJIFILM Wako Pure Chemical Industries)] to cultivate mycobacterium strains. Seed and production media consisted of 1.0% malt extract (Becton, Dickinson and Company), 0.4% yeast extract (Becton, Dickinson and Company), and 0.4% glucose (FUJIFILM Wako Pure Chemical Industries) to cultivate all actinomycetal strains.

2.2. Silkworms

Fertilized silkworm eggs of *Bombyx mori* (Hu·Yo × Tukuba·Ne) were purchased from Ehime Sansyu (Ehime, Japan) and fed an artificial diet (Silk Mate 2S; Nihon Nosan Kogyo, Kanagawa, Japan, and Silkmate; Katakura Industries, Tokyo, Japan) until the fourth-instar larval stage.

2.3. Preparation of the mycobacterial suspension

M. avium JCM15430 and *M. intracellulare* JCM6384 were obtained from the Riken BioResource Research Center (Ibaraki, Japan). Both strains were stored in 20% glycerol at -80°C. Frozen stock culture (500 μL, approximately 5.0×10^8 colony-forming unit (CFU)/mL) was inoculated into Middlebrook 7H9 broth (10 mL) in a T-25 flask (TPP Techno Plastic Products AG, Trasadingen, Switzerland) and cultured under static conditions at 37°C for 14 days (up to approximately 1.0×10^9 CFU/mL).

2.4. Assessment of minimum inhibitory concentration (MIC) values using the liquid microdilution method

The MIC values of anti-tuberculosis antibiotics (isoniazid, rifampicin, pyrazinamide, ethambutol, streptomycin, kanamycin, and clarithromycin) and four microbial metabolites (**1**-**4**) against *M. avium* and *M. intracellulare* were evaluated using the liquid microdilution method according to a previously established method (*11,21*). Each test strain was adjusted to 1.0×10^6 CFU/mL in Middlebrook 7H9 broth. The suspension (95 μL) was added to each well of a 96-well microplate (AS ONE, Osaka, Japan) with or without test samples (5 μL in methanol or saline) and incubated at 37°C for 5 days. Absorbance was measured at 550 nm using an absorption spectrometer (MTP-500, Corona Electric Co., Ltd., Ibaraki, Japan). The MIC value was defined as the lowest sample concentration that inhibited the growth of *M. avium* or *M. intracellulare* by 90%.

2.5. Silkworm infection model with *M. avium* and *M. intracellulare*

Hatched silkworm larvae were raised by feeding an artificial diet containing antibiotics (Silk Mate 2S) in an incubator at 27°C until the fourth molting stage. On the first day of the fifth-instar larval stage, silkworms were fed an antibiotic-free artificial diet (Silk Mate) for 24 hours. On the second day, a three-fold serially diluted *M. avium* JCM15340 or *M. intracellulare* JCM6384

suspension (0.83×10^7 to 7.5×10^7 CFU/larva·g in 50 µL saline) was injected into the hemolymph of silkworms through the dorsal surface (2.0 g, $n = 5$) using a disposable 1-mL syringe with a 27-G needle (TERUMO, Tokyo, Japan). Infected silkworms were raised without feed at 37°C unless stated otherwise, and their survival rate was measured every 3 hours after the sample injection.

2.6. Assessment of 50% effective dose (ED_{50}) values in the silkworm infection model with *M. avium* and *M. intracellulare*

The *M. avium* or *M. intracellulare* suspension (2.5×10^7 CFU/larva·g in 50 µL saline) was injected into the hemolymph of silkworm larvae (2.0 g, $n = 5$), followed by an injection of anti-tuberculosis antibiotics and microbial compounds (50 µL in saline or 10% dimethyl sulfoxide) within 30 minutes. Silkworms were then raised at 37ºC. The survival rate at the indicated drug dose was assessed 72 hours after its injection. ED_{50} values were defined as the amount of a drug required for a 50% survival rate, normalized per 1 g of silkworm.

2.7. Isolation of **1**-**4**

Ohmyungsamycins A (**1**) and B (**2**): Actinomycete strain TMPU-A0334 was isolated from marine sediment collected from Tokyo Bay, Japan at a depth of 6.4 m. This strain was fermented with seed medium containing 3.64% Marine art Hi (Osaka Yakken Co., Ltd., Osaka, Japan) on a rotary shaker (180 rpm, 27°C) for 3 days, followed by a production culture on a rotary shaker (180 rpm, 27°C) for 21 days. The culture broth obtained (5.0 L) was centrifuged to separate mycelia and supernatant. After mycelia had been treated with acetone (1.0 L), the mixture was filtered and concentrated *in vacuo* to remove acetone. Aqueous solution (300 mL) was adjusted to pH 9 and extracted with an equal volume of ethyl acetate (EtOAc). The EtOAc layer was then evaporated *in vacuo* to yield a solid black material (206 mg). This material was dissolved in a small amount of methanol, applied to a Sep-Pak C18 column cartridge (5 g, Waters, MA, USA), and eluted stepwise with 0, 20, 40, 60, 80, and 100% acetonitrile in water (20 mL each). The 80% acetonitrile eluate (12.5 mg) containing **1** and **2** were purified by preparative high-performance liquid chromatography (HPLC) [Column, PEGASIL ODS SP100 (Senshu Scientific Co., Tokyo, Japan, i.d. 10 mm × 250 mm); mobile phase, 55% acetonitrile in 50 mM sodium phosphate buffer (pH 7); flow rate, 3.0 mL/min; detection, UV at 210 nm]. Under these conditions, **1** (3.1 mg, retention time (t_R) = 26 min) and **2** (3.5 mg, t_R = 34 min) were isolated as white powders.

Chartreusin (**3**): Actinomycete strain TMPU-A0405 was isolated from soil collected in Tottori prefecture, Japan. 14-day-old culture broth (1.0 L) fermented under static conditions at 27°C was extracted with acetone (600 mL) and concentrated *in vacuo* to remove acetone. The remaining aqueous solution was extracted with EtOAc (pH 3, 500 mL), and the organic layer was concentrated *in vacuo* to give a yellow solid material (259 mg). This material dissolved in a small volume of methanol was applied to a Sep-Pak C18 column cartridge (5 g) and eluted stepwise with 0, 20, 40, 60, 80, and 100% acetonitrile in H_2O (20 mL each). The 60% acetonitrile eluate (12.3 mg) containing **3** was evaporated, and the residue was treated with methanol (1 mL) to obtain a methanol-insoluble substance as a yellow powder of **3** (3.5 mg).

Griseoviridin (**4**): Actinomycete strain KTM7-6 was isolated from deep sea water collected from Kumejima island, Japan. 14-day-old whole culture broth fermented by the rotary shaker (180 rpm, 27°C) was extracted with acetone (600 mL), concentrated *in vacuo* to remove acetone, and extracted with EtOAc (200 mL) to obtain the EtOAc extract (86.6 mg). The extract dissolved in methanol was subjected to a Sep-Pak C18 column cartridge (5 g) and eluted stepwise with 0, 20, 40, 60, 80, and 100% acetonitrile in water (20 mL each). The 60% acetonitrile eluate was evaporated *in vacuo*, and **4** was isolated as a white powder (3.5 mg).

The structures of **1**-**4** were identified by comparing their various spectroscopic data, including nuclear magnetic resonance (NMR) and mass spectrometry (MS) experiments, with those described in the literature (*17-20*) as ohmyungsamycin A (**1**), ohmyungsamycin B (**2**), chartreusin (**3**), and griseoviridin (**4**), respectively (Figure 1).

3. Results

3.1. Establishment of the silkworm infection model with *M. avium* and *M. intracellulare*

To establish the silkworm model with *M. avium* and *M. intracellulare*, the cell concentrations of the mycobacterium injected into silkworms were examined. Silkworms were infected with three different concentrations (0.83×10^7, 2.5×10^7, and 7.5×10^7 CFU/larva·g) and observed for 96 hours under the incubation at 37ºC. Silkworms infected with *M. avium* and *M. intracellulare* died in a cell concentration-dependent manner. All silkworms infected with *M. avium* at 0.83×10^7, 2.5×10^7, and 7.5×10^7 CFU/larva·g died within 81, 72, and 64 hours, respectively (Figure 2A). The infection with *M. intracellulare* at 0.83×10^7, 2.5×10^7, and 7.5×10^7 CFU/larva·g caused death within 81, 68, and 60 hours, respectively (Figure 2B). Therefore, the cell concentrations of *M. avium* and *M. intracellulare* were fixed at 2.5×10^7 CFU/larva·g. The supernatant or autoclaved suspensions of *M. avium* and *M. intracellulare* had no pathogenicity against silkworms (data not shown). Based on these results, the

silkworm model with *M. avium* and *M. intracellulare* was established; these mycobacteria were injected into the silkworm hemolymph at 2.5×10^7 CFU/larva·g, and infected silkworms were then raised at 37°C. Under these conditions, all silkworms died within 72 hours.

3.2. *In vitro* anti-*M. avium* and *M. intracellulare* activities of anti-tuberculosis antibiotics

The *in vitro* anti-*M. avium* and *M. intracellulare* activities of clinically used anti-tuberculosis drugs (clarithromycin, kanamycin, streptomycin, amikacin, ciprofloxacin, rifampicin, ethambutol, isoniazid, and pyrazinamide) were compared using the liquid microdilution method. MIC values are summarized in Table 1. Clarithromycin, kanamycin, streptomycin, amikacin, ciprofloxacin, rifampicin, ethambutol, and isoniazid inhibited the growth of *M. avium* with MIC values of 0.098, 3.1, 1.6, 1.6, 0.20, 0.20, 13, and 1.6 µg/mL, respectively. The anti-*M. intracellulare* activities of clarithromycin, kanamycin, streptomycin, amikacin, ciprofloxacin, rifampicin, ethambutol, and isoniazid showed MIC values of 0.012, 1.6, 0.78, 1.6, 0.39, 0.049, 1.6, and 3.1 µg/mL, respectively. However, pyrazinamide did not exhibit anti-*M. avium* or *M. intracellulare* activity, even at 50 µg/mL.

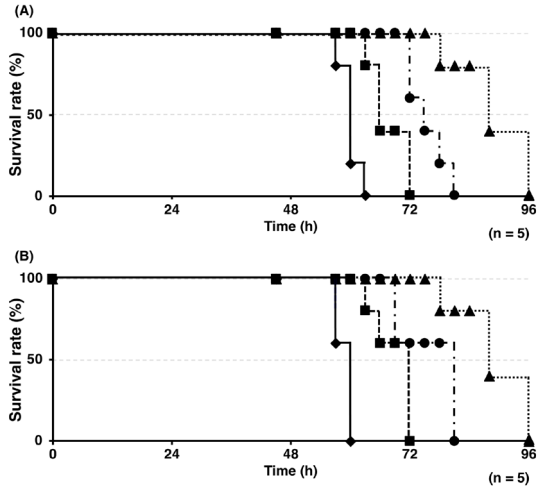

Figure 2. Silkworm-killing abilities of (A) *M. avium* and (B) *M. intracellulare*. Suspensions of the *M. avium* JCM15340 and *M. intracellulare* JCM6384 strains were diluted to the indicated cell number and injected into the silkworm hemolymph. Infected silkworms were incubated at 37°C. The number of surviving silkworms was counted 96 h after the injection. ♦: 7.5×10^7, ■: 2.5×10^7, ●: 0.83×10^7, ▲: 0 CFU/larva·g, Experiments were performed three times and reproducible data were observed.

3.3. Therapeutic effects of anti-tuberculosis antibiotics in the silkworm infection model with *M. avium* and *M. intracellulare*

Anti-tuberculosis antibiotics were then assessed in the established silkworm model with *M. avium* and *M. intracellulare* ($n = 5$), and their ED_{50} values are listed in Table 1. Treatments with clarithromycin, kanamycin, streptomycin, amikacin, and ciprofloxacin exerted therapeutic effects in the silkworm model with *M. avium* in a dose-dependent manner with ED_{50} values of 23, 23, 20, 140, and 140 µg/larva·g, respectively (Table 1, Figure 3). Similarly, clarithromycin, kanamycin, streptomycin, and amikacin exerted therapeutic effects in the silkworm model with *M. intracellulare* with ED_{50} values of 42, 27, 84, and 160 µg/larva·g (Table 1, Figure 4). However, rifampicin, ethambutol, isoniazid, and pyrazinamide did not exert therapeutic effects, even at 200 µg/larva·g (Table 1, Figures 3 and 4). Moreover, none of the anti-tuberculosis antibiotics (200 µg/larva·g)

Table 1. Anti-microbial properties of anti-mycobacterium agents and compounds 1-4 against *M. avium* and *M. intracellulare*

	Mycobacterium avium			*Mycobacterium intracellulare*		
	MIC (µg/mL)	ED_{50} (µg/larva·g)	ED_{50}/MIC	MIC (µg/mL)	ED_{50} (µg/larva·g)	ED_{50}/MIC
Clarithromycin	0.098	23	230	0.012	42	3500
Kanamycin	3.1	23	7.4	1.6	27	17
Streptomycin	1.6	20	13	0.78	84	110
Amikacin	1.6	140	88	1.6	160	100
Ciprofloxacin	0.20	140	700	0.39	> 200	−
Rifampicin	0.20	> 200	−	0.049	> 200	−
Ethambutol	13	> 200	−	1.6	> 200	−
Isoniazid	1.6	> 200	−	3.1	> 200	−
pyrazinamide	> 50	> 200	−	> 50	> 200	−
Ohmyungsamycin A (**1**)	0.39	8.5	22	0.20	40	200
Ohmyungsamycin B (**2**)	1.6	42	26	1.6	> 50	−
Chartreusin (**3**)	3.1	23	7.4	3.1	> 50	−
Griseoviridin (**4**)	1.6	35	22	0.78	> 50	−

The MIC value was defined as the lowest compound concentration that inhibited the growth of *M. avium* and *M. intracellulare* by 90%. The ED_{50} value was defined as the amount of the compound required for 50% survival, normalized per 1 g of silkworm. Experiments were performed three times and reproducible data were observed.

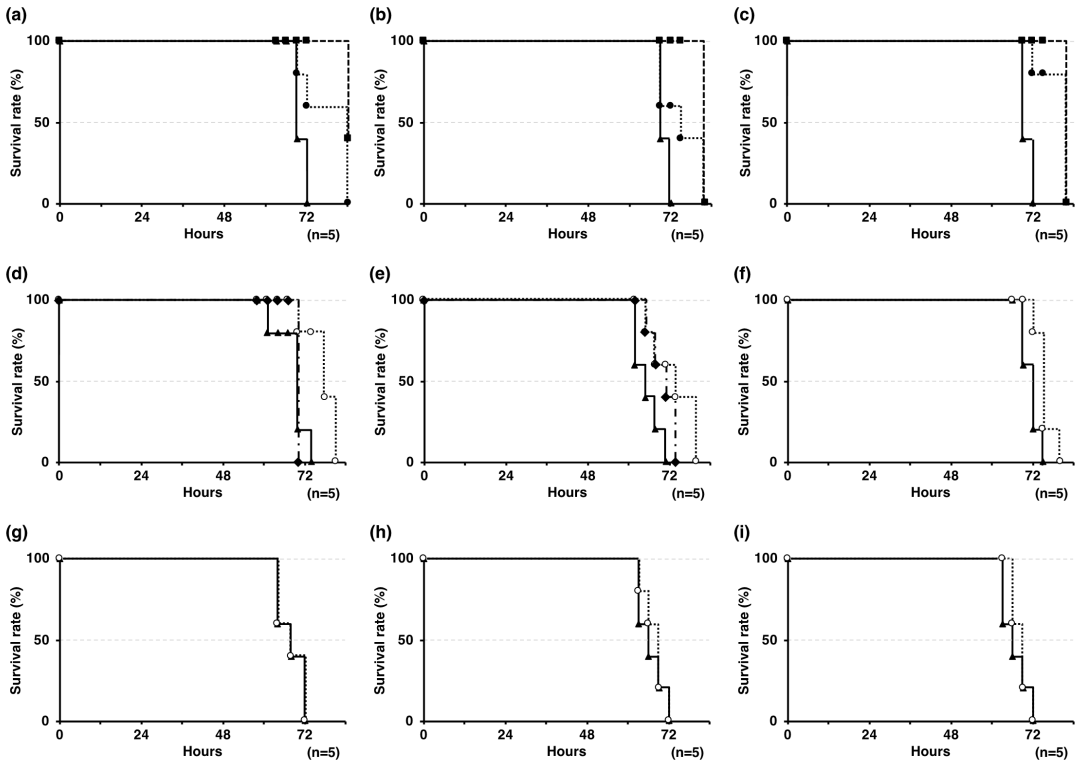

Figure 3. Therapeutic effects of anti-mycobacterium drugs in the silkworm infection assay with *M. avium*. (a) Clarithromycin (CAM), **(b)** kanamycin (KM), **(c)** streptomycin (SM), **(d)** amikacin (AMK), **(e)** ciprofloxacin (CPFX), **(f)** rifampicin (RFP), **(g)** ethambutol (EB), **(h)** isoniazid (INH), and **(i)** pyrazinamide (PZA). ○: 200, ♦: 100, ■: 50, ●: 25, ▲: 0 μg/larva·g. Experiments were performed three times and reproducible data were observed.

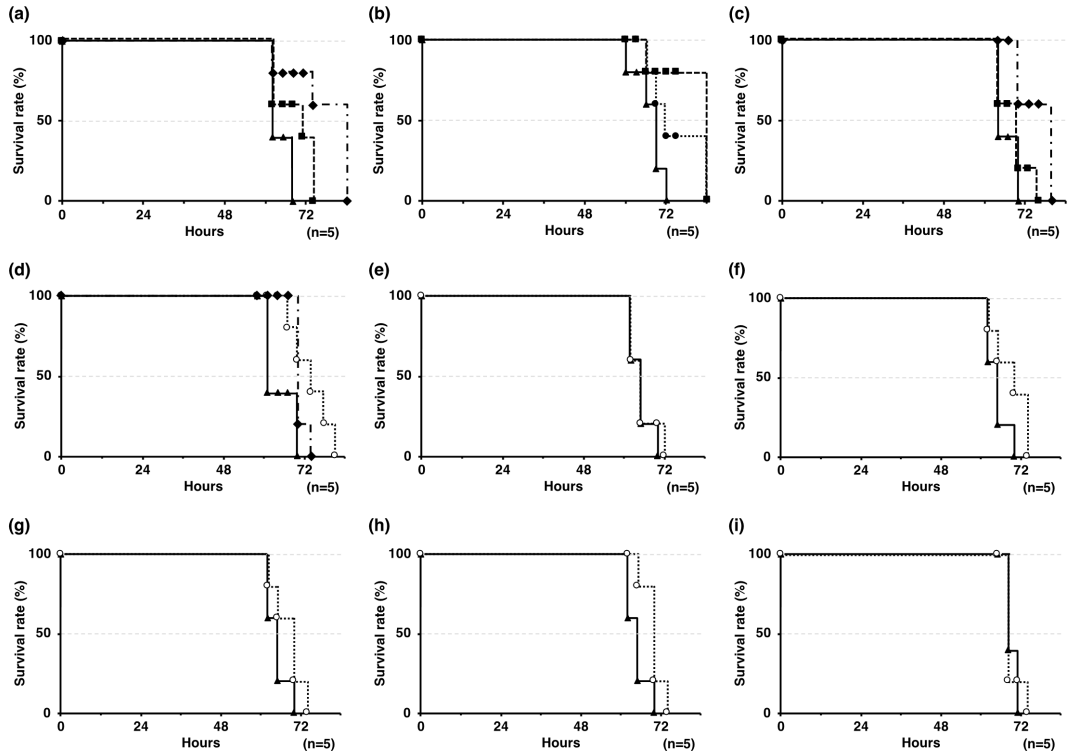

Figure 4. Therapeutic effects of anti-mycobacterium drugs in the silkworm infection assay with *M. intracellulare*. (a) Clarithromycin (CAM), **(b)** kanamycin (KM), **(c)** streptomycin (SM), **(d)** amikacin (AMK), **(e)** ciprofloxacin (CPFX), **(f)** rifampicin (RFP), **(g)** ethambutol (EB), **(h)** isoniazid (INH), and **(i)** pyrazinamide (PZA). ○: 200, ♦: 100, ■: 50, ●: 25, ▲: 0 μg/larva·g. Experiments were performed three times and reproducible data were observed.

exhibited toxicity against silkworms, at least for 72 hours (data not shown).

3.4. Screening of anti-*M. avium* and *M. intracellulare* compounds in the silkworm infection model

We started screening for new types of anti-*M. avium* and *M. intracellulare* compounds using the established silkworm model; approximately 1,500 microbial broths of terrestrial and marine fungi and actinomycetes were evaluated. Consequently, three culture broths of actinomycete strains TMPU-A0334, TMPU-A0405, and KTM7-6 exerted therapeutic effects in the silkworm model. The bioactivity-guided separation of the broths led to the isolation of four microbial metabolites, ohmyungsamycins A (**1**) and B (**2**) from strain TMPU-A0334, chartreusin (**3**) from strain TMPU-A0405, and griseoviridin (**4**) from strain KTM7-6. Compounds **1** and **2** were initially reported as cyclic peptides produced by the marine-derived *Streptomyces* sp. in 2013 (*17*), and the structure of **2** was revised by a total synthesis study in 2018 (*18*). Compound **3** was discovered in various actinomycetal culture broths following its first isolation from *Streptomyces* sp. in 1955 (*19*). Furthermore, **4** was initially isolated from *Streptomyces* sp. in 1956 (*20*), and we recently rediscovered its *in vitro* growth inhibitory activity against *M. avium* and *M. intracellulare* (*21*).

3.5. *In vitro* anti-*M. avium* and *M. intracellulare* activities of **1-4**

The *in vitro* anti-*M. avium* and *M. intracellulare* activities of **1-4** were measured using the liquid microdilution method. Compound **1** showed the most potent *in vitro* anti-*M. avium* activity with a MIC value of 0.39 g/mL, while **2-4** had MIC values of 1.6, 3.1, and 1.6 g/mL, respectively (Table 1). The MIC values of **1-4** against *M. intracellulare* were equivalent to those against *M. avium*.

3.6. Therapeutic effects of **1-4** in the silkworm infection model with *M. avium* and *M. intracellulare*

Compounds **1-4** were evaluated in the silkworm model with *M. avium* and *M. intracellulare* (n = 5), and their ED_{50} values are summarized in Table 1. As shown in Figure 5, when **1-4** were administered to silkworms infected with *M. avium*, moderate therapeutic effects were confirmed in a dose-dependent manner with ED_{50} values of 8.5, 42, 23, and 35 g/larva·g, respectively. However, in the silkworm model with *M. intracellulare*, only silkworms treated with **1** survived (ED_{50}; 40 g/larva·g), and **2-4** showed no effects in the *M. intracellulare* infection model, even at 50 g/larva·g (Figure 6). Compounds **1-4** did not exhibit any toxicity toward silkworms at least for 72 hours (data not shown).

The *in vitro* and *in vivo* experimental values of **1-4** were used to calculate ED_{50}/MIC ratios, an index of the drug potential of antibiotics (*22*), which were listed in Table 1. Among them, **3** showed the best ED_{50}/MIC rate (7.4) in the silkworm model with *M. avium*, while **1**, **2**, and **4** showed similar rates (22 to 26). In contrast, only **1** exhibited a high ED_{50}/MIC rate (200) in the silkworm model with *M. intracellulare*.

4. Discussion

We herein successfully established an *in vivo*-mimic silkworm infection model with *M. avium* and *M. intracellulare*, which are slowly growing mycobacteria. We previously reported that silkworms infected with *M. smegmatis* (1.3×10^7 CFU/larva·g) and *My. abscessus* (3.8×10^7 CFU/larva·g), which are rapidly growing mycobacteria, died within 48 hours of infection (*11,12*). Based on these findings, further investigations showed that silkworms needed a longer time (for 72 hours) and a higher cell concentration (2.5×10^7 CFU/larva·g) for death due to infection with *M. avium* and *M. intracellulare*.

Clarithromycin is currently the standard therapy for MAC disease as the first-line drug in clinical practice. Combination therapy with rifampicin and ethambutol is simultaneously used to prevent the emergence of *M. avium* and *M. intracellulare* resistant to clarithromycin. The intravenous administration of aminoglycosides (streptomycin, kanamycin, or amikacin) twice or thrice weekly for at least two months is recommended in severe cases. The *in vitro* and *in vivo* anti-mycobacterial activities of various anti-tuberculosis drugs against MAC bacteria have been reported, as described below. The majority of these drugs were found to be active *in vitro*, except for pyrazinoic acid (*23*), the active metabolite converted from pyrazinamide. Among them, only clarithromycin (50-200 mg/kg) and aminoglycosides (kanamycin; 20 mg/kg, streptomycin; 150 mg/kg, and amikacin; 100-220 mg/kg) exerted therapeutic effects as a single agent in *in vivo* mouse infection models with MAC bacteria. On the other hand, rifampicin (10 mg/kg), isoniazid (40 mg/kg), ethambutol (20-100 mg/kg), and ciprofloxacin (40 mg/kg) had marginal effects (*24-28*). However, high doses of fluoroquinolones (moxifloxacin; 100 mg/kg and levofloxacin; 200 mg/kg) exerted therapeutic effects in MAC-infected mice, suggesting that ciprofloxacin also needs to be administered at higher doses to achieve greater therapeutic effects (*29*). These findings are consistent with the present results obtained using the silkworm model with *M. avium*. In comparisons, the therapeutic effects of these drugs were weaker in the silkworm model with *M. intracellulare* than in the model with *M. avium*. *M. intracellulare* has been reported to be more pathogenic and refractory than *M. avium* in clinical practice (*30,31*), which is consistent with the results obtained in the silkworm model.

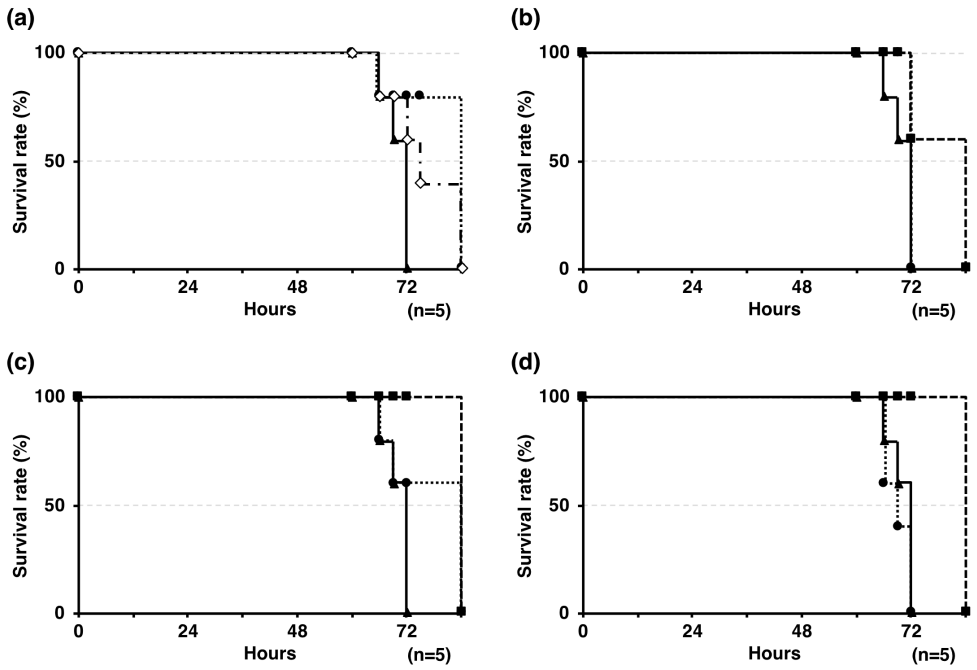

Figure 5. Therapeutic effects of compounds 1-4 in the silkworm infection assay with *M. avium*. (a) Ohmyungsamycin A (**1**), **(b)** ohmyungsamycin B (**2**), **(c)** chartreusin (**3**), and **(d)** griseoviridin (**4**). ■: 50, ●: 25, ◊: 13, ▲: 0 μg/larva·g. Experiments were performed three times and reproducible data were observed.

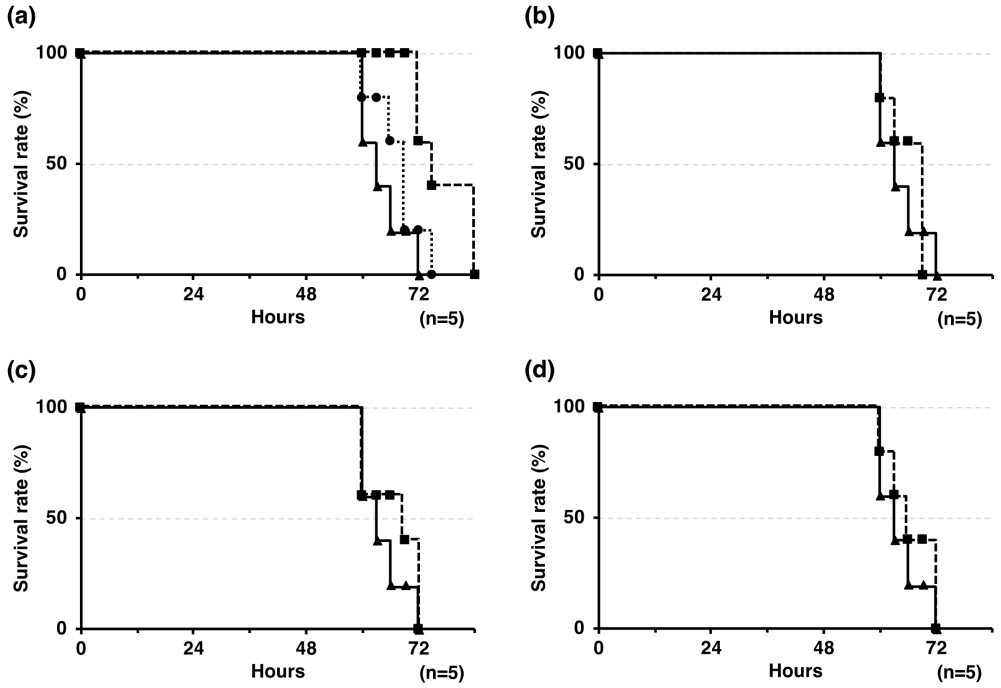

Figure 6. Therapeutic effects of compounds 1-4 in the silkworm infection assay with *M. intracellulare*. (a) Ohmyungsamycin A (**1**), **(b)** ohmyungsamycin B (**2**), **(c)** chartreusin (**3**), and **(d)** griseoviridin (**4**). ■: 50, ●: 25, ▲: 0 μg/larva·g. Experiments were performed three times and reproducible data were observed.

Accordingly, we concluded that the silkworm model may be used to evaluate the *in vivo* effects of anti-MAC drug candidates.

Hamamoto and co-workers previously reported that the ED_{50}/MIC ratio, indicating an index of drug potential, of common clinical antibiotics was less than 10 (*22*). In the present study, the ratio of kanamycin had the best score of 7.4 in the silkworm model with *M. avium*, while those of clarithromycin, streptomycin, amikacin, and ciprofloxacin were higher than 10, suggesting that the efficiencies of the majority of the anti-tuberculosis drugs tested were poor in the silkworm

model with *M. avium*.

We then screened our microbial broth library using the silkworm model, and identified four potential compounds, ohmyungsamycins A and B (**1** and **2**), chartreusin (**3**), and griseoviridin (**4**), from the actinomycete strains TMPU-A0334, TMPU-A0405, and KTM7-6, respectively. Compounds **1** to **4** exerted therapeutic effects in a dose-dependent manner in the silkworm model with *M. avium*. Of these, **1** exerted potent therapeutic effect with the lowest ED_{50} value of 8.5 μg/larva·g in all tested compounds, including anti-tuberculosis drugs. Moreover, the ED_{50}/MIC ratios of **1**, **2**, and **4** were relatively high (ratio; 22 to 26), while that of **3** only was < 10 (ratio; 7.4), similar to that of KM. Therefore, the therapeutic effects of **1** and **3** need to be examined in a mouse model.

We previously discovered a unique lasso peptide lariatin A, produced by *Rhodococcus jostii* K01-B0171, in the screening of anti-tuberculosis antibiotics using *M. smegmatis* (*13*). Lariatin A also exerted therapeutic effects in the silkworm model with *M. smegmatis* (ED_{50}; 0.5 μg/larva·g) and *My. abscessus* (ED_{50}; 4.4 μg/larva·g) (*11,12*). In the present study, lariatin A exhibited anti-*M. avium* and anti-*M. intracellulare* activities with MIC values of 1.56 and 1.56 μg/mL, respectively, in the microdilution assay (data not shown), but no therapeutic effects in the silkworm model with *M. avium* and *M. intracellulare* (ED_{50}; > 50 μg/larva·g). Interestingly, the therapeutic effects of **1**, which were potent in the silkworm model with *M. avium* and *M. intracellulare*, were negligible in the silkworm model with *M. smegmatis* and *My. abscessus* (*12*). Many pathogenic mycobacteria are generally slow-growing. Therefore, the evaluation of test compounds by silkworm models using mycobacteria with different growth rates is critical for obtaining a more detailed understanding of actual medicinal effects that cannot be distinguished by *in vitro* activity.

In summary, we herein established silkworm models with *M. avium* and *M. intracellulare* to screen and develop new anti-MAC drugs. The reliability of the silkworm model was supported by comparisons of the therapeutic effects of clinically used anti-mycobacterium drugs between the silkworm and mouse models. The evaluation period of test compounds in the silkworm model was successfully reduced from 4 weeks in the mouse model to 4 days in the silkworm model. Furthermore, we identified four compounds as potential anti-MAC candidates from our microbial broth collection within a short period. Thus, the silkworm model has potential as a practical *in vivo*-mimic model for discovering a new class of anti-MAC drugs with therapeutic effects.

Acknowledgements

We thank the captain and crew of the training vessel "Hiyodori" of Tokyo University of Marine Science and Technology for their assistance in collecting marine sediments.

Funding: This work was supported by JSPS KAKENHI Grant Numbers 19J15511 (to AY) and 16H05095 (to RU).

Conflict of Interest: There is no conflict of interest to disclose.

References

1. Adjemian J, Olivier KN, Seitz AE, Holland SM, Prevots DR. Prevalence of nontuberculous mycobacterial lung disease in U.S. Medicare beneficiaries. Am J Respir Crit Care Med. 2012; 185:881-886.
2. Namkoong H, Kurashima A, Morimoto K, Hoshino Y, Hasegawa N, Ato M, Mitarai S. Epidemiology of pulmonary nontuberculous mycobacterial disease, Japan. Emerg Infect Dis. 2016; 22:1116-1117.
3. Griffith DE, Aksamit T, Brown-Elliott BA, *et al.* An official ATS/IDSA statement: diagnosis, treatment, and prevention of nontuberculous mycobacterial diseases. Am J Respir Crit Care Med. 2007; 175:367-416.
4. Shirley M. Amikacin liposome inhalation suspension: a review in *Mycobacterium avium* complex lung disease. Drugs. 2019; 79:555-562.
5. Hamamoto H, Urai M, Ishii K, *et al.* Lysocin E is a new antibiotic that targets menaquinone in the bacterial membrane. Nat Chem Biol. 2015; 11:127-133.
6. Uchida R, Iwatsuki M, Kim YP, Ohte S, Ōmura S, Tomoda H. Nosokomycins, new antibiotics, discovered in an *in vivo*-mimic infection model using silkworm larvae. I. Fermentation, isolation and biological properties. J Antibiot. 2010; 63:151-155.
7. Uchida R, Iwatsuki M, Kim YP, Ōmura S, Tomoda H. Nosokomycins, new antibiotics, discovered in an *in vivo*-mimic infection model using silkworm larvae. II. Structure elucidation. J Antibiot. 2010; 63:157-163.
8. Uchida R, Hanaki H, Matsui H, Hamamoto H, Sekimizu K, Iwatsuki M, Kim YP, Tomoda H. *In vitro* and *in vivo* anti-MRSA activities of nosokomycins. Drug Discov Ther. 2014; 8:249-254.
9 Uchida R, Namiguchi S, Ishijima H, Tomoda H. Therapeutic effects of three trichothecenes in the silkworm infection assay with *Candida albicans*. Drug Discov Ther. 2016; 20:44-48.
10. Tominaga T, Uchida R, Koyama N, Tomoda H. Anti-*Rhizopus* activity of tanzawaic acids produced by the hot spring-derived fungus *Penicillium* sp. BF-0005. J Antibiot. 2018; 71:626-632.
11. Yagi A, Uchida R, Hamamoto H, Sekimizu K, Kimura K, Tomoda H. Anti-*Mycobacterium* activity of microbial peptides in a silkworm infection model with *Mycobacterium smegmatis*. J Antibiot. 2017; 70:685-690.
12. Hosoda K, Koyama N, Hamamoto H, Yagi A, Uchida R, Kanamoto A, Tomoda H. Evaluation of anti-mycobacterial compounds in a silkworm infection model with *Mycobacteroides abscessus*. Molecules. 2020; 25:4971.
13. Iwatsuki M, Uchida R, Takakusagi Y, Matsumoto A, Jiang CL, Takahashi Y, Arai M, Kobayashi S, Matsumoto M, Inokoshi J, Tomoda H, mura S. Lariatins, novel anti-

mycobacterial peptides with a lasso structure, produced by *Rhodococcus jostii* K01-B0171. J Antibiot. 2007; 60:357-363.
14. Koyama N, Kojima S, Nonaka K, Masuma R, Matsumoto M, Ōmura S, Tomoda H. Calpinactam, a new anti-mycobacterial agent, produced by *Mortierella alpina* FKI-4905. J Antibiot. 2010; 63:183-186.
15. Kimura K, Kanou F, Takahashi H, Esumi Y, Uramoto M, Yoshihama M. Propeptin, a new inhibitor of prolyl endopeptidase produced by *Microbispora*. I. Fermentation, isolation and biological properties. J Antibiot. 1997; 50:373-378.
16. Pascard C, Ducruix A, Lunel J, Prang T. Highly modified cysteine-containing antibiotics. Chemical structure and configuration of nosiheptide. J Am Chem Soc. 1977; 99:6418-6423.
17. Um S, Choi TJ, Kim H, Kim BY, Kim SH, Lee SK, Oh KB, Shin J, Oh DC. Ohmyungsamycins A and B: cytotoxic and antimicrobial cyclic peptides produced by *Streptomyces* sp. from a volcanic island. J Org Chem. 2013; 78:12321-12329.
18. Hur J, Jang J, Sim J, *et al.* Conformation-enabled total syntheses of ohmyungsamycins A and B and structural revision of ohmyungsamycin B. Angew Chem Int Ed Engl. 2018; 57:3069-3073.
19. Byron EL, Kenneth MC, LeRoy EJ, Charlotte MT, William GJ. Chartreusin, a new antibiotic produced by *Streptomyces chartreusis*, a new species. J Am Chem Soc. 1953; 75:4011-4012.
20. Anderson LE, Ehrlich J, Sun SH, Burkholder PR. Strains of *Streptomyces*, the sources of azaserine, elaiomycin, griseoviridin, and viridogrisein. Antibiot Chemother. 1956; 6:100-105.
21. Hosoda K, Koyama N, Kanamoto A, Tomoda H. Discovery of nosiheptide, griseoviridin, and etamycin as potent anti-Mycobacterial agents against *Mycobacterium avium* complex. Molecules. 2019; 24:1495
22. Hamamoto H, Kurokawa K, Kaito C, Kamura K, Razanajatovo IM, Kusuhara H, Santa T, Sekimizu K. Quantitative evaluation of the therapeutic effects of antibiotics using silkworms infected with human pathogenic microorganisms. Antimicrob Agents Chemother. 2004; 48:774-779.
23. Cynamon MH, Klemens SP, Chou TS, Gimi RH, Welch JT. Antimycobacterial activity of a series of pyrazinoic acid esters. J. Med. Chem. 1992; 35:1212-1215.
24. Kuze F. Experimental chemotherapy in chronic *Mycobacterium avium-intracellulare* infection of mice. Am Rev Respir Dis. 1984; 129:453-459.
25. Klemens SP, DeStefano MS, Cynamon MH. Activity of clarithromycin against *Mycobacterium avium* complex infection in beige mice. Antimicrob Agents Chemother. 1992; 36:2413-2417.
26. Fattorini L, Xiao Y, Mattei M, Li Y, Iona E, Ricci ML, Thoresen OF, Creti R, Orefici G. Activities of isoniazid alone and in combination with other drugs against *Mycobacterium avium* infection in beige mice. Antimicrob Agents Chemother. 1998; 42:712-714.
27. Inderlied CB, Kolonoski PT, Wu M, Young LS. Amikacin, ciprofloxacin, and imipenem treatment for disseminated *Mycobacterium avium* complex infection of beige mice. Antimicrob Agents Chemother. 1989; 33:176-180.
28. Gangadharam PR, Ashtekar DR, Flasher DL, Düzgüneş N. Therapy of *Mycobacterium avium* complex infections in beige mice with streptomycin encapsulated in sterically stabilized liposomes. Antimicrob Agents Chemother. 1995; 39:725-730.
29. Kohno Y, Ohno H, Miyazaki Y, Higashiyama Y, Yanagihara K, Hirakata Y, Fukushima K, Kohno S. *In vitro* and *in vivo* activities of novel fluoroquinolones alone and in combination with clarithromycin against clinically isolated *Mycobacterium avium* complex strains in Japan. Antimicrob Agents Chemother. 2007; 51:4071-4076.
30. Han XY, Tarrand JJ, Infante R, Jacobson KL, Truong M. Clinical significance and epidemiologic analyses of *Mycobacterium avium* and *Mycobacterium intracellulare* among patients without AIDS. J Clin Microbiol. 2005; 43:4407-4412.
31. Koh WJ, Jeong BH, Jeon K, Lee NY, Lee KS, Woo SY, Shin SJ, Kwon OJ. Clinical significance of the differentiation between *Mycobacterium avium* and *Mycobacterium intracellulare* in *M avium* complex lung disease. Chest. 2012; 142:1482-1488.

Received October 26, 2020; Revised November 15, 2020; Accepted November 22, 2020.

**Address correspondence to:*
Ryuji Uchida, Department of Natural Product Chemistry, Faculty of Pharmaceutical Sciences, Tohoku Medical and Pharmaceutical University, 4-4-1 Komatsushima, Aoba-ku, Sendai, Miyagi 981-8558, Japan.
E-mail: uchidar@tohoku-mpu.ac.jp

Released online in J-STAGE as advance publication November 30, 2020.

Original Article

DOI: 10.5582/ddt.2020.03118

Preparation and *in vitro* tumor growth inhibitory effect of oligo (L-lactate) nanoparticles

Akihiro Matsumoto[1], Satoshi Murao[1], Chie Watanabe[1,2], Masahiro Murakami[1,*]

[1] Laboratory of Pharmaceutics, Faculty of Pharmacy, Osaka Ohtani University, Osaka, Japan;
[2] Laboratory of Clinical Pathology, Faculty of Pharmacy, Josai University, Saitama, Japan.

SUMMARY Oligo L-lactates (oligolactates) that have low molecular weights less than 2000 have been reported to inhibit tumor growth and extend the survival of experimental animals. Because oligolactates are scarcely soluble in water, they require a solvent or a solubilizing agent, such as a surfactant, to be dissolved in water. However, these agents are generally cytotoxic, an *in vitro* assay appropriate to evaluate the inhibitory effect on tumor growth has not been developed yet. Here, we prepared a solid nanodispersion of oligolactates using an oil-in-water emulsion solvent evaporation method to evaluate its tumor inhibitory activity *in vitro* without a solvent or surfactant. Polyol solutions containing polyvinyl alcohol (PVA) were used as a continuous phase. The formation of nanoparticles depended on the concentrations of polyol and PVA in the continuous phase. The nanoparticles with a particle size of approximately 100 nm were obtained using 10-15% PVA and 60% propylene glycol. The obtained aqueous nanodispersion of oligolactates inhibited the growth of B16-BL6 melanoma cells *in vitro*, whereas the medium alone did not affect tumor cell growth. Therefore, oligo(L-lactate) nanoparticles may be useful in the research and development of oligolactates as a remedy for cancer.

Keywords oligo(L-lactate), solid nanodispersion, polyol, solvent evaporation method, tumor growth inhibition, melanoma

1. Introduction

Polylactides are linear lactic acid polymers with high molecular weights which are inert; thus, they are used as green plastics or inactive biodegradable ingredients. A collegium on L-lactic acid oligomers (oligolactates), which was established in 1996 and sponsored by Tokai Education Instruments Co., Ltd. (Kanagawa, Japan) and Amato Pharmaceutical Products, Ltd. (Osaka, Japan), suggested that cyclic and linear oligolactates of molecular weights below 2000 exhibit various physiological activities such as antihyperglycemic and anti-allergic activities, suppression of anaerobic glycolysis, and mitochondrial proliferation (not published). The substances were originally discovered in a conditioned medium harvested from cultured HeLa cells (not published). Some fractions of the conditioned medium showed growth inhibition or tumoricidal effects against HeLa cells and other tumor cells. Subsequent investigations revealed that oligolactates from the conditioned medium showed a tumor static effect. Moreover, the collegium developed a method for synthesizing oligolactates with a degree of polymerization from 3-13 (*1*) and confirmed that these oligolactates show *in vivo* tumor static effects in mice. The oligolactates inhibit the anaerobic activity of tumor cells. Thus, they effectively inhibit the growth of FM3A ascites tumors (*2*). Other studies have also reported that an extract containing cyclic poly-L-lactates inhibited the cell growth of leukemic (*3,4*) and carcinoma cells (*5*). However, oligolactates are water-insoluble substances and require a water-miscible organic solvent such as dimethyl sulfoxide or a solubilizing agent such as a surfactant to be dissolved in water; unfortunately, these agents are generally cytotoxic or affect cell proliferation. Consequently, an *in vitro* assay to evaluate the inhibitory effect of oligolactates on tumor growth has not been developed yet.

Macromolecular compounds and microparticles are generally membrane-impermeable, and their cellular uptake can occur *via* endocytosis, *i.e.*, pinocytosis and phagocytosis. For the uptake of particles in non-phagocytes, the necessity for keeping particles between 10 and 100 nm to enter endocytic vesicles was postulated and became the foundation for the current definition of nanomedicine by various agencies worldwide (*6*). Thus, it can be a strategy for formulating nanoparticles by increasing the cellular uptake of water-

insoluble macromolecules.

Several techniques for reducing particle size have been proposed, including micro/nanomization (*7-10*), solubilization (*11,12*), and self-emulsification (*13-16*). Among the size reduction methods, the solvent diffusion method is often used for preparing polymeric nanoparticles (*17-21*). A dispersed phase of an organic polymer solution is injected into a continuous phase of a miscible solvent. Being miscible, the interfacial tension between dispersed and continuous phase is reduced, and the deposition of the polymer occurs as nano-sized particles. In general, acetone and water are used as the dispersed and continuous phase, respectively. However, because commercially available oligolactates are insoluble in acetone, it is difficult to apply the solvent diffusion method to fabricate oligo(L-lactate) nanoparticles. In addition, this method typically generates nanoparticles of around 200 nm, and it is difficult to obtain nanoparticles around/below 100 nm. Thus, the particles are in a size range that promotes cellular uptake.

Because oligolactates are soluble in methylene chloride, the emulsion-based solvent evaporation method is suitable to fabricate oligolactates particles. For further size reduction using this method, the interfacial tension must be reduced between the dispersed phase containing the polymer and the continuous phases. Additionally, the hydrophobicity between the two phases must be closer. The addition of polyols such as propylene glycol and butylene glycol to water as a continuous phase can increase the hydrophobicity of the solution. Moreover, polyol aqueous solution can dissolve PVA at high concentrations. PVA, a synthetic water-soluble polymer, is very less toxic and commonly used for producing polymer emulsions in the preparation of nano/microparticles, which is advantageous to reduce the interfacial tension between dispersed and continuous phases. Hence, in this study, to obtain nanoparticles of oligolactates around 100 nm or smaller, we used the oil-in-water (o/w) type emulsion solvent-evaporation method with a polyol aqueous solution as the continuous phase and a polymeric organic solvent as the dispersed phase.

The objectives of this study were to develop an alternative fabrication method for oligo(L-lactate) nanoparticles, which are difficult to fabricate using conventional methods for polymeric nanoparticles, such as a solvent diffusion method, and confirm the tumor toxicity of oligolactates *in vitro*. We investigated the feasibility of implementing an o/w type emulsion solvent evaporation method using a polyol aqueous solution to obtain oligo(L-lactate) nanoparticles of various sizes. The aqueous nanodispersion can apply to *in vitro* cell culture without an organic solvent or surfactant. Our study will lead to a reasonable evaluation of the activity of oligolactates *in vitro* and help in developing oligolactates and their derivatives as a new type of antitumor agent in the future.

2. Materials and Methods

2.1. Materials

CPL, a commercial oligolactate mixture synthesized using a decompression and dehydration condensation method, was kindly gifted by Shumeido Co., Ltd. (Yamaguchi, Japan). Polyvinyl alcohol (PVA; JP03) was obtained from Japan VAM & POVAL Co., Ltd. (Osaka, Japan). Dulbecco's modified Eagle's medium (D-MEM) were purchased from Wako Pure Chemical Industry, Ltd. (Osaka, Japan). Dulbecco's phosphate-buffered saline (D-PBS), non-essential amino acids, penicillin, streptomycin, and Cell Count Reagent SF were purchased from Nacalai Tesque, Inc. (Kyoto, Japan). Fetal bovine serum (FBS) was purchased from Biowest (Nuaillé, France). All other chemicals used were of reagent grade. There are no ethical aspects to declare in this study.

2.2. Cell lines and culture

Murine B16-BL6 melanoma cells were kindly provided by Dr. Y. Hayakawa (University of Toyama) and routinely incubated and maintained in complete medium (DMEM containing 10% FBS, non-essential amino acids, 100 U/mL penicillin, and 100 U/mL streptomycin, pH 7.4) at 37°C in a humidified atmosphere containing 5% carbon dioxide.

2.3. Synthesis of low molecular weight oligolactates

Oligolactates were synthesized by dehydration polycondensation to obtain oligolactates with a lower molecular weight than CPL. L-Lactic acid (500 mL) was placed into a three-necked flask fitted with a distillation head and condenser, a thermometer for monitoring the temperature of the solution, and an inlet for inert nitrogen gas (300 mL/min). The vessel was heated at 145°C for 3 h using a mantle heater. The pressure and temperature were then changed stepwise to 150 mmHg at 145°C for 3 h, 3 mmHg at 155°C for 3 h, and 3 mmHg at 185°C for 1.5 h. The obtained mixture was mixed well with ethanol (100 mL) and methanol (400 mL) at 100°C, and then cooled to room temperature overnight. The obtained suspension was filtered to remove participants, dried under reduced pressure, and filtered to remove participants once again before the dry substance was dissolved in acetonitrile (200 mL). The solution was purified using reverse phase Octa decyl silyl (ODS) column (Biotage® sfär C18 Duo 100Å 30 μm, Biotage AB, Uppsala, Sweden) through stepwise elution of 0.01 M hydrochloride -30% acetonitrile, 0.01 M hydrochloride -50% acetonitrile, and 0.01 M hydrochloride -100% acetonitrile. The elute collected with 100% acetonitrile was dried under reduced pressure to obtain oligolactates. Hereinafter,

the obtained oligolactates are referred to as "synthesized oligolactates".

To prepare the oligo(L-lactate) nanoparticles used in the *in vitro* tumor growth inhibition study, we used oligolactates washed with water to remove water-soluble components. Namely, 1 g of oligolactates was dissolved in 2 mL of methylene chloride, washed with 10 mL water by shaking for 30 min, and dried under reduced pressure.

2.4. Preparation of commercial or synthesized oligo(L-lactate) nanoparticles

CPL- or synthesized oligo(L-lactate) nanoparticles were prepared using the o/w type emulsion solvent evaporation method. CPL or the synthesized oligolactates were dissolved in methylene chloride to obtain the oil phase. The oil phase was emulsified in 5 mL of PVA solution containing propylene glycol at 20,000 rpm using a homogenizer (ULTRA-TURRAX T18, IKA®-Werke GmbH & Co., KG, Staufen, Germany) for 5 min at 20-23°C. The resulting o/w type emulsion was added to 100 mL of water, and the diluted emulsion was stirred at 20-23°C for 180 min to remove the solvent. The aggregates generated during the manufacturing process were removed using a 20-μm stainless mesh or 0.45-μm membrane filter if necessary. For the *in vitro* tumor growth inhibition study, the obtained nanoparticle suspension was washed and replaced with a complete medium by ultrafiltration using a 100 kDa filter at 4°C.

2.5. Characterization of nanoparticles

The size and zeta potential of the nanoparticles were measured using dynamic light scattering (DLS) with a zeta (ζ) potential analyzer (ELSZ-2, Otsuka Electronics Co. Ltd., Osaka, Japan). The cumulant size obtained by DLS was used as the hydrodynamic diameter.

2.6. Characteristics of CPL and synthesized oligolactates

CPL and the synthesized oligolactates were dissolved in tetrahydrofuran, mixed with 3-indoleacrylic acid (Tokyo Chemical Industry Co., Ltd., Tokyo, Japan), and characterized by matrix-assisted laser desorption/ionization-time of flight-mass spectrometry (MALDI-TOF-MS). The mass spectrometry was performed using an AXIMA® Confidence™ running LAUNCHPAD 2.8.4 (Shimadzu Co., Ltd., Kyoto, Japan). The wavelength of the laser was 337 nm.

2.7. Transmission electron microscope imaging

The nanoparticles were absorbed onto formvar film-coated copper grids and negatively stained by treating them with 2% phosphotungstic acid solution (pH 7.0) for a few seconds. The samples were observed using a transmission electron microscope (TEM; JEM-1400Plus, JOEL Ltd., Tokyo, Japan) at 100 kV. Digital images were captured with a CCD camera (EM-14830RUBY2, JOEL Ltd., Tokyo, Japan).

2.8. *In vitro* tumor growth inhibition study

The influence of CPL and the synthesized oligo(L-lactate) nanoparticles on *in vitro* B16-BL6 cell growth was evaluated using the water-soluble tetrazolium (WST) method. In brief, 1×10^4 cells/mL of the exponentially growing B16-BL6 cells (100 μL) in a complete medium was plated in a 96-well plate. After a 24-h incubation at 37°C in a humidified atmosphere containing 5% carbon dioxide to allow cell attachment, the cells were treated with varying concentrations of the synthesized oligo(L-lactate) nanoparticles dispersed in the complete medium and incubated for 48 h under the same conditions. After 4 h of incubation under the same conditions, followed by the addition of 10 μL of Cell Count Reagent SF, the supernatant was measured spectrophotometrically at 450 nm using a hybrid multimode microplate reader (Synergy H4; BioTek Instruments, Winooski, VT, USA).

2.9. Statistical analysis

Experiments were performed at least three times. The results are presented as the mean ± standard deviation. The differences between the means for the two groups were statistically analyzed using Williams' test for multiple comparisons. P-values < 0.05 indicated significant differences.

3. Results

3.1. Characteristics of CPL and synthesized oligolactates based on MALDI-TOF-MS analysis

Figure 1 shows the mass spectra of CPL and the synthesized oligolactates, and Table 1 lists the detected molecular weights. The measurement in positive mode provided molecular ion peaks corresponding to protonated, sodium, and ammoniated oligolactates ions. For CPL, the peaks corresponding to polymerization degree 4-31 indicating linear structure and 5-12 indicating cyclic structure were detected. For the synthesized oligolactates, peaks corresponding to polymerization degrees 2-12 (linear) and 2-8 (cyclic) were detected.

The complicated stepwise change in pressure and temperature in the dehydration polycondensation method for synthesizing oligolactates was aimed at increasing the yield of cyclic lactides. However, some of the major molecular weight peaks were identified as linear oligolactates through MALDI-TOF-MS. This indicates that a large quantity of linear oligolactates

is among the oligolactates synthesized in this study as well as in CPL.

3.2. Influence of fabrication conditions on the characteristics of CPL nanoparticles

Table 2 summarizes the particle sizes of CPL nanoparticles in various continuous phases during the emulsification process. The increase in PVA concentration resulted in smaller CPL nanoparticles, and the particle sizes were below 200 nm in continuous phases containing more than 5% PVA concentration in the case of 60% propylene glycol (Figure 2a). With the addition of polyol, an increase in propylene glycol concentration up to 60% resulted in a smaller particle size (Figure 2b); however, 80% propylene glycol-10% PVA solution could not be used as a continuous phase because of its gelation at room temperature. The reduction in particle size by the addition of polyols was in the order of 1,3-butylene glycol = propylene glycol > glycerin, and butylated glycol and propylene glycol provided particle sizes below 150 nm in the case of 10% PVA. When glycerin was used as a polyol, the aggregates

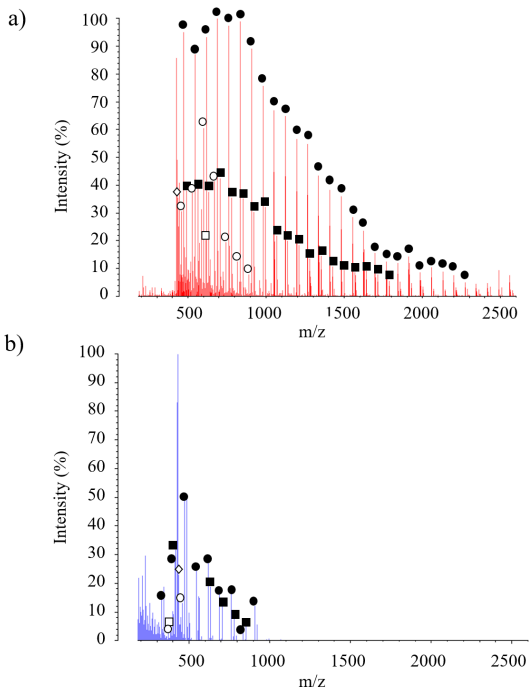

Figure 1. MALDI-TOF-MS spectra. a) CPL and **b)** synthesized oligolactates. The molecular weight of peaks corresponds to ●: [linear oligolactates-Na]$^+$, ■: [linear oligolactates-K]$^+$, ○: [cyclic oligolactates-Na]$^+$, □: [cyclic oligolactates-K]$^+$, ◊: [cyclic oligolactates-H]$^+$.

Table 1. List of detected cyclic oligolactates in CPL and synthesized oligolactates

Molecular weight	Degree of polymerization	Adduction	Area percentage of cyclic oligolactates*	
			CPL	Synthesized oligolactates
144	2	$-NH_4^+$	-	1.84
216	3	$-H^+$	-	2.48
		$-NH_4^+$	-	0.56
		$-Na^+$	-	0.95
		$-K^+$	-	3.00
288	4	$-H^+$	-	0.19
		$-NH_4^+$	-	0.24
		$-Na^+$	-	1.04
		$-K^+$	-	1.64
360	5	$-NH_4^+$	0.45	0.07
		$-Na^+$	-	1.09
		$-K^+$	-	0.06
432	6	$-H^+$	1.77	5.23
		$-Na^+$	1.52	2.93
		$-K^+$	1.42	1.16
504	7	$-H^+$	0.18	0.07
		$-Na^+$	1.85	-
		$-K^+$	0.70	-
576	8	$-H^+$	-	0.19
		$-Na^+$	3.02	-
		$-K^+$	1.01	-
648	9	$-Na^+$	2.05	-
		$-K^+$	0.59	-
720	10	$-Na^+$	0.97	-
792	11	$-Na^+$	0.62	-
864	12	$-Na^+$	0.40	-
Total (%)			16.57	22.75

*[cyclic oligolactates]/[linear and cyclic oligolactates] × 100. CPL: brand name of commercial oligolactates.

Table 2. Composition of continuous phase and hydrodynamic diameter of the fabricated nanoparticles

Number	Composition of continuous phase	Mean size	Polydispersity index
#1	10% PVA	435.0 ± 48.5 nm	0.202 ± 0.030
#2	10% PVA-60% glycerol	1609 ± 220 nm	0.648 ± 0.088
#3	10% PVA-60% propylene glycol	117.1 ± 4.3 nm	0.098 ± 0.018
#4	10% PVA-60% 1,3 butylene glycol	137.1 ± 7.5 nm	0.075 ± 0.013
#5	15% PVA-60% propylene glycol	99.1 ± 3.3 nm	0.131 ± 0.027
#7	5% PVA-60% propylene glycol	162.7 ± 1.9 nm	0.062 ± 0.013
#8	2.5% PVA-60% propylene glycol	200.8 ± 6.5 nm	0.066 ± 0.017
#9	0.5% PVA-60% propylene glycol	278.7 ± 9.5 nm	0.136 ± 0.031
#10	10% PVA-80% propylene glycol	-	-
#11	10% PVA-50% propylene glycol	123.3 ± 4.6 nm	0.114 ± 0.012
#12	10% PVA-40% propylene glycol	165.5 ± 12.9 nm	0.111 ± 0.041
#13	10% PVA-20% propylene glycol	245.2 ± 3.5 nm	0.107 ± 0.018

Data are represented as mean ± S.D. (n = 3 batches). PVA, polyvinyl alcohol; S.D., standard deviation.

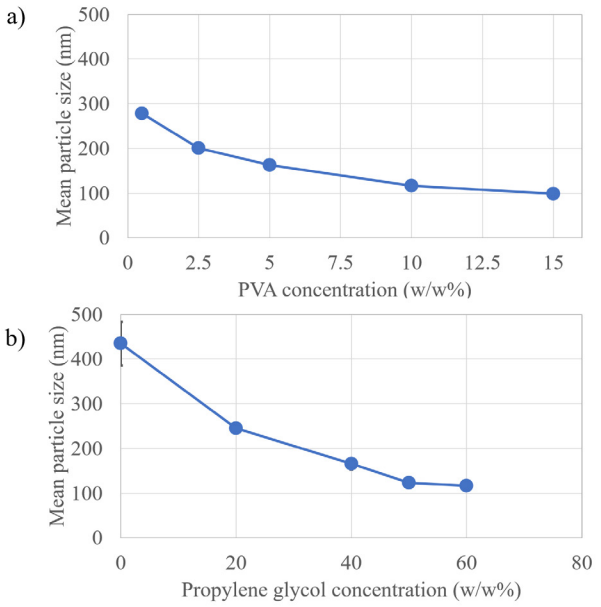

Figure 2. Effect of the continuous phase composition on the hydrodynamic diameter of nanoparticles. a) Effect of PVA concentration in 60% propylene glycol solution, **b)** Effect of propylene glycol concentration in 10% PVA solution. Data are represented as mean ± S.D. (n = 3 batches)

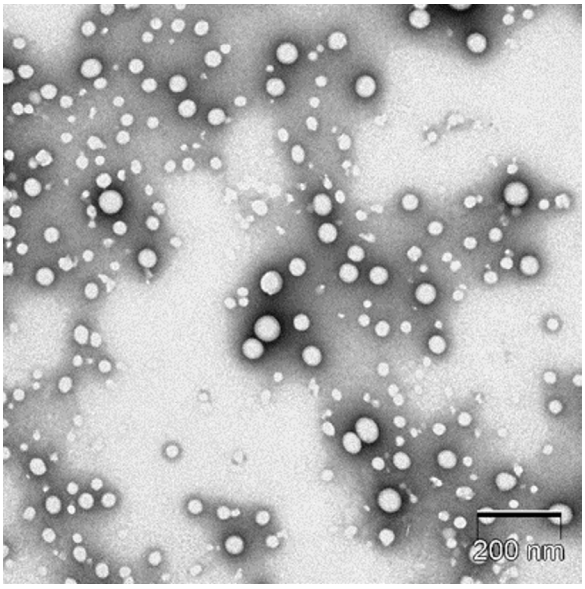

Figure 3. Transmission electron micrographs of the typical CPL nanoparticles. The nanoparticles were fabricated using 15% PVA-60% propylene glycol as a continuous phase.

of 55.2 ± 14.1% over a size of 20 μm were generated. Figure 3 shows the transmission electron micrographs of the typical CPL nanoparticles (hydrodynamic diameter: 117.5 nm). Transmission electron microscopy images confirmed spherical nanoparticles in the size range of 1.7 nm to 66.4 nm (number mean size 25.6 nm).

3.3. Evaluation of tumor growth inhibition

The oligo(L-lactate) nanoparticles were evaluated for their growth inhibition by the WST assay at various concentrations. The nanoparticles used in this study were well-dispersed at the size of 126.3 nm (polydispersity index: 0.129) and ζ-potential of -4.64 mV for CPL, and 149.4 nm (polydispersity index: 0.181) and ζ-potential of -16.78 mV for the synthesized oligolactates in a D-MEM culture medium without aggregates (Figures 4a and 4b). The results of the inhibitory effect on the *in vitro* growth of B16-BL6 melanoma cells are shown in Figure 4c. The synthesized oligo(L-lactate) nanoparticles significantly induced growth inhibition at a concentration of 5 mg/mL with an IC_{50} of 9.7 mg/mL. On the other hand, CPL nanoparticles showed no growth inhibition at concentrations up to 10 mg/mL.

4. Discussion

To fabricate oligo(L-lactate) nanoparticles, we employed an o/w emulsion solvent evaporation method. We used the detergent (D) phase emulsification technique using a polyol-surfactants solution as continuous phase (*22*) to produce fine emulsions, which involves the formation of an oil-in-surfactant gel emulsion by dispersing oil in the surfactant solution. Consequently, we obtained nanoparticles of around 100 nm in hydrodynamic diameter from DLS analysis.

For the D phase emulsification method, a ternary system composed of water, polyol, and surfactant was used as the continuous phase. The role of polyol in this method is as follows: 1) the enhancement of the interaction between water and surfactant and the effective attachment of surfactant on oil droplets, and 2) the suppression of the liquid crystalline formation of a surfactant such as a hexagonal liquid crystal and increase in the region of the detergent phase (*22*). In the case of the ternary system of water, propylene glycol, and PVA used in this study, the effective attachment of PVA on oil droplets is indicated by the result that the influence of the PVA concentration on the size of the obtained particles was less sensitive than that of the propylene glycol concentration. On the other hand, the mechanism of the suppression of liquid crystalline formation in the D phase emulsification method may not be applied to the ternary system of water, propylene glycol, and PVA. However, the association between PVA is suppressed by propylene glycol. PVA has intermolecular hydrogen bonding, which leads to reduced efficiency as an emulsifier, especially at high concentrations. Polyols are used as plasticizers in PVA (*23*). It is known that hydrogen bonds between plasticizer and PVA chains are formed. It has been reported that the intermolecular interactions in the PVA solutions were notably reduced by propylene glycol because of its hydrogen bond breaking effects (*24*). This indicates that PVA in propylene glycol can effectively act as a monomeric emulsifier. This can account for the fact that nanoparticles were obtained by the addition of propylene glycol concentrations.

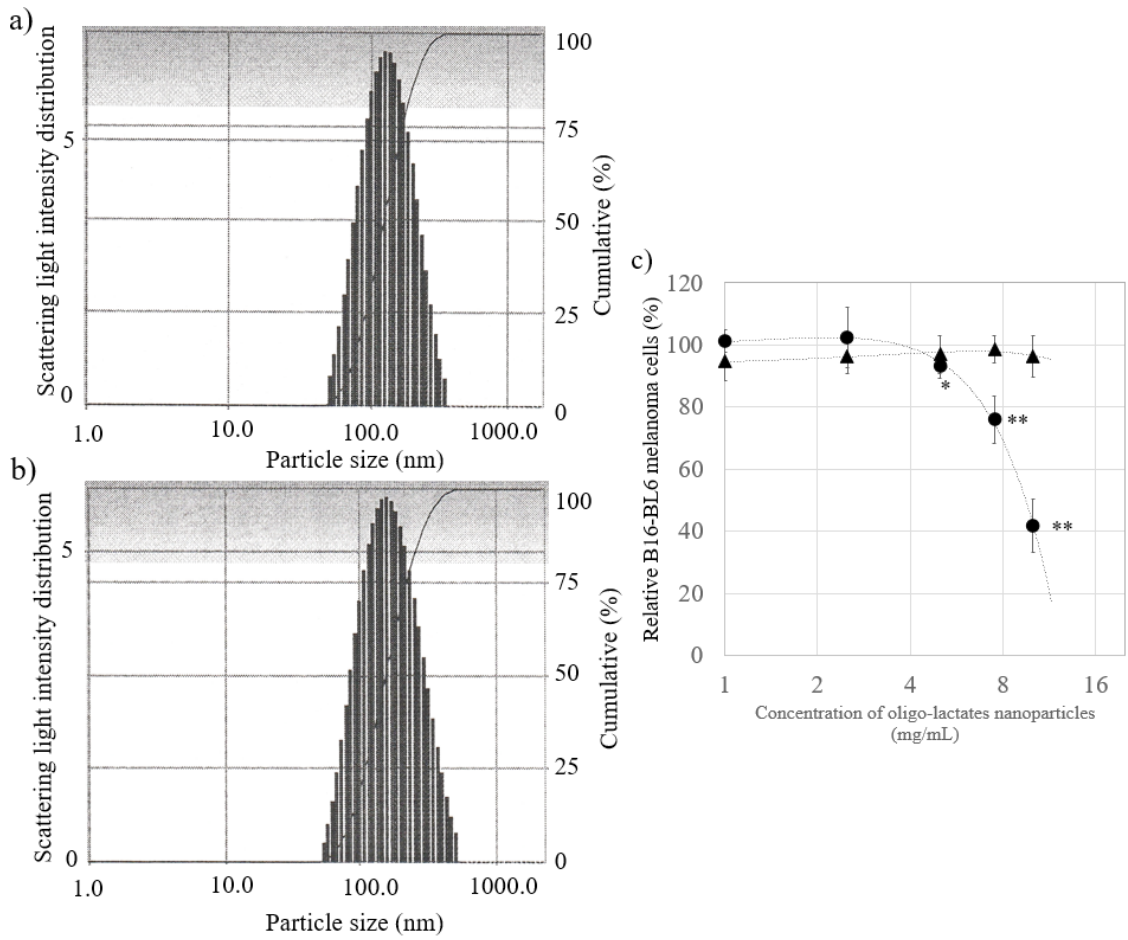

Figure 4. *In vitro* growth inhibition of B16-BL6 melanoma cells by CPL/synthesized oligo(L-lactate) nanoparticles. The graphs show the size distribution of **a)** CPL-nanoparticles and **b)** synthesized oligo(L-lactate) nanoparticles applied to *in vitro* growth inhibitory study. **c)** The graph shows *in vitro* dose inhibitory curve of CPL/synthesized oligo(L-lactate) nanoparticles to B16-BL6 melanoma cells. B16-BL6 melanoma cells were grown in 96-well microplates in a complete medium (10% FBS D-MEM, pH 7.4). Nanoparticles of various concentrations were added to each well and the cells were incubated for 48 h. Data are represented as mean ± S.D. ($n = 7$) of the relative B16-BL6 melanoma cells, percentages of treated group (▲: CPL nanoparticles, ●: synthesized oligo(L-lactate) nanoparticles) to non-treated group. * and ** represent significant differences between non- and nanoparticle-treated group at $p < 0.05$ and $p < 0.025$, respectively.

It has been reported that the hydrogen bond breaking effects of propylene glycol on PVA became dominant between 20 and 30 wt% in a PVA/propylene glycol film (*23*). Moreover, propylene glycol bonded to PVA may increase its affinity to the surface of oil droplets due to its hydrophobicity. This hypothesis explains why glycerol did not provide nanoparticles. The effective attachment of PVA on the surface of the oil phase by the inhibition of intermolecular interactions and the hydrophobicity of propylene glycol and butylene glycol contributed to the production of nanoparticles.

The data from the WST assay demonstrated that the synthesized oligolactates could inhibit the growth of B16-BL6 cells when administered as the nanoparticles. On the other hand, CPL did not show growth inhibition up to 10 mg/mL. CPL and synthesized oligolactates can be degraded to produce lactic acid by hydrolysis and may show cytotoxic effect by the acidification of a medium; however, the nanoparticle-dispersed D-MEM medium was confirmed to remain at a low pH of 6.9 (initial pH 7.4) after incubation at 37°C for 2 days. Hence, the growth inhibition is not due to the acidification of the medium. The synthesized oligolactates contain lower molecular weight components than CPL, based on MALDI-TOF-MS analysis, although cyclic oligolactates were also detected in both CPL and the synthesized oligolactates, indicating that the observed growth inhibition can attribute to the lower molecular weight components. It is difficult to identify the ratio of the lower molecular weight cyclic structure in the synthesized oligolactates and CPL from MALDI-TOF-MS analysis because the detection sensitivity of MALDI-TOF-MS may be different between linear and cyclic oligolactates and between molecular weights. However, it could be supposed that the synthesized oligolactates have higher contents of growth inhibition components than CPL. The growth inhibition activity of the synthesized oligo(L-lactate) nanoparticles was weak in comparison with that of doxorubicin, which showed approximately 9.5% at a concentration of 10 μg/mL in the relative percentage of cells in treated versus non-treated groups. Considering this weak activity of oligolactates, the active fraction and,

furthermore the active substance, should be separated from the mixtures to improve the tumor inhibitory effect.

It seems difficult for oligolactate molecule to pass through cell membrane by diffusion as a solute. The growth inhibition activity of the nanodispersion may be related to the cellular uptake of the nanoparticles by endocytosis, which is mainly determined by particle size and surface properties. For the size, it is reported that relative to internalized 50 nm beads, the uptake of the 100 nm beads was diminished by approximately 3-4-fold, whereas the internalization of the 200 and 500 nm beads was reduced by approximately 8-10 times in non-phagocytic B16 cells (*25*). In the present study, we obtained nanoparticles of around 150 nm in hydrodynamic diameter, although the median volume and number size from DLS were calculated to be 68.6 nm and 52.8 nm for the synthesized oligo(L-lactate) nanoparticles, respectively (data not shown). This suggests that further downsizing in hydrodynamic diameter may be effective to enhance the tumor growth inhibitory effect of oligo(L-lactate) nanoparticles. For the surface properties, endocytosis is also influenced by the particle's charge besides the size. In this study, we used negatively charged nanoparticles without surface modification. In general, positively charged particles show better interaction with the cellular membrane and internalization properties than negatively charged particles because the cellular membrane possesses negative charge. Therefore, we should investigate the fabrication of oligo(L-lactate) nanoparticles with surface charge modification further to improve their affinity to cells.

There are two more limitations on this study. One is that the long-term *in vitro* effects of oligolactates on tumor cell growth remains to be investigated. CPL was found to induce morphological changes of tumor cells during long-term administration *in vivo* (*2*). Another is that energy metabolism in tumor cells was not evaluated in this study. Tumor growth inhibition is related to energy metabolism and the suppression of anaerobic glycolysis by oligolactates and thereby mitochondrial proliferation are indicated. Thus, further investigation is needed to clarify the relationship between tumor growth inhibition and energy metabolism changes over time during incubation with oligolactates *in vitro*.

In conclusion, we developed a new method to produce oligo(L-lactate) nanoparticles of around 100 nm hydrodynamic diameter through o/w emulsion solvent evaporation using PVA-polyol aqueous solution as a continuous phase. Moreover, it was demonstrated that tumor growth is inhibited by the synthesized oligo(L-lactate) nanoparticles in an *in vitro* study using B16-BL6 melanoma cells. Thus, it was suggested that the nanoparticle is useful for an *in vitro* assay of effects of oligolactates and in development of various dosage forms for their clinical use, which may also help in developing oligolactates and their derivatives as a new type of antitumor agent in the future.

Acknowledgements

We thank Mr. Tatsuma Kobayashi and Ms. Ayaka Inoyama (Faculty of Pharmacy, Osaka Ohtani University) for their technical assistance. We thank Dr. Yoshihiro Hayakawa (Institute of Natural Medicine, University of Toyama, Japan) for providing us with B16-BL6 cells. We thank Shumeido Co., Ltd. (Kanagawa, Japan) for gifting oligolactates to facilitate our research. Furthermore, we thank Fuji Molecular Planning Co., Ltd. (Yokohama, Japan) for synthesizing oligolactates of low molecular weight on contract. We thank the Osaka Research Institution of Industrial Science and Technology for renting their MALDI-TOF-MS facilities to us. We also thank Tokai Electron Microscopy, Inc. (Nagoya, Japan) for analyzing the transmission electron microscopic images on contract.

Funding: None.

Conflict of Interest: The authors have no conflicts of interest to disclose.

References

1. Osaka I, Watanabe M, Takama M, Murakami M, Arakawa R. Characterization of linear and cyclic polylactic acids and their solvolysis products by electrospray ionization mass spectrometry. J Mass Spectrom. 2006; 41:1369-1377.
2. Takada S, Nagato Y, Yamamura M. Effect of cyclic polylactates on tumor cells and tumor bearing mice. Biochem Mol Biol Int. 1997; 43:9-17.
3. Harada T, Nagasu M, Tsuboi I, Koshinaga M, Kanno H, Aizawa S. Cyclic polylactate inhibited growth of cloned leukemic cells through reducing glycolytic enzyme activities. Oncol Rep. 2005; 14:501-505.
4. Aizawa S, Shimizu N, Handa H, Hiramoto M, Hoshi H, Nagasu M, Kanno H, Nagasu Y, Imanishi Y. Effects of cyclic polylactate (CPL) on the growth of cloned leukemic cells *in vitro*. Hematol Oncol. 2000; 18:51-60.
5. Campbell JH, Edsberg L, Meyer AE. Polylactide inhibition of carcinoma cell growth *in vitro*. J Oral Maxillofac Surg. 1994; 52:49-51.
6. Sahay G, Alakhova DY, Kabanov AV. Endocytosis of nanomedicines. J Control Release. 2010; 145:182-195.
7. Cheng KT, Seltzer SE, Adams DF, Blau M. The production and evaluation of contrast-carrying liposomes made with an automatic high-pressure system. Invest Radiol. 1987; 22:47-55.
8. Lidgate DM, Fu RC, Byars NE, Foster LC, Fleitman JS. Formulation of vaccine adjuvant muramyldipeptides. 3. Processing optimization, characterization, and bioactivity of an emulsion vehicle. Pharm Res. 1989; 6:748-752.
9. Alliod O, Almouazen E, Nemer G, Fessi H, Charcosset C. Comparison of three processes for parenteral nanoemulsion production: ultrasounds, microfluidizer, and premix membrane emulsification. J Pharm Sci. 2019; 108:2708-2717.

10. Wan J, Zhong S, Schwarz P, Chen B, Rao J. Physical properties, antifungal and mycotoxin inhibitory activities of five essential oil nanoemulsions: impact of oil compositions and processing parameters. Food Chem. 2019; 291:199-206.
11. Mandl I, Grauer A, Neuberg C. Solubilization of insoluble matter in nature; I. The part played by salts of adenosinetriphosphate. Biochim Biophys Acta. 1952; 8:654-663.
12. Mandl I, Grauer A, Neuberg C. Solubilization of insoluble matter in nature. II. The part played by salts of organic and inorganic acids occurring in nature. Biochim Biophys Acta. 1953; 10:540-569.
13. Kim HJ, Yoon KA, Hahn M, Park ES, Chi SC. Preparation and *in vitro* evaluation of self-microemulsifying drug delivery systems containing idebenone. Drug Dev Ind Pharm. 2000; 26:523-529.
14. Postolache P, Petrescu O, Dorneanu V, Zanini AC. Cyclosporine bioavailability of two physically different oral formulations. Eur Rev Med Pharmacol Sci. 2002; 6:127-131.
15. Holm R, Porter CJ, Edwards GA, Müllertz A, Kristensen HG, Charman WN. Examination of oral absorption and lymphatic transport of halofantrine in a triple-cannulated canine model after administration in self-microemulsifying drug delivery systems (SMEDDS) containing structured triglycerides. Eur J Pharm Sci. 2003; 20:91-97.
16. Abdelmonem R, Azer MS, Makky A, Zaghloul A, El-Nabarawi M, Nada A. Development, characterization, and in-vivo pharmacokinetic study of lamotrigine solid self-nanoemulsifying drug delivery system. Drug Des Devel Ther. 2020; 14:4343-4362.
17. Niwa T, Takeuchi H, Hino T, Kunou N, Kawashima Y. *In vitro* drug release behavior of D,L-lactide/glycolide copolymer (PLGA) nanospheres with nafarelin acetate prepared by a novel spontaneous emulsification solvent diffusion method. J Pharm Sci. 1994; 83:727-732.
18. Fresta M, Cavallaro G, Giammona G, Wehrli E, Puglisi G. Preparation and characterization of polyethyl-2-cyanoacrylate nanocapsules containing antiepileptic drugs. Biomaterials. 1996; 17:751-758.
19. Kawashima Y, Yamamoto H, Takeuchi H, Hino T, Niwa T. Properties of a peptide containing DL-lactide/glycolide copolymer nanospheres prepared by novel emulsion solvent diffusion methods. Eur J Pharm Biopharm. 1998; 45:41-48.
20. Kawashima Y, Serigano T, Hino T, Yamamoto H, Takeuchi H. A new powder design method to improve inhalation efficiency of pranlukast hydrate dry powder aerosols by surface modification with hydroxypropylmethylcellulose phthalate nanospheres. Pharm Res. 1998; 15:1748-1752.
21. Chen SQ, Wang C, Song YQ, Tao S, Yu FY, Lou HY, Hu FQ, Yuan H. Quercetin covalently linked lipid nanoparticles: multifaceted killing effect on tumor cells. ACS Omega. 2020; 5:30274-30281.
22. Sagitani H, Nabeta K, Nagai M. A new preparing method for fine O/W emulsions by D phase emulsification and their application to cosmetic industry. J Jpn Oil Chem Soc. 1991; 40:988-994.
23. Mohsin M, Hossin A, Haik Y. Thermal and mechanical properties of poly(vinyl alcohol) plasticized with glycerol. J Appl Polym Sci. 2011; 122:3102-3109.
24. Cho YH, Kim BC, Dan KS. Effects of propylene glycol on the physical properties of poly(vinyl alcohol) solutions and films. Macromol Res 2009; 17:591-596.
25. Rejman J, Oberle V, Zuhorn IS, Hoekstra D. Size-dependent internalization of particles *via* the pathways of clathrin- and caveolae-mediated endocytosis. Biochem J. 2004; 377:159-169.

Received November 28, 2020; Revised December 25, 2020; Accepted December 30, 2020.

**Address correspondence to:*
Masahiro Murakami, Laboratory of Pharmaceutics, Faculty of Pharmacy, Osaka Ohtani University, 3-11-1 Nishikori-kita, Tondabayashi, Osaka 584-0854, Japan.
E-mail: murakam@osaka-ohtani.ac.jp

Original Article

DOI: 10.5582/ddt.2020.03112

5-Aminolevulinic acid combined with sodium ferrous ameliorated liver injury in a murine acute graft-versus-host disease model by reducing inflammation responses through PGC-1α activation

Zhidan Wang[1,2], Kuai Ma[1], Chi Liu[1], Xin Hu[1], Weitao Que[1], Hidenori Ito[3], Kiwamu Takahashi[3], Motowo Nakajima[3], Tohru Tanaka[3], Ke Ren[4], Wen-Zhi Guo[5], Shuang-Qin Yi[2,*], Xiao-Kang Li[1,4,5,*]

[1] Division of Transplantation Immunology, National Research Institute for Child Health and Development, Tokyo, Japan;
[2] Laboratory of Functional Morphology Graduate School of Human Health Sciences Tokyo Metropolitan University, Tokyo, Japan;
[3] SBI Pharmaceuticals Co., Ltd., Tokyo, Japan;
[4] Project Division for Healthcare Innovation, Graduate School of Human Health Sciences, Tokyo Metropolitan University, Tokyo, Japan;
[5] Department of Hepatobiliary and Pancreatic Surgery, The First Affiliated Hospital of Zhengzhou University, Zhengzhou, China.

SUMMARY Acute graft-versus-host disease (aGvHD) remains lethal as a life-threatening complication after allogeneic hematopoietic stem cell transplantation (HSCT). Inflammatory responses play an important role in aGvHD. 5-Aminolevulinic acid combined with sodium ferrous citrate (5-ALA/SFC) has been widely reported to have a major effect on the anti-inflammatory response; however, these effects in aGvHD models have never been reported. In this study, a murine aGvHD model was developed by transferring spleen cells from donor B6/N (H-2k^{b}) mice into recipient B6D2F1 (H-2k$^{b/d}$) mice. In addition to evaluating manifestations in aGvHD mice, we analyzed the serum ALT/AST levels, liver pathological changes, infiltrating cells and mRNA expression of inflammation-related cytokines and chemokines. 5-ALA/SFC treatment significantly ameliorated liver injury due to aGvHD and decreased the population of liver-infiltrating T cells, resulting in a reduced expression of pro-inflammatory cytokines and chemokines. Furthermore, the mRNA expression proliferator-activated receptor-γ coactivator (PGC-1α) was enhanced, which might explain why 5-ALA/SFC treatment downregulates inflammatory signaling pathways. Our results indicated that 5-ALA/SFC can ameliorate liver injury induced by aGvHD through the activation of PGC-1α and modulation of the liver mRNA expression of inflammatory-related cytokines and chemokines. This may be a novel strategy for treating this disease.

Keywords 5-aminolevulinic acid, acute graft-versus-host disease, liver injury, inflammatory cytokines, PGC-1α.

1. Introduction

Allogeneic hematopoietic stem cell transplantation (HSCT) is the most efficient treatment for many hematological malignancies and for primary immunodeficiencies (*1,2*). However, transplants also contain mature T cells, which can induce acute graft-versus-host disease (aGvHD), a life-threatening complication of allogeneic HSCT (*3*).

The immune response causes activated donor T cells to gain a cytolytic capacity and attack recipient tissue in order to eliminate foreign antigen-bearing cells. These donor T cells infiltrate target organs where the inflammatory response plays a very important role, including the skin, liver, lung and gastrointestinal tract, and ultimately induce end-organ tissue damage (*4,5*). Therefore, the major goals of HSCT are to modulate alloreactivity by donor allogeneic T cells without causing GvHD and to preserve the graft-versus-leukemia and graft-versus-infection effects.

Several strategies are being reported to treat aGVHD, and current therapies include the administration of extracellular mediators and receptors, regulation of intracellular signaling pathways, and regulation of translation and transcription (*6*). The successful reduction in inflammatory responses is a major strategy for dealing with aGvHD.

5-Aminolevulinic acid (5-ALA) is a precursor of heme found in plants, bacteria, fungi, and animals (*7*). It is an endogenous amino acid in animals and the first

compound produced by 5-ALA synthase in the heme biosynthetic pathway. Growing evidence supports the notion that 5-ALA combined with sodium ferrous citrate (5-ALA/SFC) exerts antioxidant, anti-inflammatory and anti-fibrotic properties (*8-11*). In addition, 5-ALA/SFC has been used to treat a variety of animal models, including inflammatory disease, transplantation, autoimmune disease and sclerodermatous issues induced by chronic GvHD, which may explain its anti-inflammatory, immunoregulation and cytoprotective properties exerted *via* the upregulation of heme oxygenase (HO)-1 expression and release of heme metabolites (*12,13*).

In the present study, we investigated the effects of 5-ALA/SFC treatment modulating inflammatory responses and liver injury in aGvHD mice. Evidence supporting the anti-inflammatory, immunoregulation and cytoprotective properties of 5-ALA/SFC was obtained, and possible mechanisms underlying these effects were confirmed. Such evidence included direct amelioration of liver injury, reduction in liver-infiltrating T lymphocytes and modulation of the liver mRNA expression of inflammatory-related cytokines and chemokines. Furthermore, 5-ALA/SFC treatment also enhanced the proliferator-activated receptor-γ coactivator (PGC-1α) expression in liver tissue, potentially explaining the downregulation of the inflammatory signaling pathways in the aGvHD model treated with 5-ALA/SFC.

2. Materials and Methods

2.1. Mice

Male 7- to 8-week-old C57BL/6NJcl × DBA/2NJcl (B6D2F1, H-2k$^{b/d}$) and 8- to 12-week-old C57BL/6NJcl (B6/J, H-2k^{b}) mice were purchased from CLEA Japan, Inc. (Tokyo, Japan). Mice were maintained on a 12-h light-dark cycle and given free access to food and water except during the period of caloric restriction for the pair-feeding group. All animal manipulations were performed according to the recommendations of the Committee on the Care and Use of Laboratory Animals at the National Research Institute for Child Health and Development in Tokyo, Japan (Permission number: A2009-010-C11).

2.2. Experimental procedure for the aGvHD model and grouping

Spleens were aseptically harvested from B6/J mice separately, and the tissue was dissociated by rubbing to generate a single-cell suspension. Red blood cells were lysed using 10× phosphate-buffered saline (PBS) and pure water, viable cells were counted by trypan blue dye exclusion on a hemocytometer, and individual cells were resuspended in RPMI 1640 (Gibco BRL, Grand Island, NY). aGvHD was induced by the intravenous injection of 1 × 10^8 B6/J donor splenocytes into unirradiated B6D2F1 recipients.

The mice were pair-fed, and body weight was monitored weekly. At the indicated time point on days 7 and 14, mice were sacrificed, and the serum, liver and spleen tissue were collected for the measurement of serum enzymes alanine transaminase (ALT) and aspartate transaminase (AST) levels, counting of liver-infiltrating cells and mRNA expression analyses.

Mice were randomly assigned to two groups: those receiving 5-ALA hydrochloride (100 mg/kg; neo ALA Co. Ltd, Tokyo, Japan) and SFC (157 mg/kg) (Komatsuya Corporation, Osaka, Japan) daily from days 0 to 7 or 14 as the 5-ALA/SFC-group, those receiving distilled water as the control group.

2.3. Histopathological analyses

For the histopathological examination, liver samples were collected after the animals were sacrificed by anesthesia and fixed in 10% formaldehyde, then embedded in paraffin. Sections of 4 μm were processed and stained with hematoxylin-eosin (HE; MUTO PURE CHEMICALS, Osaka, Japan) according to a previously described method (*14*). A light microscopic analysis was performed to assess the overall cellularity and liver damage using a digital camera (BX51, OLYMPUS, Tokyo, Japan). To facilitate a semiquantitative assessment of aGVHD, grading of aGVHD was confined to analysis of the liver. The histological assessment was performed according to the scoring system with slight modification (*15*). Inflammatory cell infiltrates in the portal tract and around the central veins were graded on a scale of 1 to 5 as follows: Grade 1, normal or minimal perivascular cuffing; Grade 2, perivascular cuffing, 1-2 cells in thickness, involving up to 10% of vessels; Grade 3, perivascular cuffing, 1-4 cells in thickness, involving 10-30% of vessels; Grade 4, perivascular cuffing, 3-6 cells in thickness, involving 30-50% of vessels; Grade 5, perivascular cuffing, ≥7 cells in thickness, involving > 50% of vessels. Scoring was performed in a blinded manner.

2.4. Liver enzyme measurements

Serum levels of ALT and AST are commonly used as biochemical indicators of liver injury. Blood samples were obtained to evaluate serum ALT and AST levels using commercially available kits (Fujifilm, Tokyo, Japan) measured by an automatic biochemical analyzer (DRI-CHEM 3500i; Fujifilm) according to the manufacturer's protocol.

2.5. Isolation of nonparenchymal cells (NPCs) from the liver

Mice were chosen randomly from each group on day 7 and 14 after the lymphocyte injection. The liver was

mashed and passed through a 70-μm nylon cell strainer on ice; then, the tissue liquid was centrifugated at 4°C for 1 min at 60 g, and the supernatant was collected for washing twice with PBS. NPCs were purified by centrifugation at room temperature for 25 mins over a 40% discontinuous Percoll gradient (Sigma-Aldrich, St. Louis, MO). The NPCs were then suspended in PBS for flow cytometry (FCM) and RLT buffer for a quantitative real-time polymerase chain reaction (PCR) analysis.

2.6. Flow Cytometer (FCM) analysis

NPCs and splenocytes were incubated with directly labeled antibodies for 30 mins, washed with PBS and fixed in 1% paraformaldehyde. Immune cell composition was determined *via* FCM. Liver NPCs and splenocytes were then treated with purified anti-mouse CD16/32 (BioLegend, San Diego, CA) and stained with a defined panel containing Live/Dead stain (L34957; Thermo Fisher Scientific, Waltham, MA) to mark the living and dead cells. In addition, liver NPCs in all panels were stained with anti-CD45 (30-F11; BioLegend) to gate the white blood cells (WBCs). NPCs and splenocytes then were stained with anti-CD3 (145-2C11), anti-CD4 (GK1.5), anti-CD8 (53-6.7), anti-NKp46 (29A1.4), anti-CD11b (M1-70), anti-CD11c (N418), anti-B220 (RA3-6B2), anti-Ly6G (1A8), anti-Ly6C (HK1.4), anti-IA/IE (M5/114.15.2), anti-CD40 (3/23), anti-CD80 (16-10A1) and anti-CD86 (GL-1) mAbs conjugated with a particular fluorochrome, and corresponding isotype controls were used (BioLegend). The analysis of stained cells was performed with a BD FACS LSR Fortessa, Franklin Lakes, NJ), and analyzed by the FlowJo software program (Version 10.5.0; BD Biosciences).

2.7. RNA preparation and quantitative real-time PCR

To measure the inflammation and cytokine gene expression in liver tissue, total RNAs of liver were isolated with the Trizol reagent (Invitrogen, Carlsbad, CA). A total of 800 ng of each RNA sample was reverse-transcribed to cDNA using oligo (dT) primers and Super Script reverse transcriptase (Invitrogen). The target-specific primers and probes listed in Table 1 were designed based on the reported cDNA sequences and synthesized by Biosearch Technologies (Novato, CA). Four-step PCR was performed for 45 cycles. Quantitative real-time PCR was performed using the TaqMan and SYBR® Green-based system with an Applied Biosystem PRISM7700 (Thermo Fisher Scientific). 18s was used as the housekeeping gene. The final result was analyzed by the $2^{-\Delta\Delta}$Ct method.

2.8. Statistical analysis

The results were expressed as the mean ± standard deviation (SD). All data were analyzed using the GraphPad Prism software program (version 7.0, GraphPad Software, San Diego, CA). A one-tailed unpaired Student's *t*-test were used to compare two groups, and a one-tailed Wilcoxon's matched-pairs signed rank test was used to compare two groups. In cases with a normal distribution, a one-way analysis of variance (ANOVA) with Tukey's multiple comparisons test was used to compare multiple groups, while in cases with a non-normal distribution, a one-way ANOVA with Dunn's multiple comparisons test was used to compare multiple groups. P values of < 0.05 were considered to indicate statistical significance.

3. Results

3.1. 5-ALA/SFC treatment ameliorated liver injury in aGvHD

To investigate the therapeutic effect of 5-ALA/SFC on liver injury, we used a mouse model of aGvHD, established by transferring 1×10^8 spleen cells from donor B6/J (H-$2k^b$) mice into recipient B6D2F1 (H-$2k^{b/d}$) mice, and recipient mice were treated with a combination of 5-ALA and SFC orally administered at 100 mg/kg and 157 mg/kg daily, respectively. In the aGvHD control group, the mouse weight loss was obvious. However, in the 5-ALA/SFC treatment group, the weight decreased significantly more slowly (Figure 1A). In addition, we also examined the serum levels of ALT and AST at the baseline before treatment as well as on days 7 and 14 in aGvHD mice. As shown as in Figure 1B, compared with the control group on day 14, the serum ALT and AST levels of the mice in the 5-ALA/SFC-treated group were significantly decreased. Furthermore, pathological changes in the liver were observed by light microscopy after HE staining. The histology of the representative liver specimen of aGvHD mice was observed after HE staining on days 7 and 14. The samples showed lymphoid cell infiltration, and the histology score was determined. 5-ALA/SFC treatment prevents pathological changes in the liver, and improvements in the liver samples of the 5-ALA/SFC treatment group were observed in all samples (Figure 1C).

3.2. 5-ALA/SFC treatment decreased the liver-infiltrating T cells on day 14 in aGvHD

In order to understand how 5-ALA/SFC treatment modulates the cellular response in aGvHD, we performed a multicolor FCM analysis on 5-ALA/SFC-treated mice on days 7 and 14 after the spleen cells had been transplanted. As shown as in Figure 2, we found that, compared with naïve mice, the populations of liver-infiltrating cells and spleen cells were increased on days 7 and 14 in the aGvHD model mice, indicating that liver and spleen inflammation was induced after donor cell transplantation. In addition, the total number of $CD3^+$ T

Table 1. The sequences information of the primers and probes used in the study

Genes	Forward (5'- 3') primers	Reverse (5'- 3') primers	Probes
Taqman primers and probes			
PGC-1α	CATTTGATGCACTGACAGATGGA	CCGTCAGGCATGGAGGAA	CCGTGACCACTGACAACGAGGCC
HO-1	CAGGGTGACAGAAGAGGCTAAGAC	TCTTTGTGTTCCTCTGTCAGCAGT	TCCTGCTCAACATTGAGCTGTTTGAGGA
Nrf-2	GCCCTCAGCATGATGGACTTG	TGCCTCCAAAGGATGTCAATCAA	AGTTGCCACCGCCAGGACTACAGTCC
Sirt-1	CAGCATCTTGCCTGATTTGTAAATAC	CACCGAGGAACTACCTGATTAAAAA	TCTCCACGAACAGCTTCACAATCAACT
IFN-γ	AAGCGTCATTGAATCACACCTGA	ACCTGTGGGTTGTTGACCTCAA	ACTACCTTCTTCAGCAACAGCAAGGCGA
TNF-α	TGTCTACTGAACTTCGGGGTGAT	AACTGATGAGAGGGAGGCCAT	TCCCCAAAGGGATGAGAAGTTCCCAA
IL-1β	ACCCCAAAAGATGAAGGGCTG	GTGCTGCTGCGAGATTTGAAG	TCTCATCAGGACAGCCCAGGTCAAAGGT
CCL-2	GTTGGCTCAGCCAGATGCAG	GTAGCTCTCCAGCCTACTCATTG	CCCACTCACCTGCTGCTACTCATTCACC
CCL-3	TCCCAGCCAGGTGTCATTTTC	AGGCATTCAGTTCCAGGTCAG	ACCCAGGTCTCTTTGGAGTCAGCGCA
CCR-2	CCTGTAAATGCCATGCAAGTTCA	CCGTGGATGAACTGAGGTAACATA	ACCAGAAGAGGGCATTGGATTCACCACAT
NF-κB	TGTCTGCCTCTCTCGTCTTCCT	CACCACTGTCACAGACGCTGT	CGAGGCAGCACATAGATGAACTCCGG
18s	ATGAGTCCACTTTAAATCCTTTAACGA	CTTTAATATACGCTATTGGAGCTGGAA	ATCCATTGGAGGGCAAGTCTGGTGC
SYBR green primers and probes			
Sulf-2	ATCCAGACCTTCTATTTCCAGGC	GTTGGGCCGGATGTTCCTG	
18s	ATGAGTCCACTTTAAATCCTTTAACGA	CTTTAATATACGCTATTGGAGCTGGAA	

cells was significantly increased on day 14, that of $CD4^+$ T cells was increased on day 7, and that of $CD8^+$ T cells was increased on day 14 (data not shown), indicating that $CD4^+$ and $CD8^+$ T cells play important roles in different phases of aGvHD.

Regarding the effect of 5-ALA/SFC treatment, we found that, compared with the control group, the T cell percentage among the liver-infiltrating $CD45^+$ cells was reduced in the 5-ALA/SFC treatment group. In addition, we detected other immune cells in the liver and spleen after splenocyte transplantation into recipient mice. As shown in Supplementary Figure S1A (*http://www.ddtjournal.com/action/getSupplementalData.php?ID=68*), compared with the data on day 7 the percentages of NK cells, NKT cells, neutrophils, monocytes, macrophages and dendritic cells among the liver-infiltrating cells were reduced on day 14, although there were no significant differences between the control and 5-ALA/SFC-treated groups, indicating that T cells are the main cells involved in aGvHD, and after 5-ALA/SFC treatment, the population of liver-infiltrating T cells is significantly decreased, with improvements in liver inflammation noted. Furthermore, we found that the populations of T cells, neutrophils, monocytes and macrophages were increased in the spleens of recipient mice, demonstrating spleen injury in aGvHD mice (Supplementary Figure S1B, *http://www.ddtjournal.com/action/getSupplementalData.php?ID=68*).

3.3. 5-ALA/SFC treatment upregulated the PGC-1α expression in the liver tissue of aGvHD mice

Next, we wanted to determine the possible mechanism by which 5-ALA/SFC modulates the inflammatory response. PGC-1α regulates the molecular pathway linking oxidative stress and mitochondrial metabolism with the inflammatory response and metabolic syndrome (*16*). We therefore explored the expression of PGC-1α, which exerts a protective effect against inflammation in the liver tissue (*17-19*), as one potential cause of these phenomena.

As shown in Figure 3, we found that the mRNA expression of PGC-1α was significantly higher in 5-ALA/SFC-treated mice than in control mice. In addition, 5-ALA/SFC treatment enhanced the expression of mRNA from HO-1 and nuclear factor erythroid 2-related factor 2 (Nrf-2), which activate the transcription factor Sirtuin-1 (Sirt-1) to promote mitochondrial fusion and biogenesis, partly through an increase in the mRNA expression of PGC-1α. Thus, these data indicated that the activation of PGC-1α by 5-ALA/SFC through enhanced HO-1, Nrf-2, and Sirt-1 expression resulted in the improved modulation of the inflammatory response.

3.4. 5-ALA/SFC treatment decreased the mRNA expression of inflammation-related genes in the liver tissue of aGvHD mice

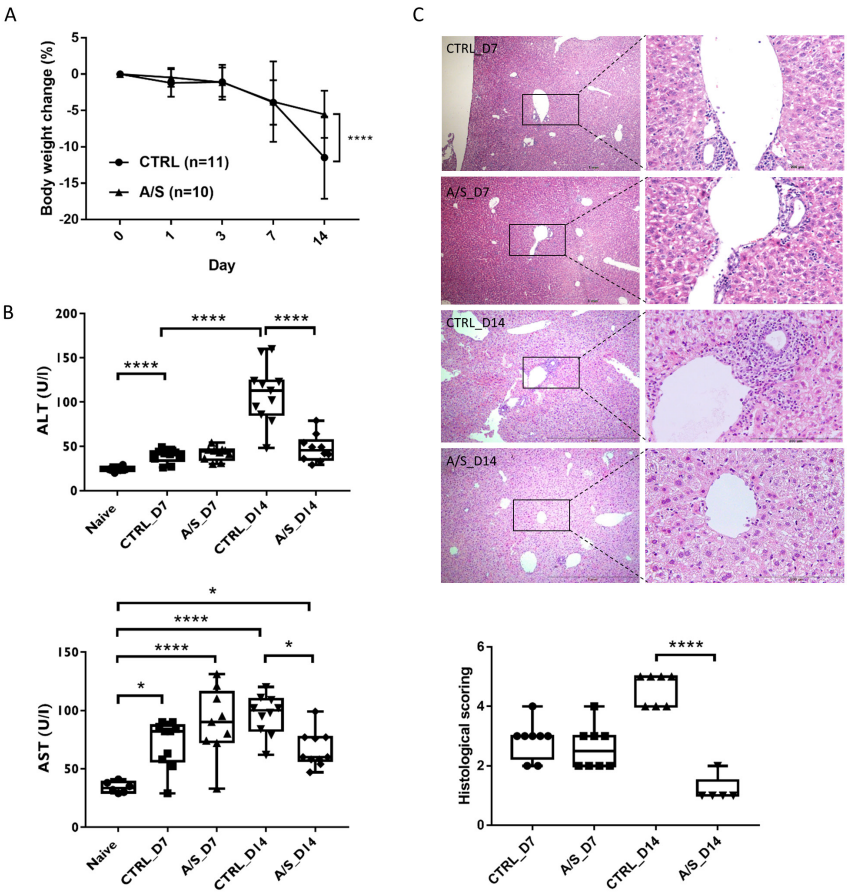

Figure 1. 5-ALA/SFC treatment ameliorated liver injury in aGvHD mice. A. The weight loss of the control group was markedly reduced during aGvHD, and in the 5-ALA/SFC-treated group, the weight reduced more slowly. Data were analyzed and presented as the mean ± SEM; $^{****}p < 0.0001$ compared with the control group. **B.** Serum ALT and AST levels were measured. Compared with the control group, the serum ALT and AST levels in the 5-ALA/SFC-treated group were significantly decreased. Data were analyzed and presented as the means ± SD; $^{*}p < 0.05$, $^{****}p < 0.0001$. **C.** The representative histological changes of the liver were observed on days 7 and 14 from aGvHD mice after HE staining, revealing inflammatory cell infiltration, which had improved in the liver samples from the 5-ALA/SFC treatment groups. Based on HE staining, the histology score was determined. 5-ALA/SFC treatment prevents pathological changes in the liver. Values are shown as the means ± SD; $^{****}p < 0.0001$.

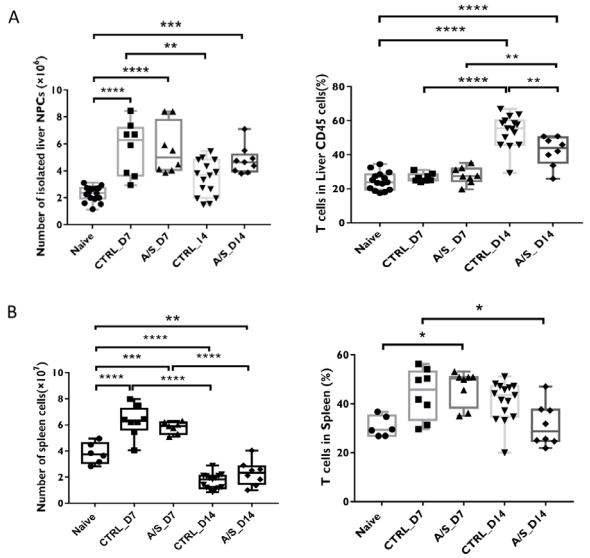

Figure 2. 5-ALA/SFC treatment alleviated the activation of liver-infiltrating T cells in aGvHD mice. Compared with the naïve group, the number of isolated liver NPCs on days 7 and 14 was increased in the aGvHD groups. Among the total lymphocytes, representative data showed that gated T cells were decreased in the 5-ALA/SFC-treated group. Percentages represent the means ± SD; $^{*}p < 0.05$, $^{**}p < 0.01$, $^{***}p < 0.001$, $^{****}p < 0.0001$.

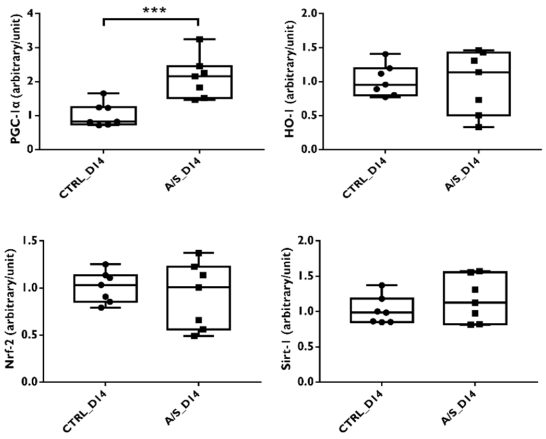

Figure 3. 5-ALA/SFC treatment increased the mRNA expression of PGC-1α in aGvHD mice. Liver tissue was collected on day 14, and the mRNA expression of PGC-1α, HO-1, Nrf-2 and Sirt-1 was analyzed by qRT-PCR, as described in the Materials and Methods. Compared with the control group, the mRNA levels were significantly different in the liver tissues of the 5-ALA/SFC group. Values are shown as the means ± SD; $^{***}p < 0.001$.

In order to analyze how 5-ALA/SFC ameliorated liver injury, we conducted quantitative real-time PCR for several kinds of inflammatory cytokines and chemokines in liver tissue that are known to be major contributors to the development of aGvHD and lead to liver injury. As shown as in Figure 4, the expression of TNF-α, IFN-γ, IL-1β, CC chemokine ligands 2 and 3 (CCL-2 and CCL-3, respectively) and NF-κB was increased in aGvHD mice, but 5-ALA/SFC treatment significantly reduced the expression of these genes. In addition, we found that 5-ALA/SFC treatment enhanced the mRNA expression of CC chemokine receptor 2 (CCR-2), which controls leukocyte migration during inflammatory processes and has dual pro- and anti-inflammatory actions. Furthermore, we found that, compared with control mice, the expression of heparan sulfate 6-O-endosulfatase (Sulf)-2, an extracellular sulfatase that acts on heparan sulfate proteoglycans and modulates multiple signaling pathways (*20*) was decreased after 5-ALA/SFC treatment.

4. Discussion

aGvHD was briefly induced by donor T cells attacking recipient tissue contained in the transplant. Based on previous experimental models, the development of aGvHD involves three stage: first, activation of antigen-presenting cells (APCs); then, donor T cell activation, proliferation, differentiation and migration; finally, target tissue destruction (*21,22*). Therefore, in addition to end-organ damage, aGvHD also results in the immune response of T-cell activation and expansion. Thus far, several strategies for combatting aGvHD have been proposed, include targeting mediators of cytokine storm, such as TNF-α and IL-1/IL-1β, with antagonists (*23*), as well as reducing the intensity of conditioning regimens to avoid causing excessive inflammation (*22*).

In the present study, we transferred B6/J splenocytes into recipient B6D2F1 mice to develop an aGvHD model and investigated the therapeutic effect of 5-ALA/SFC on this disease. During the development of this model, on days 7 and 14, the mice showed liver and spleen injury in addition to weight reduction. After treatment with a 5-ALA/SFC, however, an assessment of the serum and pathological features indicated that the liver damage had been ameliorated (Figure 1).

Many reports in addition to our own have shown that 5-ALA/SFC has an anti-inflammatory effect in different kinds of diseases (*24-33*). Liver injury is a major end-organ damage that occurs in aGvHD, wherein the inflammatory response dominates the disease phase (*21*). However, while there are already many strategies for dealing with this kind of disease, previous approaches have had a rather broad spectrum and often affect the overall immune system reconstruction (*34*). Few reports have described the inhibitory effect of 5-ALA/SFC on aGvHD, especially in liver injury. Therefore, in the present study, we administered 5-ALA/SFC to a murine aGvHD model to determine whether or not it had a protective effect against liver damage.

Regarding immune cells of the liver and spleen, recent studies have reported that donor T cells occupy a central role in mediating aGvHD. In our study, on day 14, although the total cells isolated from the liver were fewer than had been noted on day 7, the population of liver-infiltrating T cells, specially $CD8^+$ T cells, was increased, indicating that T cells play a central role in aGvHD. This population was significantly decreased following 5-ALA/SFC treatment, and a decrease was also noted in spleen cells compared with the control mice (Figure 2). This finding may explain the reduced weight, reduced serum level and pathological features of liver damage, although

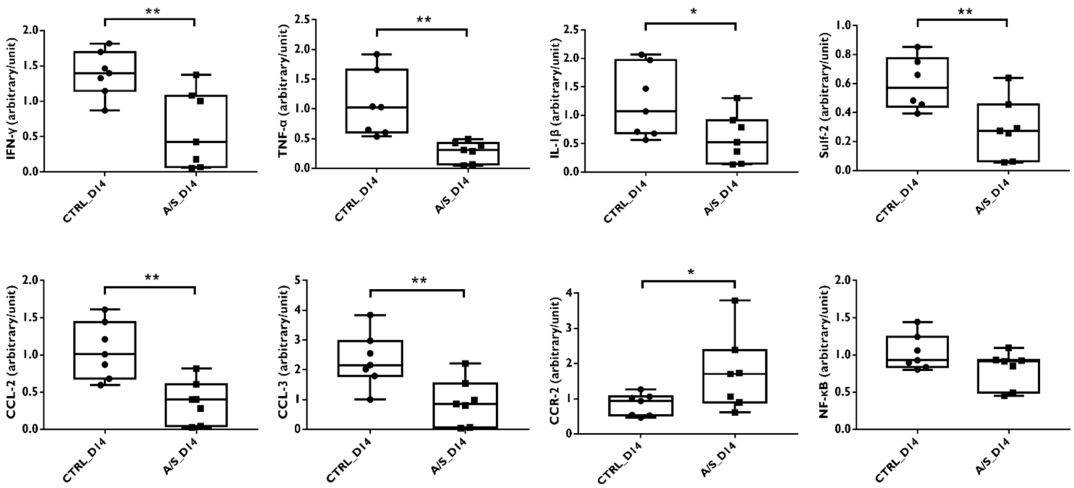

Figure 4. 5-ALA/SFC treatment decreased the mRNA expression of inflammatory-related genes in aGvHD mice. Liver were collected on day 14, and the mRNA expression of IFN-γ, TNF-α, IL-1β, CCL-2, CCL-3, CCR-2, Sulf-2 and NF-κB was analyzed by RT-PCR, as described in the Materials and Methods. Compared with the control group, the mRNA levels were significantly different in the liver tissues of the 5-ALA/SFC group. Values are shown as the means ± SD; $^{*}p < 0.05$, $^{**}p < 0.01$.

there were no significant differences in other immune cells, including NK cells, NKT cells, macrophages and dendritic cells, in the liver and spleen. However, the numbers of neutrophils and monocytes were significantly increased in the spleen following 5-ALA/SFC treatment (Supplementary Figure S1, *http://www.ddtjournal.com/action/getSupplementalData.php?ID=68*). These results indicate that 5-ALA/SFC treatment mainly targets T cells, which are primarily involved in aGvHD, resulted in the amelioration of liver inflammation and improvement in its function.

PGC-1α plays a beneficial role in the regulation of hepatic steatosis and insulin resistance by enhancing the IL-10-mediated anti-inflammatory response (*35,36*). In addition, inflammation can be regulated through changes in cellular reactive oxygen species induced by PGC-1α (*37*). Future studies should endeavor to identify the molecular mechanisms involved in the PGC-1α-mediated downregulation of inflammatory signaling pathways. Regarding the possible protective mechanism of 5-ALA/SFC against liver injury in the aGvHD model, we hypothesized that the activation of PGC-1α signaling might be intimately involved. We demonstrated that the mRNA expression of PGC-1α was significantly increased in the 5-ALA/SFC treatment group compared with the control group, which might be sufficient to enhance the mitochondrial function and ameliorate hepatic inflammatory cell infiltration (Figure 3). Therefore, we proposed that PGC-1α might played a vital role in our aGvHD mouse model by mediating the inflammatory response and reducing oxidative damage. In addition to an increased expression of PGC-1α, 5-ALA/SFC treatment also resulted in an increased mRNA expression of HO-1, Nrf-2 and Sirt-1, suggesting that the upregulation of PGC-1α might be achieved *via* the Nrf-2, HO-1 and Sirt-1 pathway, which enhances the mitochondrial function *in vitro* (*38,39*). Of note, Sirt-1 can deacetylate downstream targets, such as NF-κB, which is a key transcriptional factor in pro-inflammation responses (Figure 3) (*40*). Our data showed that with the expression of Sirt-1 and PGC-1α was increased while that of NF-κB was reduced (Figure 4). HO-1's oxidative stress-protective effects are strongly associated with Sirt-1 upregulation. The increases in both Sirt-1 and HO-1 found in this study point to the existence of a common mechanism mediating the anti-inflammatory, anti-proliferative and cytoprotective effects, all of which result from oxidative stress induced by both Sirt-1 and HO-1 (*41*). Taken together, our data show that 5-ALA/SFC treatment significantly increased the PGC-1α expression in liver tissue, highlighting a possible mechanism underlying the protective effect of 5-ALA/SFC.

Because inflammatory cytokines and chemokines are well-known inducers of leukocyte trafficking and activation and contribute to the pathogenesis of aGvHD (*2*), we detected the mRNA expression of related cytokines and chemokines in the liver. We found that 5-ALA/SFC treatment significantly reduced the expression of IFN-γ, TNF-α, IL-1β, CCL-2 and CCL-3 while increasing the CCR-2 expression (Figure 4). CCR-2 and its main ligand, CCL-2, are a chemokine receptor-ligand pair that controls leukocyte migration during inflammatory processes (*42*). It is important to note that CCR-2 has both pro- and anti-inflammatory actions. The proinflammatory role of CCR-2 is dependent on APCs and T cells, whereas the anti-inflammatory role is dependent on its expression in regulatory T cells (*43*). In our study, the enhancement of CCR-2 was attributed to an anti-inflammatory function, resulting in the inhibition of the release of cytokines, such as TNF-α, INF-γ and IL-1β (Figure 4). However, in the present study, we found that, compared with control mice, the expression of Sulf-2 was reduced after 5-ALA/SFC treatment (Figure 4). This result suggested that Sulf-2 would offer considerable advantages as a therapeutic target, playing a protective role against epithelial injury and inflammation of the liver in aGvHD (*44*). Taken together, these results were consistent with the findings of an increased expression of PGC-1α and the liver pathologic features, indicating that 5-ALA/SFC can modulate the inflammatory response *via* the HO-1, Nrf-2, Sirt-1 and PGC-1α pathways.

In conclusion, our data showed that 5-ALA/SFC was effective for treating liver injury by modulating the inflammatory response in aGvHD mice. The mechanistically therapeutic effect of 5-ALA/SFC may rely on PGC-1α activation and reducing the liver mRNA expression of inflammatory-related cytokines and chemokines. Our research may offer a novel therapeutic option for aGvHD, and these data may encourage future studies of this promising therapeutic agent for the treatment of aGvHD.

Acknowledgements

The authors thank Yuko Sato for her invaluable technical assistance.

Funding: This study was supported by research grants from the Grants of Ministry of Education, Culture, Sports, Science and Technology of Japan (Grants-in-Aid 16K11064, 24/17H04277, 18K08558); and grants from the National Center for Child Health and Development (26-22).

Conflict of Interest: HI, KT, MN and TT are employees of SBI Pharmaceuticals Co., Ltd.

References

1. Kitazawa Y, Li XK, Liu Z, Kimura H, Isaka Y, Hunig T, Takahara S. Prevention of graft-versus-host diseases by *in vivo* supCD28mAb-expanded antigen-specific nTreg cells.

Cell Transplant. 2010; 19:765-774.
2. Weissman IL. Translating stem and progenitor cell biology to the clinic: barriers and opportunities. Science. 2000; 287:1442-1446.
3. Blazar BR, Korngold R, Vallera DA. Recent advances in graft-versus-host disease (GVHD) prevention. Immunol Rev. 1997; 157:79-109.
4. Billingham RE. The biology of graft-versus-host reactions. Harvey Lect. 1966; 62:21-78.
5. Sackstein R. A revision of Billingham's tenets: the central role of lymphocyte migration in acute graft-versus-host disease. Biol Blood Marrow Transplant. 2006; 12:2-8.
6. Magenau J, Reddy P. Next generation treatment of acute graft-versus-host disease. Leukemia. 2014; 28:2283-2291.
7. Kang Z, Zhang J, Zhou J, Qi Q, Du G, Chen J. Recent advances in microbial production of delta-aminolevulinic acid and vitamin B12. Biotechnol Adv. 2012; 30:1533-1542.
8. Fujino M, Nishio Y, Ito H, Tanaka T, Li XK. 5-Aminolevulinic acid regulates the inflammatory response and alloimmune reaction. Int Immunopharmacol. 2016; 37:71-78.
9. Ito H, Nishio Y, Hara T, Sugihara H, Tanaka T, Li XK. Oral administration of 5-aminolevulinic acid induces heme oxygenase-1 expression in peripheral blood mononuclear cells of healthy human subjects in combination with ferrous iron. Eur J Pharmacol. 2018; 833:25-33.
10. Mahmoudi K, Garvey KL, Bouras A, Cramer G, Stepp H, Jesu Raj JG, Bozec D, Busch TM, Hadjipanayis CG. 5-aminolevulinic acid photodynamic therapy for the treatment of high-grade gliomas. J Neurooncol. 2019; 141:595-607.
11. Nakai Y, Inoue K, Tsuzuki T, Shimamoto T, Shuin T, Nagao K, Matsuyama H, Oyama M, Furuse H, Ozono S, Miyake M, Fujimoto K. Oral 5-aminolevulinic acid-mediated photodynamic diagnosis using fluorescence cystoscopy for non-muscle-invasive bladder cancer: A multicenter phase III study. Int J Urol. 2018; 25:723-729.
12. Hou J, Cai S, Kitajima Y, Fujino M, Ito H, Takahashi K, Abe F, Tanaka T, Ding Q, Li XK. 5-Aminolevulinic acid combined with ferrous iron induces carbon monoxide generation in mouse kidneys and protects from renal ischemia-reperfusion injury. Am J Physiol Renal Physiol. 2013; 305:F1149-1157.
13. Liu C, Yang X, Zhu P, Fujino M, Ito H, Takahashi K, Nakajima M, Tanaka T, Wang J, Zhuang J, Zou H, Li XK. Combination of 5-aminolevulinic acid and iron prevents skin fibrosis in murine sclerodermatous graft-versus-host disease. Exp Dermatol. 2018; 27:1104-1111.
14. Li S, Fujino M, Ichimaru N, Kurokawa R, Hirano S, Mou L, Takahara S, Takahara T, Li XK. Molecular hydrogen protects against ischemia-reperfusion injury in a mouse fatty liver model *via* regulating HO-1 and Sirt1 expression. Sci Rep. 2018; 8:14019.
15. Song EK, Yim JM, Yim JY, *et al.* Glutamine protects mice from acute graft-versus-host disease (aGVHD). Biochem Biophys Res Commun. 2013; 435:94-99.
16. Rius-Perez S, Torres-Cuevas I, Millan I, Ortega AL, Perez S. PGC-1alpha, inflammation, and oxidative stress: An integrative view in metabolism. Oxid Med Cell Longev. 2020; 2020:1452696.
17. Handschin C, Spiegelman BM. The role of exercise and PGC1alpha in inflammation and chronic disease. Nature. 2008; 454:463-469.
18. Singh S, Simpson RL, Bennett RG. Relaxin activates peroxisome proliferator-activated receptor gamma (PPARgamma) through a pathway involving PPARgamma coactivator 1alpha (PGC1alpha). J Biol Chem. 2015; 290:950-959.
19. St-Pierre J, Drori S, Uldry M, Silvaggi JM, Rhee J, Jager S, Handschin C, Zheng K, Lin J, Yang W, Simon DK, Bachoo R, Spiegelman BM. Suppression of reactive oxygen species and neurodegeneration by the PGC-1 transcriptional coactivators. Cell. 2006; 127:397-408.
20. Singer MS, Phillips JJ, Lemjabbar-Alaoui H, Wang YQ, Wu J, Goldman R, Rosen SD. SULF2, a heparan sulfate endosulfatase, is present in the blood of healthy individuals and increases in cirrhosis. Clin Chim Acta. 2015; 440:72-78.
21. Ferrara JL, Levine JE, Reddy P, Holler E. Graft-versus-host disease. Lancet. 2009; 373:1550-1561.
22. Schroeder MA, DiPersio JF. Mouse models of graft-versus-host disease: advances and limitations. Dis Model Mech. 2011; 4:318-333.
23. Uberti JP, Ayash L, Ratanatharathorn V, *et al.* Pilot trial on the use of etanercept and methylprednisolone as primary treatment for acute graft-versus-host disease. Biol Blood Marrow Transplant. 2005; 11:680-687.
24. Machado MP, Rocha AM, de Oliveira LF, *et al.* Autonomic nervous system modulation affects the inflammatory immune response in mice with acute Chagas disease. Exp Physiol. 2012; 97:1186-1202.
25. Cao W, Guo XW, Chen K, Xu RX, Zheng HZ, Wang J. Inhibition of hypoxia and serum deprivation-induced apoptosis by salvianolic acid in rat mesenchymal stem cells. J Tradit Chin Med. 2012; 32:222-228.
26. Chen T, Liu W, Chao X, Zhang L, Qu Y, Huo J, Fei Z. Salvianolic acid B attenuates brain damage and inflammation after traumatic brain injury in mice. Brain Res Bull. 2011; 84:163-168.
27. Fu J, Fan HB, Guo Z, Wang Z, Li XD, Li J, Pei GX. Salvianolic acid B attenuates spinal cord ischemia-reperfusion-induced neuronal injury and oxidative stress by activating the extracellular signal-regulated kinase pathway in rats. J Surg Res. 2014; 188:222-230.
28. Jiang P, Guo Y, Dang R, Yang M, Liao D, Li H, Sun Z, Feng Q, Xu P. Salvianolic acid B protects against lipopolysaccharide-induced behavioral deficits and neuroinflammatory response: involvement of autophagy and NLRP3 inflammasome. J Neuroinflammation. 2017; 14:239.
29. Lin M, Zhai X, Wang G, Tian X, Gao D, Shi L, Wu H, Fan Q, Peng J, Liu K, Yao J. Salvianolic acid B protects against acetaminophen hepatotoxicity by inducing Nrf2 and phase II detoxification gene expression *via* activation of the PI3K and PKC signaling pathways. J Pharmacol Sci. 2015; 127:203-210.
30. Liu B, Cao B, Zhang D, Xiao N, Chen H, Li GQ, Peng SC, Wei LQ. Salvianolic acid B protects against paraquat-induced pulmonary injury by mediating Nrf2/Nox4 redox balance and TGF-beta1/Smad3 signaling. Toxicol Appl Pharmacol. 2016; 309:111-120.
31. Lv H, Wang L, Shen J, Hao S, Ming A, Wang X, Su F, Zhang Z. Salvianolic acid B attenuates apoptosis and inflammation *via* SIRT1 activation in experimental stroke rats. Brain Res Bull. 2015; 115:30-36.
32. Zhang HS, Wang SQ. Salvianolic acid B from *Salvia miltiorrhiza* inhibits tumor necrosis factor-alpha (TNF-alpha)-induced MMP-2 upregulation in human aortic smooth muscle cells *via* suppression of NAD(P)H

oxidase-derived reactive oxygen species. J Mol Cell Cardiol. 2006; 41:138-148.
33. Zhou Z, Liu Y, Miao AD, Wang SQ. Salvianolic acid B attenuates plasminogen activator inhibitor type 1 production in TNF-alpha treated human umbilical vein endothelial cells. J Cell Biochem. 2005; 96:109-116.
34. Markey KA, MacDonald KP, Hill GR. The biology of graft-versus-host disease: experimental systems instructing clinical practice. Blood. 2014; 124:354-362.
35. Wan X, Zhu X, Wang H, *et al.* PGC1alpha protects against hepatic steatosis and insulin resistance *via* enhancing IL10-mediated anti-inflammatory response. FASEB J. 2020; 34:10751-10761.
36. Leveille M, Besse-Patin A, Jouvet N, Gunes A, Sczelecki S, Jeromson S, Khan NP, Baldwin C, Dumouchel A, Correia JC, Jannig PR, Boulais J, Ruas JL, Estall JL. PGC-1alpha isoforms coordinate to balance hepatic metabolism and apoptosis in inflammatory environments. Mol Metab. 2020; 34:72-84.
37. Buler M, Aatsinki SM, Skoumal R, Komka Z, Toth M, Kerkela R, Georgiadi A, Kersten S, Hakkola J. Energy-sensing factors coactivator peroxisome proliferator-activated receptor gamma coactivator 1-alpha (PGC-1alpha) and AMP-activated protein kinase control expression of inflammatory mediators in liver: induction of interleukin 1 receptor antagonist. J Biol Chem. 2012; 287:1847-1860.
38. Wu Z, Puigserver P, Andersson U, Zhang C, Adelmant G, Mootha V, Troy A, Cinti S, Lowell B, Scarpulla RC, Spiegelman BM. Mechanisms controlling mitochondrial biogenesis and respiration through the thermogenic coactivator PGC-1. Cell. 1999; 98:115-124.
39. Schreiber SN, Emter R, Hock MB, Knutti D, Cardenas J, Podvinec M, Oakeley EJ, Kralli A. The estrogen-related receptor alpha (ERRalpha) functions in PPARgamma coactivator 1alpha (PGC-1alpha)-induced mitochondrial biogenesis. Proc Natl Acad Sci U S A. 2004; 101:6472-6477.
40. Yu Q, Dong L, Li Y, Liu G. SIRT1 and HIF1alpha signaling in metabolism and immune responses. Cancer Lett. 2018; 418:20-26.
41. Davis PA, Pagnin E, Dal Maso L, Caielli P, Maiolino G, Fusaro M, Paolo Rossi G, Calo LA. SIRT1, heme oxygenase-1 and NO-mediated vasodilation in a human model of endogenous angiotensin II type 1 receptor antagonism: implications for hypertension. Hypertens Res. 2013; 36:873-878.
42. Charo IF, Peters W. Chemokine receptor 2 (CCR2) in atherosclerosis, infectious diseases, and regulation of T-cell polarization. Microcirculation. 2003; 10:259-264.
43. Deshmane SL, Kremlev S, Amini S, Sawaya BE. Monocyte chemoattractant protein-1 (MCP-1): an overview. J Interferon Cytokine Res. 2009; 29:313-326.
44. Yue X. Epithelial deletion of Sulf2 exacerbates bleomycin-induced lung injury, inflammation, and mortality. Am J Respir Cell Mol Biol. 2017; 57:560-569.

Received December 4, 2020; Revised December 21, 2020; Accepted December 27, 2020.

**Address correspondence to:*
Xiao-Kang Li, Division of Transplantation Immunology, National Research Institute for Child Health and Development, 2-10-1 Okura, Setagaya-ku, Tokyo, 157-8535 Japan.
E-mail: ri-k@ncchd.go.jp

Shuang-Qin Yi, Laboratory of Functional Morphology, Graduate School of Human Health Sciences, Tokyo Metropolitan University, 7-2-10, Higashiogu, Arakawa-Ku, Tokyo, 116-8551 Japan.
E-mail: yittmniu@tmu.ac.jp

Released online in J-STAGE as advance publication December 30, 2020.

Original Article

DOI: 10.5582/ddt.2020.03089

Leucocytosis and early organ involvement as risk factors of mortality in adults with dengue fever

Upendra Baitha[1], Sujay Halkur Shankar[1], Parul Kodan[1], Paras Singla[1], Jatin Ahuja[1], Samagra Agarwal[1], Anant Gupta[2], Pankaj Jorwal[1], Manish Soneja[1], Piyush Ranjan[1], Arvind Kumar[1], Kalpana Baruah[3], Ashutosh Biswas[1,*]

[1] Department of Medicine, All India Institute of Medical Sciences, New Delhi, India;
[2] Department of Hospital Administration, All India Institute of Medical Sciences, New Delhi, India;
[3] Additional Director cum Head of Office, Directorate of National Vector Borne Disease Control Programme, Directorate General of Health Services, Ministry of Health and Family Welfare, Government of India.

SUMMARY The clinical profile and risk factors for mortality in dengue fever have evolved over the years. The all-cause mortality in admitted dengue patients is around 6%. We aimed to evaluate the recent change in trends of the clinical characteristics and risk factors for in-hospital mortality in adults with dengue fever. This is a retrospective study on adults with confirmed dengue fever admitted in a medical unit of a tertiary care center in North India. Medical records of confirmed dengue fever patients admitted between January 2011, and December 2016 were reviewed. Chi-squared tests with Bonferroni correction for multiple testing were used to identify risk factors for mortality. 232 records were included, of which 66.8% were males. The mean age was 31.6 ± 14 years. There were 17 deaths with an all-cause mortality rate of 7.3% with 76.5% being classified as severe dengue at admission. Among the 17 mortality cases, dyspnea (47%), tachypnea (86.7%), leucocytosis (58.8%), raised urea (80%), and elevated serum creatinine (52.9%) at presentation were significantly associated with mortality ($p < 0.001$). Shock at any time during the hospital stay (58.8%) was also found to be significantly associated with mortality ($p < 0.001$). We found that dyspnea, tachypnea, acute kidney injury, and leucocytosis at presentation was significantly associated with in-hospital mortality. Based on our results, we recommend aggressive management of patients with severe dengue and those with mild/moderate disease with the above risk factors.

Keywords Dengue, clinical presentation, mortality, India, retrospective

1. Introduction

Dengue fever is rapidly re-emerging as an epidemic in the Indian subcontinent and spreading to newer areas across the globe (*1*). It continues to be a significant cause of morbidity and mortality, particularly in resource-limited settings in the countries of South-East Asia. A 2018 meta-analysis reported a pooled case fatality rate of 2.6% in India (*2*). The national statistics, however, puts the case fatality rate for 2019 to be about 0.09%. It is a matter of urgent public health priority for endemic countries like India (*3*).

Dengue can have a myriad of manifestations ranging from being asymptomatic to mild fever to having fatal complications. The in-hospital all-cause mortality for dengue fever is reported to be 5.9% as a result of referral bias (*4*). It is crucial to identify clinical and laboratory features which portend severe illness and are risk factors for poor outcomes. In the initial research around the risk factors for mortality, bleeding, and thrombocytopenia were given much importance (*5,6*). It was later discovered that bleeding is a marker for severity and thrombocytopenia did not portend poor outcomes. The focus later shifted to systemic and other organ involvement. The knowledge of mortality risk factors will help in better triage of patients and the efficient utilization of limited healthcare resources. The available evidence is, however, scarce and difficult to interpret.

We aimed to perform a retrospective analysis of the clinical characteristics of adult patients admitted with confirmed dengue fever. We further analyzed the admission characteristics that are risk factors for mortality in these patients.

2. Materials and Methods

This is a retrospective observational study on confirmed cases of dengue fever in adults. Ethical clearance was obtained from the institutional ethics committee. Medical records of confirmed cases of dengue fever admitted under the medical unit between January 2011 and December 2016 were reviewed. These records were classified under the codes A90 and A91 of the 10th Revision of the International Classification of Diseases (ICD)-10.

Inclusion criteria included admitted patients with either a positive Enzyme-Linked Immunosorbent Assay (ELISA) based NS-1 antigen test or a positive anti-dengue IgM antibody capture ELISA (MAC-ELISA) test. Any patient aged less than 14 years was excluded from the study. The cases were classified as mild, moderate, and severe dengue based on the national guidelines for the clinical management of dengue fever (*3*).

Mild dengue is fever without complications, signs of capillary leak, and organ involvement. Any patient with warning signs like recurrent vomiting, abdominal pain, lethargy, hepatomegaly, or signs of a capillary leak is classified as moderate dengue. Patient with extremes of age, pregnancy, diabetes, hypertension, coronary artery disease (CAD), hemoglobinopathy, immunosuppression, are at high risk and classified as moderate dengue. Dengue fever with significant bleeding, severe metabolic abnormalities, shock, or multiple organ involvement is classified as severe dengue.

Data were extracted to a predesigned proforma containing demographic details, presentation, investigations, and outcomes of the patients. This was analyzed using Stata 12 software (Stata Corp [2011], College Station, TX). Categorical variables are represented as frequency (percentage), while continuous variables are presented as mean (standard deviation) or median (interquartile range). Demographic details, presentation, and investigations were categorized into clinically meaningful subgroups. These were then analyzed using a Chi-square test or Fisher's exact test to identify differences based on the outcome of the patient (death *vs*. survival). Significance was considered at an alpha of 0.05 and a 95% confidence interval. The analysis was subjected to a Bonferonni correction to account for multiple tests. Following this, the *p*-value for significance was considered at a value < 0.002.

Table 1. Demographic characteristics of the study population.

Characteristics	Frequency (%)
Age	
14-30 years	138 (59.5)
31-45 years	57 (24.6)
46-60 years	26 (11.2)
> 60 years	11 (4.7)
Sex	
Male	155 (66.8)
Female	77 (33.2)
Hospital stay	
Less than 5 days	113 (48.7)
5-10 days	100 (43.1)
> 10 days	19 (8.2)
Comorbidities	
Hypertension	12 (5.2)
Diabetes Mellitus	07 (3.0)
Chronic kidney disease	04 (1.7)
Chronic liver disease	02 (0.9)
Others	19 (8.2)

3. Results

3.1. Demographic data and clinical profile at presentation

A total of 232 cases of confirmed dengue fever were included in the study after satisfying the inclusion criteria. The mean age was 31.6 ± 14 years, and 66.8 % were males. The demographic details are presented in Table 1. The median number of comorbidities in our cases was 0 (0, 0) with the maximum being three. 94.4% of the patients were from Delhi and the neighboring states of Haryana and Uttar Pradesh. The number of cases distributed by year is depicted in Figure 1.

Of the 232 patients, 42.7% of patients were classified as mild, 39.6% of patients were classified as moderate, and 17.7% had severe dengue. 47.8% presented between the 4th and 6th day of onset of fever (critical phase) with the mean duration of illness at a presentation being 5.7 ± 4.8 days. 15.1% of the patients were admitted beyond the 6th day of fever (recovery phase).

The clinical presentation of the patients is depicted in Table 2. Patients presenting with bleeding manifestations had a significantly lower platelet count at admission (32,000 cells/mm^3) when compared to those who did not present with bleeding manifestations (48,000 cells/mm^3). The most common sites of bleeding included mucosal bleed (21%) followed by bleeding from venipuncture site (21%). Menorrhagia in females (16% of females) was a common presenting complaint. Severe bleeding in the form of massive hematemesis or retroperitoneal hematoma was seen in 3% of the patients.

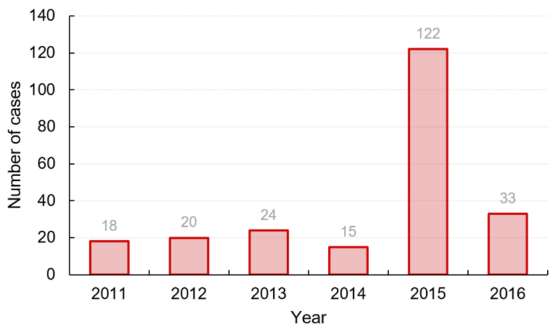

Figure 1. Year-wise distribution of cases in the study population (*n* = 232).

Table 2. Clinical profile of the study population (n = 232).

Clinical characteristic	Number of patients [n (%)]
Symptoms	
Fever	232 (100)
Myalgia	129 (55.6)
Recurrent vomiting	116 (50.0)
Headache	110 (47.4)
Abdominal pain	087 (37.5)
Bleeding	081 (34.9)
Oral	17 (21.0)
Venipuncture site	17 (21.0)
Malena	10 (12.3)
Hematemesis	08 (9.9)
Epistaxis	06 (7.4)
Hematuria	06 (7.4)
Hematochezia	04 (4.9)
Others	14 (17.3)
Rash	052 (22.4)
Arthralgia	039 (16.8)
Examination findings	
Pulse rate (mean ± SD)	88.7 ± 15.3
Systolic blood pressure (mmHg); (mean ± SD)	114.9 ± 20.44
Diastolic blood pressure (mmHg); (mean ± SD)	74.13 ± 15.17
Respiratory rate (mean ± SD)	19 ± 4.7
Hepatomegaly	20 (8.6)
Serositis (Ascites/pleural effusion)	47 (20.2)

Table 3. Risk factors for in-hospital mortality

Characteristic	Mortality [n (N)]	Survivor [n (N)]	p value
Demographic			
Age > 45 years	8 (17)	38 (215)	0.003
Male sex	13 (17)	142 (215)	0.380
Symptoms			
Rash	3 (17)	49 (214)	0.618
Bleeding manifestation	9 (17)	72 (212)	0.115
Headache	4 (17)	106 (213)	0.037
Abdominal pain	10 (17)	77 (213)	0.064
Dyspnea*	8 (17)	19 (213)	< 0.001
Arthralgia	1 (17)	38 (213)	0.21
Vomiting	9 (17)	107 (213)	0.83
Myalgia	6 (17)	123 (213)	0.073
Examination			
Pulse Rate > 100 bpm	6 (17)	11 (212)	0.060
Respiratory Rate > 20/min*	13 (15)	83 (209)	< 0.001
Shock*	10 (17)	10 (202)	< 0.001
Investigations			
Hemoglobin < 10 g/dL*	10 (17)	188 (207)	< 0.001
Corrected hematocrit > 20%	5 (15)	32 (208)	0.071
TLC < 4000 cells/mm^3	0 (17)	70 (205)	0.004
TLC > 11000 cells/mm^3*	10 (17)	20 (205)	< 0.001
Platelet < 50000 cells/mm^3	12 (17)	118 (213)	0.224
Urea > 20 mg/dL*	12 (15)	61 (185)	< 0.001
Serum creatinine > 1.2 mg/dL*	9 (17)	18 (186)	< 0.001
Transaminitis	8 (12)	92 (156)	0.60
Albumin < 3.5 g/dL	9 (12)	64 (147)	0.035

*Significance considered at $p < 0.002$ after Bonferroni correction

3.2. Organ system involvement

Acute kidney injury (AKI) was defined as serum creatinine greater than 1.2 mg/dL without a previous history or imaging evidence of chronic kidney disease. This was seen in 14.6% of our study population at presentation. A Fisher's exact test showed a significant association between hypotension at any point in the hospital stay and the presence of AKI (χ^2 = 26.45, df = 1, p = 0.002).

Transaminitis was defined as an elevation of alanine transaminase (ALT) or aspartate transaminase (AST) beyond three times the upper limit of normal (> 120 IU/L). This was seen in a total of 51.6% of 172 patients with available liver enzyme data. When transaminitis was present, the median AST/ALT ratio was 1.8 (1.3, 2.6), and the median total bilirubin level was 0.7 (0.4, 1.4). Hepatomegaly was seen in 20 patients. A Fisher's exact test showed no significant difference in the presence of hepatomegaly between those with and those without transaminitis (χ^2 = 0.006, df = 1, p = 0.9). There was also no significant difference in the presence of vomiting or pain abdomen at admission between those with and those without transaminitis (χ^2 = 0.21, df = 1, p = 0.64).

Complications involving the central nervous system (CNS) in the form of altered sensorium, drowsiness, seizures, or any features of encephalopathy or encephalitis were seen in 11.6% of the patients. One patient was diagnosed with dengue encephalitis with an initial presentation of fever, seizures, and headaches. Blood and CSF IgM antibodies for dengue were positive. Other causes of viral encephalitis (Herpes, Japanese encephalitis) were ruled out in this patient.

Twenty-five patients required invasive mechanical ventilation during their hospital stay. Respiratory failure (defined as a pf ratio < 300) was the indication in 48% of the patients.

3.3. Mortality and its risk factors

Seventeen patients died, leading to an all-cause mortality rate of 7.3%. Among the mortality cases, 13 were classified as severe dengue at admission. 11 out of the 17 patients did not have any comorbidities. A Mann Whitney U test did not show any significant differences in the number of comorbidities between the mortality and the survival cases. 15 out of the 17 mortality cases required invasive mechanical ventilation with eight being intubated for respiratory failure.

The demographic characteristics, symptoms, and laboratory investigations were categorized. Chi-square tests and Fisher's exact tests were done with Bonferroni corrections for multiple testing to identify differences between mortality cases and those that survived. This is depicted in Table 3. Dyspnea (χ^2 = 22.1, df = 1, p < 0.001), respiratory rate > 20/min (χ^2 = 12.6, df = 1, p < 0.001), total leucocyte count > 11,000 cells/mm^3 (χ^2 = 32.3, df = 1, p < 0.001), urea > 20 mg/dL (χ^2 = 13.2, df = 1, p < 0.001), and serum creatinine > 1.2 mg/dL (χ^2 = 25.3, df = 1, p < 0.001) at presentation were significantly associated with mortality. Shock at anytime during the hospital

Table 4. Clinical spectrum during hospital stay and outcome of cases categorized by severity of Dengue fever

Characteristic	Mild Dengue (N = 99)	Moderate Dengue (N = 92)	Severe Dengue (N = 41)
Day of illness at admission (Median (IQR))	4 (6, 7)	4.75 (6, 8)	4 (5, 9)
Number of patients with 1 or more risk factors (N (%))	0 (0)	26 (28.3)	14 (34.1)
Organ Involvement (N (%))			
Hepatic (Bilirubin > 2 mg/dL)	3 (3.0)	5 (5.4)	11 (26.8)
Renal (Creatinine > 1.2 mg/dL)	4 (4.0)	11 (11.9)	16 (39.0)
Neurologic (GCS < 15)	5 (5.1)	8 (8.7)	14 (34.1)
Respiratory (p/f ratio < 300)	1 (1.0)	7 (7.6)	12 (29.3)
Cardiovascular (MAP < 65 mmHg)	1 (1.0)	6 (6.5)	13 (31.7)
Mortality (N (%))	0 (0)	4 (4.3)	13 (31.7)

stay was also found to be significantly associated with mortality ($\chi^2 = 57.8$, df = 1, $p < 0.001$).

Among organ failures, we found that hepatic, renal, neurologic, respiratory, cardiovascular, and acute kidney injury were higher in patients with severe dengue (Table 4).

3.4. Co-infections

Twelve patients (~5%) were identified to have co-infections with other tropical fevers. Seven patients tested positive for malaria where all patients were infected with vivax malaria and one infected with mixed species of Plasmodium. Five patients were positive for IgM Chikungunya. All of these patients had an uneventful recovery.

4. Discussion

Our study analyzed dengue cases spanning over six years. In our analysis, we found that dyspnea, tachypnea, leucocytosis, and acute kidney injury at presentation were significantly associated with in-hospital mortality. The year 2015 contributed to the bulk of the cases in our study. This is in keeping with the national statistics as India experienced its worst outbreak in 2015 with a total of 99,913 recorded cases (*7*).

The initial assessment and triage of patients as mild, moderate, or severe can be useful during admission and management decision making. 13 out of the 17 deaths were classified as severe dengue at admission. This further emphasizes the need to classify and manage severe cases aggressively. Untreated severe dengue has a mortality as high as 20%. With treatment, this number can be as low as 1-2% (*8*). The mortality rate in our study is 7.3% reflecting a berksonian bias as our hospital is a tertiary care referral center.

We found that 100% of our cases presented with a history of fever. Asymptomatic disease is known in dengue and is thought to be a reservoir of infection during epidemics (*1*). However, in symptomatic dengue, fever is the most common symptom as described in our study. Special attention and close monitoring are recommended in pregnancy as they are prone to have a rapid downhill course. Among our study population, two women were admitted in the second trimester of pregnancy, and both were discharged without any feto-maternal complications. A study by Agarwal *et al.* who retrospectively analyzed 62 dengue cases in pregnancy concluded that dengue hemorrhagic fever (DHF)/dengue Shock Syndrome (DSS) was associated with significant maternal morbidity and mortality (*9*). Pregnancy-related management of dengue fever does not differ from the usual empirical treatment. However, monitoring of the patient and the fetus is required with interdepartmental coordination with Obstetrics and Gynecology.

AKI was present in 14.6% of our patients which is in keeping with existing quotes between 13 and 16% (*10,11*). Our study shows a 11.6% prevalence of neurologic manifestations. The quoted prevalence of neurologic manifestations (both central and peripheral) ranges between 0.5-20% (*12*). We did not note the presence of any peripheral nervous manifestations of dengue. Transaminitis was seen in nearly half the patients with available enzyme data. Our results suggest that dengue hepatitis consists of anicteric hepatitis wherein the bilirubin levels are normal/marginally elevated when compared to transaminases. The AST/ALT ratio is also greater than 1 in our study, which is classical of dengue hepatitis. It has been proposed that liver involvement in dengue is heralded by abdominal pain and vomiting, with some cases showing hepatomegaly (*13*). We, however, found that transaminitis is not significantly associated with abdominal pain, vomiting, or hepatomegaly. We would like to propose that this may be the case because abdominal pain and vomiting may also hint at an intestinal manifestation of dengue (dengue enteritis). Bowel wall oedema in the critical phase also manifests similarly, which may out shadow hepatitis which is usually seen late in the clinical course.

We found that shortness of breath and tachypnea at presentation was the only clinical features significantly associated with mortality. Tachypnea in dengue patients can be attributed to direct lung involvement, Acute Respiratory Distress Syndrome (ARDS), fluid overload, renal involvement, myocarditis,

or improper fluid management. It is important to note that neither thrombocytopenia nor bleeding manifestations at presentation were predictors of mortality. Thrombocytopenia, as a risk factor for mortality, was considered initially (*5,6*). Recent studies, however, show that thrombocytopenia is not a predictor for mortality. Some studies show that bleeding manifestations do predict mortality (*5,14*). We state that bleeding manifestations are a presentation of severe dengue and do not directly predict mortality. We found anemia (Hemoglobin < 10 g/dL) to be in much higher proportion in the survivor group. The explanation for the same is beyond us. However, we believe it hints at the presence of hemoconcentration at presentation and the need for appropriate fluid resuscitation. This, however, needs to be decided on a case-by-case basis.

Among organ failures, we found that acute kidney injury was associated with morality as supported by existing literature (*15*). While severe hepatitis (transaminitis > 1,000 IU/L) has been proposed as a predictor of mortality, we did not find such an association with transaminitis or severe hepatitis (*6,15*). Leucopenia is a known manifestation of dengue fever. It is interesting to note that we found a significant association between leucocytosis at presentation and mortality. This has been scarcely reported so far (*4*). We believe that these markers are an indication of close monitoring and aggressive management.

Seven patients in this study tested positive for malaria (all *Plasmodium vivax* and one mixed malaria), and five patients had IgM Chikungunya ELISA positive. This is an important observation as co-infections require a prompt diagnosis. Identification of one cause of the febrile illness may mask and delay the diagnosis of others. This may affect clinical outcomes and prognosis. Previous studies have also reported cases of co-infection (*16*). This finding highlights the importance of awareness of the possibility of concurrent infections. In countries like India, with the presence of seasonal epidemics of acute febrile illness, it becomes crucial to test broadly and rule out causes that have specific treatment modalities.

Atypical cases of dengue fever in our cohort included one case of CSF confirmed dengue encephalitis and one case of dengue with hemophagocytic lymphohistiocytosis (HLH). Dengue encephalitis is a rare manifestation attributed to the direct neurotropic effect of the virus (*12*). In highly endemic settings, dengue should also be suspected as an etiological agent in the evaluation of acute encephalitis syndrome. HLH is a hyper-inflammatory condition that may occur secondary to dengue infection, possibly due to the dysregulated immune system triggered by the virus. This patient had persistent fever, organomegaly, high ferritin, pancytopenia, low fibrinogen, and evidence of haemophagocytosis on bone marrow. He required steroids for management and was discharged in stable condition. This has been previously described only in case reports (*17,18*).

In conclusion, early diagnosis and close dynamic monitoring remain the key to the management of dengue fever. We found that shortness of breath and tachypnea at presentation was the only clinical features significantly associated with mortality. Acute kidney injury and leucocytosis at presentation were other markers that were significantly associated with in-hospital mortality. Based on our results, we recommend aggressive management of patients with severe dengue and those with mild/moderate disease with the above risk factors.

Funding: None.

Conflict of Interest: The authors have no conflicts of interest to disclose.

References

1. Bhatt S, Gething PW, Brady OJ, *et al*. The global distribution and burden of dengue. Nature. 2013; 496:504-507.
2. Ganeshkumar P, Murhekar MV, Poornima V, Saravanakumar V, Sukumaran, K, Anandaselvasankar A, Jonny D, Mehendale SM. Dengue infection in India: A systematic review and meta-analysis. PLoS Negl Trop Dis. 2018; 12:e0006618.
3. Dutta AK, Biswas A, Baruah K, Dhariwal AC. National guidelines for diagnosis and management of dengue fever/dengue haemorrhagic fever and dengue shock syndrome. J Indian Med Assoc. 2011; 109:30-35.
4. Jain S, Mittal A, Sharma SK, Upadhyay AD, Pandey RM, Sinha S, Soneja M, Biswas A, Jadon RS, Kakade MB, Dayaraj C. Predictors of dengue-related mortality and disease severity in a tertiary care center in North India. Open Forum Infect Dis. 2017; 4:ofx056.
5. Pinto RC, Castro DB de, Albuquerque BC de, Sampaio VS, Passos RA, Costa CF, Sadahiro M, Braga JU. Mortality predictors in patients with severe dengue in the state of Amazonas, Brazil. PLoS One. 2016; 11:e0161884.
6. Thomas L, Brouste Y, Najioullah F, Hochedez P, Hatchuel Y, Moravie V, Kaidomar S, Besnier F, Abel S, Rosine J, Quenel P, Cesaire R, Cabie A. Predictors of severe manifestations in a cohort of adult dengue patients. J Clin Virol. 2010; 48:96-99.
7. DENGUE/DHF SITUATION IN INDIA. National Vector Borne Disease Control Programme (NVBDCP) Available from: *https://nvbdcp.gov.in/index4.php?lang=1&level=0&linkid=431&lid=3715* (Accessed July 24, 2020).
8. Dengue and severe dengue. Available from: *https://www.who.int/news-room/fact-sheets/detail/dengue-and-severe-dengue* (Accessed July 24, 2020).
9. Agarwal K, Malik S, Mittal P. A retrospective analysis of the symptoms and course of dengue infection during pregnancy. Int J Gynaecol Obstet. 2017; 139:4-8.
10. Patel ML, Himanshu D, Chaudhary SC, Atam V, Sachan R, Misra R, Mohapatra SD. Clinical characteristic and risk factors of acute kidney injury among dengue viral infections in adults: A retrospective analysis. Indian J

Nephrol. 2019; 29:15.
11. Khalil MAM, Sarwar S, Chaudry MA, Maqbool B, Khalil Z, Tan J, Yaqub S, Hussain SA. Acute kidney injury in dengue virus infection. Clin Kidney J. 2012; 5:390-394.
12. Li GH, Ning ZJ, Liu YM, Li XH. Neurological manifestations of dengue infection. Front Cell Infect Microbiol. 2017; 7:449.
13. Samanta J, Sharma V. Dengue and its effects on liver. World J Clin Cases. 2015; 3:125-131.
14. dos Remédios Freitas Carvalho Branco M, de Albuquerque Luna EJ, Júnior LLB, de Olivera RV, Rios LTM, do Socorro da Silva M, Medeiros MNL, Silva GF, Nina FC, Lima TJ, Brito JA, de Oliveira AC, Pannuti CS. Risk factors associated with death in Brazilian children with severe dengue: a case-control study. Clinics (Sao Paulo). 2014; 69:55-60.
15. Huang HS, Hsu CC, Ye JC, Su SB, Huang CC, Lin HJ. Predicting the mortality in geriatric patients with dengue fever. Medicine (Baltimore). 2017; 96:e7878.
16. Bhat R, Kodan P, Shetty MA. Medley of infections-a diagnostic challenge. Asian Pac J Trop Biomed. 2015; 5:418-420.
17. Ray S, Kundu S, Saha M, Chakrabarti P. Hemophagocytic syndrome in classic dengue fever. J Glob Infect Dis. 2011; 3:399-401.
18. Kodan P, Chakrapani M, Shetty M, Pavan R, Bhat P. Hemophagocytic lymphohistiocytosis secondary to infections: a tropical experience! J Postgrad Med. 2015; 61:112-115.

Received September 19, 2020; Revised October 30, 2020; Accepted December 13, 2020.

**Address correspondence to:*
Ashutosh Biswas, Room No. 3094A, 3rd Floor, Teaching Block, Department of Medicine, All India Institute of Medical Sciences, Ansari Nagar, New Delhi – 110029, India.
E-mail: drashutoshbiswas@gmail.com

Released online in J-STAGE as advance publication December 27, 2020.

Original Article

DOI: 10.5582/ddt.2020.03098

Patient satisfaction with oral health check-ups at a community pharmacy and their effect on oral self-care habits and dental consultation behavior

Hiroki Iwata[1,2], Koichi Shibano[1], Mitsuhiro Okazaki[3,4], Kotaro Fujimaki[5,6], Noriko Kobayashi[1,2], Kazuko Fujimoto[1], Naoko Hayashi[1,2], Tomoyuki Goto[6,7], Katsunori Yamaura[1,2,*]

[1] Division of Social Pharmacy, Center for Social Pharmacy and Pharmaceutical Care Sciences, Faculty of Pharmacy, Keio University, Tokyo, Japan;
[2] Keio University Community Pharmacy, Tokyo, Japan;
[3] Department of Drug Policy & Management, Graduate School of Pharmaceutical Sciences, The University of Tokyo, Tokyo, Japan;
[4] Health Innovation & Technology Center, Faculty of Health Sciences, Hokkaido University, Hokkaido, Japan;
[5] Bubai Ohana Dental Clinic, Tokyo, Japan;
[6] Shinjuku Shoku-Shien Kenkyukai, Tokyo, Japan;
[7] Goto Dental Office, Tokyo, Japan.

SUMMARY Maintaining good oral health is important because oral diseases are related to systemic diseases, and community pharmacies play a key role in maintaining the health of local residents. This study aimed to examine the effects of oral health check-ups and information provision at community pharmacies on oral health-associated behaviors as well as patient satisfaction. We conducted oral health check-ups and provided information about oral health self-care to 84 patients at a community pharmacy, and then asked them to complete a questionnaire survey. One month later, we sent them a follow-up questionnaire and received responses from 66.7% (56/84) of the participants. The large majority were satisfied with the salivary test (95.2%) and the information (96.4%) we provided. Most of the participants (89.3%) indicated that they wanted to use the oral health check-up service again in the future. Compared with baseline, the ratio of participants restricting their intake of sugar-rich foods and drinks significantly increased 1 month later ($p = 0.021$). About 60% of those who had not undergone a regular dental examination at baseline reported newly visiting or planning to visit a dental clinic. The results revealed high satisfaction with the oral health check-up and information about oral self-care they received at the community pharmacy. The results suggested that oral health check-ups had the potential to change both oral self-care habits and dental consultation behavior. Our findings indicate that community pharmacies can contribute to the maintenance and promotion of oral health by providing oral health check-ups to local residents.

Keywords health support, behavioral change, salivary test, information provision, dental clinic, questionnaire survey

1. Introduction

Oral diseases, such as dental caries and periodontal disease, are major public health problems worldwide (*1,2*). In Japan, about 4 million patients were estimated to have periodontal disease, making it the second most common major disease behind hypertension (*3*). Oral diseases lead not only to loss of oral function but also to lower quality of life (*4*). In addition, it is known that periodontal disease is related to systemic diseases, including diabetes mellitus (*5,6*) and atherosclerotic vascular disease (*7*). It has been reported that periodontal treatment is effective for improving glycemic control (*8*) and that regular dental care utilization reduces the risk of stroke (*9*). Therefore, maintenance of oral health is important for prolonging health expectancy and decreasing national medical expenditures.

Regular dental check-ups are essential for early detection of oral diseases. However, only 52.9% of Japanese adults have regular dental check-ups according to a survey conducted by the Ministry of Health, Labour and Welfare in 2016 (*10*), and this is much lower than the rate of regular health check-ups (71.4%) (*11*). Therefore, a strategy is needed to close this gap in behaviors.

Community pharmacies play an important role in maintaining the health of the local residents and

prolonging their health expectancy. A majority of pharmacists in Australia (*12,13*) and England (*14*) stated that it was their role to deliver oral health advice to the community and provide oral healthcare service to local residents. However, Japanese community pharmacists merely advise patients about the adverse effects of medicine in the oral cavity (*15*), and few studies have investigated the contribution of community pharmacists to the oral healthcare of local residents. In September 2015, the Ministry of Economy, Trade and Industry allowed salivary tests to be used to conduct oral health check-ups at community pharmacies (*16*). This oral health check-up could become a new tool for community pharmacies to maintain and promote the oral health of local residents. However, very few Japanese community pharmacies have introduced this service. Therefore, in the present study, we conducted oral health check-ups and provided information about oral self-care at a community pharmacy and examined the effect on oral health-associated behaviors and conducted surveys to determine satisfaction as well as how likely participants were to use the service again in the future.

2. Materials and Methods

2.1. Participants and study design

Participants were recruited from among patients who visited Keio University Community Pharmacy (Tokyo, Japan) with a prescription in June or July 2018. The researchers explained the details of the study to each patient and obtained written informed consent prior to their participation. Individuals under 20 years old were excluded. The oral health condition of the participants was checked by using a salivary test, which was free of charge, and each participant was given their results sheet. In addition, the participants received information about oral health self-care from the researchers and were asked to respond to a self-administered questionnaire. One month later, the participants were asked to respond to a follow-up questionnaire sent to their home by postal mail. The study protocol was approved by the research ethics committee of the Faculty of Pharmacy, Keio University (approval number: 180528-1).

2.2. Oral health check-up by salivary test

The oral health check-up was conducted using a salivary test system (SillHa; ARKRAY Inc., Kyoto, Japan), which assays the following six items in about 5 min: cariogenic bacteria, pH, buffer capacity (which indicates the risk of dental caries), leukocytes, protein (which indicates the risk of periodontal disease), and ammonia (which indicates oral cleanliness). This test cannot be used to diagnose oral diseases. In this study, participants provided oral rinse sample using 3 mL of distilled water, and the researchers used a dropper to transfer the sample onto the test strip. Once the assay was complete, the researchers explained the results to the participant, referencing a results sheet, on which the results of the six items were plotted on a radar chart. The participants were also told that the results were often affected by their diet and oral hygiene.

2.3. Information provision about oral health

The researchers gave each participant an original leaflet containing information about the relationship between oral diseases and systemic diseases, recommendations for dietary behaviors and oral self-care, and an explanation on the importance of regular dental check-ups, and they discussed the contents of the leaflet with each participant for a few minutes. Regarding dietary behaviors, the researchers recommended that the participants restrict their intake of sugar-rich foods and drinks, eat nutritionally balanced meals, and chew their meals wells. In addition, the researchers provided oral hygiene guidance, including the use of an interdental brush or dental floss as well as fluoride-containing toothpaste. Among the researchers were two dentists, who contributed to the creation of the information leaflet.

2.4. Questionnaire survey

At the end of the session at the community pharmacy, each participant was asked to complete a self-administered questionnaire covering the following areas: 1) basic characteristics and frequency of regular dental check-ups, 2) dietary behaviors and oral hygiene habits in daily life, and 3) satisfaction with the oral health check-up and information provided and their likelihood of using the service again in the future.

One month later, participants were asked to respond to a follow-up questionnaire sent to their home by postal mail, which asked about dietary behaviors, oral hygiene habits, and dental consultation behavior.

2.5. Statistical analysis

All analyses were performed using IBM SPSS Statistics version 25 software (IBM Corp., Armonk, NY), and McNemar's test was used to evaluate changes between baseline and 1 month later. A p-value < 0.05 was regarded as significant.

3. Results

3.1. Participant characteristics

A total of 84 patients participated in this study; their basic characteristics are shown in Table 1. Most participants (32.1%) were in their 70s and just over half (53.6%) were women. Only 9.5% were smokers. Nearly

two-thirds of the participants (64.3%) had undergone a regular dental check-up in the preceding 12 months and the rest (35.7%) had not.

3.2. Satisfaction with the oral health check-up and the information provided at the community pharmacy

Most participants (77.4%) found it beneficial to get their results on site after the oral health check-up at a community pharmacy (Figure 1A). Additionally, they said that the oral health check-up was easy (66.7%), was useful for improving their oral self-care habits (56.0%), and took a short time (51.2%). Furthermore, 79.8% of participants answered that there was no demerit about having the oral health check-up at a community pharmacy. Only a few participants felt that the presence of dental caries and periodontal disease were not confirmed by the oral health check-up (4.8%) and hesitated to provide a saliva sample for the assay (3.6%).

Nearly all the participants (95.2%) indicated that they were "satisfied" or "somewhat satisfied" with the oral health check-up at the community pharmacy (Figure 1B) and 96.4% indicated that they were "satisfied" or "somewhat satisfied" with the information they received about oral health self-care (Figure 1C). No one responded that they were "somewhat unsatisfied" or "unsatisfied" about either the oral health check-up or the information provided. Moreover, 89.3% of the participants indicated that they wanted to use the oral health check-up service at a community pharmacy again in the future (Figure 1D).

Table 1. Participant characteristics (*n* = 84)

	n (%)
Age	
20-29	4 (4.8)
30-39	4 (4.8)
40-49	12 (14.3)
50-59	18 (21.4)
60-69	14 (16.7)
70-79	27 (32.1)
80+	5 (6.0)
Sex	
Male	39 (46.4)
Female	45 (53.6)
Smoking habit	
Yes	8 (9.5)
No	76 (90.5)
Regular dental check-up in the preceding 12 months	
Yes	54 (64.3)
No	30 (35.7)

3.3. Changes in oral self-care habits and dental consultation behavior 1 month after the oral health check-up

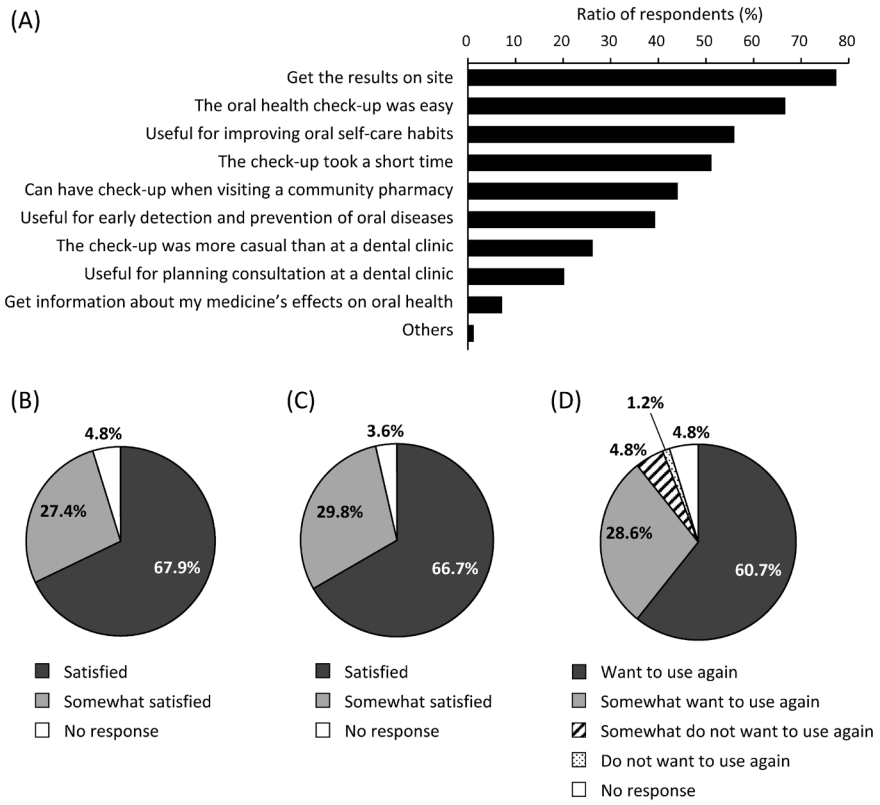

Figure 1. Satisfaction with the oral health check-up and the information provided at the community pharmacy. (A) Benefits of the oral health check-ups performed at the community pharmacy (*n* = 84, multiple answers allowed). **(B** and **C)** Degree of satisfaction with **(B)** the oral health check-up and **(C)** the information provided about oral self-care at the community pharmacy (*n* = 84). **(D)** Likelihood of using the oral health check-up service at a community pharmacy again (*n* = 84).

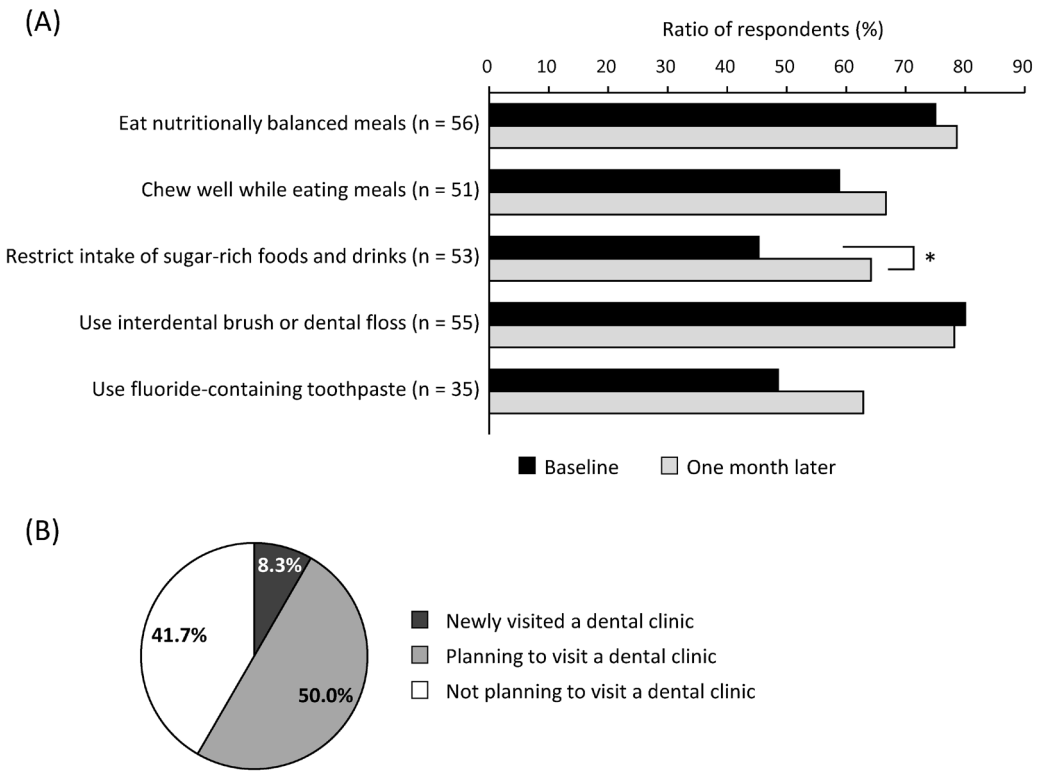

Figure 2. Changes in oral self-care habits and dental consultation behavior 1 month after the oral health check-up. (A) Comparison of oral self-care habits at baseline and 1 month after the oral health check-up performed at the community pharmacy. Data from respondents were excluded if they did not answer the same items on both questionnaires and if they answered "I don't know if my toothpaste contains fluoride" to the item on use of fluoride-containing toothpaste. The number of responses for each item are indicated in the figure. $^{*}p < 0.05$ by McNemar's test. **(B)** Dental consultation behavior 1 month after the oral health check-up performed at the community pharmacy. Figure shows data of those who had not gone to a regular dental check-up in the preceding 12 months at baseline and responded to the follow-up questionnaire 1 month later ($n = 12$).

We received responses from 66.7% (56/84) of the participants to the follow-up questionnaire we administered 1 month after the oral health check-up at the community pharmacy. The ratio of participants who performed various aspects of oral self-care at the time of the oral health check-up (baseline) to those 1 month later is shown in Figure 2A. More than 70% of the participants ate nutritionally balanced meals and used an interdental brush or dental floss at baseline, whereas less than 50% restricted their intake of sugar-rich foods and drinks and used a fluoride-containing toothpaste. Compared with baseline, the ratio of participants restricting their intake of sugar-rich foods and drink had significantly increased 1 month later (baseline, 45.3%; 1 month later, 64.2%; $p = 0.021$).

Of the 56 participants who responded to the follow-up questionnaire, 12 had not gone to a regular dental check-up in the preceding 12 months. Only one of them (8.3%) reported newly visiting a dental clinic during the month after they used the oral health check-up service at a community pharmacy, whereas half indicated plans to visit a dental clinic in the near future (Figure 2B).

4. Discussion

The results of this study showed that the majority of participants were satisfied with the oral health check-up service conducted using a salivary test as well as the information provided about oral self-care and indicated that they wanted to use the service again in the future. In addition, some of the participants reported making positive changes in their oral self-care habits and dental consultation behavior. These results suggest that providing oral health check-up services at community pharmacies could lead to improvements in oral health-associated behavior in local residents.

This is the first study to investigate oral health check-up services at a Japanese community pharmacy in terms of effectiveness, satisfaction, and likelihood of using the service again in the future. Compared with other countries (*12-14*), Japanese community pharmacies are less proactive in promoting and maintaining the oral health of local residents. The introduction of this new service comprising an oral health check-up and provision of oral self-care information is expected to help Japanese community pharmacies take a more active role in promoting and maintaining the oral health of local residents.

The results of this study showed that both the oral health check-up and the information provided about oral self-care were very well received by the participants, many of whom recognized the ease and speed with which

they could receive both the check-up and the results. In addition, the check-up procedure does not cause pain or distress because users need only provide an oral rinse sample. Furthermore, the assay takes only 5 min to complete, so it should generally be possible to complete the oral health check-up while the user is waiting for their prescription to be filled. Also, given that the large majority of participants indicated that they wanted to use the oral health check-up service again in the future, it is recommended that more Japanese community pharmacies introduce this service to accommodate the expected demand.

More than half the participants indicated that the oral health check-up and the information they received were useful for improving their oral self-care habits. Indeed, the ratio of participants restricting their intake of sugar-rich foods and drinks significantly increased 1 month after the check-up compared with baseline, suggesting that the check-up and information provision might have led to changes in their oral health-associated behaviors.

The results also suggest that the service affected the participants' dental consultation behavior because about 60% of participants who had not gone to a regular dental check-up in the preceding 12 months reported newly visiting a dental clinic or planning to do so in the near future. In this study, the participants were recommended to visit a dental clinic for a professional examination and care during the oral health check-up session. Given that oral diseases are known to be related to systemic diseases (*5-7*), it is possible that the oral health check-up conducted at community pharmacies possibly led not only to early detection of oral diseases but also to the prevention of systemic diseases.

From the results of the follow-up questionnaire survey conducted 1 month after the oral health check-up, no significant improvements were observed in chewing well while eating meals or using fluoride-containing toothpaste, and the positive effect on dental consultation behavior was limited. Regarding the effects of intervention at community pharmacies, previous studies found that repeated implementation of lifestyle advice and measurements led to reductions in blood pressure (*17*) and improvements in bone mineral density (*18*) in local residents. Although we conducted the oral health check-ups and provided information only one time, it is expected that subsequent sessions would lead to further changes in oral self-care habits and dental consultation behavior.

A limitation of this study is that we evaluated only a combination group in which both the oral health check-up was performed and the information was provided and there was no control group. Further study is required to more clearly assess the effects of the oral health check-up and information provision separately.

In conclusion, the present study demonstrated that participants were very satisfied with the oral health check-up and the information provided about oral self-care at the community pharmacy and that they wanted to use the service again in the future. Additionally, it was suggested that the oral health check-up and information provision potentially led to improvements in oral self-care and dental consultation behavior. These findings indicate that community pharmacies could possibly contribute to the promotion and maintenance of oral health in local residents by providing this service.

Acknowledgements

We are grateful to the individuals who participated in this study.

Funding: This work was supported by the Keio University Academic Development Funds for Individual Research, a grant from the OTC Self-Medication Promotion Foundation, and a JSPS KAKENHI Grant-in-Aid for Scientific Research (C; Grant Number JP20K07185).

Conflict of Interest: The authors have no conflicts of interest to disclose.

References

1. Bernabe E, Marcenes W, Hernandez CR, *et al.* Global, regional, and national levels and trends in burden of oral conditions from 1990 to 2017: A systematic analysis for the global burden of disease 2017 study. J Dent Res. 2020; 99:362-373.
2. Petersen PE, Ogawa H. The global burden of periodontal disease: towards integration with chronic disease prevention and control. Periodontol 2000. 2012; 60:15-39.
3. Ministry of Health, Labour and Welfare in Japan. Patient Survey 2017. *https://www.mhlw.go.jp/toukei/saikin/hw/kanja/17/dl/kanja-01.pdf* (accessed October 18, 2020). (in Japanese)
4. Buset SL, Walter C, Friedmann A, Weiger R, Borgnakke WS, Zitzmann NU. Are periodontal diseases really silent? A systematic review of their effect on quality of life. J Clin Periodontol. 2016; 43:333-344.
5. Ide R, Hoshuyama T, Wilson D, Takahashi K, Higashi T. Periodontal disease and incident diabetes: a seven-year study. J Dent Res. 2011; 90:41-46.
6. Taylor GW. Bidirectional interrelationships between diabetes and periodontal diseases: an epidemiologic perspective. Ann Periodontol. 2001; 6:99-112.
7. Aarabi G, Eberhard J, Reissmann DR, Heydecke G, Seedorf U. Interaction between periodontal disease and atherosclerotic vascular disease – Fact or fiction? Atherosclerosis. 2015; 241:555-560.
8. Sgolastra F, Severino M, Pietropaoli D, Gatto R, Monaco A. Effectiveness of periodontal treatment to improve metabolic control in patients with chronic periodontitis and type 2 diabetes: a meta-analysis of randomized clinical trials. J Periodontol. 2013; 84:958-973.
9. Sen S, Giamberardino LD, Moss K, Morelli T, Rosamond WD, Gottesman RF, Beck J, Offenbacher S. Periodontal disease, regular dental care use, and incident ischemic

stroke. Stroke. 2018; 49:355-362.
10. Ministry of Health, Labour and Welfare in Japan. National Health and Nutrition Survey 2016. *https://www.mhlw.go.jp/bunya/kenkou/eiyou/dl/h28-houkoku-06.pdf* (accessed October 18, 2020). (in Japanese)
11. Ministry of Health, Labour and Welfare in Japan. National Health and Nutrition Survey 2018. *https://www.mhlw.go.jp/content/000615345.pdf* (accessed October 18, 2020). (in Japanese)
12. Freeman CR, Abdullah N, Ford PJ, Taing MW. A national survey exploring oral healthcare service provision across Australian community pharmacies. BMJ Open. 2017; 7:e017940.
13. Taing MW, Ford PJ, Gartner CE, Freeman CR. Describing the role of Australian community pharmacists in oral healthcare. Int J Pharm Pract. 2016; 24:237-246.
14. Mann RS, Marcenes W, Gillam DG. Is there a role for community pharmacists in promoting oral health? Br Dent J. 2015; 218:E10.
15. Ueda M, Niki K, Ueda H, Oishi M, Uejima E. The need for medical, dental and pharmacological cooperation focused on the oral cavity functions – The role of community pharmacy on appropriate pharmacotherapy for the prevention of serious adverse effects on the oral cavity. Jpn J Pharm Health Care Sci. 2017; 43:320-327. (in Japanese).
16. Ministry of Economy, Trade and Industry in Japan. News Release (September 1, 2015) – Consciousness of the implementation of oral health check-ups with salivary tests at community pharmacies. *https://www.meti.go.jp/policy/jigyou_saisei/kyousouryoku_kyouka/shinjigyo-kaitakuseidosuishin/press/150901_press.pdf* (accessed October 18, 2020). (in Japanese)
17. Okada H, Onda M, Shoji M, Sakane N, Nakagawa Y, Sozu T, Kitajima Y, Tsuyuki RT, Nakayama T. Effects of lifestyle advice provided by pharmacists on blood pressure: The community pharmacists assist for blood pressure (COMPASS-BP) randomized trial. Biosci Trends. 2017; 11:632-639.
18. Wada Y, Wada Y, Ennyu S, Shimokawa KI, Ishii F. Ability of community pharmacists to promote self-care and self-medication by local residents [I]: Improvements in bone mineral density. Drug Discov Ther. 2017; 11:35-40.

Received October 24, 2020; Revised December 3, 2020; Accepted December 12, 2020.

**Address correspondence to:*
Katsunori Yamaura, Division of Social Pharmacy, Center for Social Pharmacy and Pharmaceutical Care Sciences, Faculty of Pharmacy, Keio University, 1-5-30 Shibakoen, Minato-ku, Tokyo 105-8512, Japan.
E-mail: yamaura-kt@keio.jp

Released online in J-STAGE as advance publication December 27, 2020.

Original Article

DOI: 10.5582/ddt.2020.03107

Finger sweating levels evaluated by video capillaroscopy system are increased in patients with systemic sclerosis compared to pre-clinical stage patients

Kayoko Tabata[1], Masatoshi Jinnin[2,*], Kanako Furukawa[1], Sayaka Tani[2], Hisako Okuhira[2], Naoya Mikita[2], Takao Fujii[1]

[1] Department of Rheumatology and Clinical Immunology, Wakayama Medical University Graduate School of Medicine, Wakayama, Japan;
[2] Department of Dermatology, Wakayama Medical University Graduate School of Medicine, Wakayama, Japan.

SUMMARY New strategies for early diagnosis and careful follow-up of systemic sclerosis are urgently needed. We unconventionally used a video capillaroscopy system to measure the amount of sweating on finger pads, and investigated its clinical significance. Thirty-three Japanese patients who were diagnosed with typical or pre-clinical stage patients of systemic sclerosis were included in this study. Five healthy subjects were also included. Among twenty-one patients with typical systemic sclerosis that fulfilled ACR/EULAR 2013 classification criteria, seven had increased sweating levels. On the other hand, among twelve pre-clinical stage patients that did not fulfill the classification criteria, no patient showed increase in finger sweating. We found that there was statistically significant difference. The ratio of diffuse cutaneous systemic sclerosis was also found to be significantly higher in subjects with increased amounts of sweating than in subjects with normal levels. Furthermore, the positivity of topoisomerase I antibody was statistically higher in patients with increased sweating levels than in those without. These results indicated that measurement of finger sweating levels may be a useful tool for early diagnosis and clarification of pathogenesis in this disease.

Keywords capillaroscopy, sweat, systemic sclerosis, skin, collagen, topoisomerase I antibody

1. Introduction

Systemic sclerosis (SSc) is a multisystemic autoimmune disease characterized by vasculopathy and excess collagen accumulation in the skin or various internal organs including the lungs and esophagus. Because pathogenesis of SSc remains unknown, diagnosis and treatment is sometimes difficult. However, progressive collagen deposition seen in SSc is often irreversible, at least clinically, and there is an urgent need to develop new strategies of early diagnosis and careful follow-up.

For that purpose, we previously reported that low serum CA9 concentration and microRNA-29 in pre-clinical stage SSc may be utilized as early diagnostic markers (*1,2*). On the other hand, accumulation of thickened collagen in SSc dermis is known to cause atrophy of the sweat glands. In the current study, we focus on the possibility that sweat volume may also be useful for early diagnosis, which has never been investigated before. We unconventionally used a video capillaroscopy system as a novel mean of evaluating sweating levels. Generally, this system is used to detect red blood cell flow by a hand-held microvideoscope. It can also be used to observe the surface of the skin to a depth of up to 2 mm (*3*). We measured the sweating levels on finger pads by this system, and investigated its clinical significance in SSc patients with the idea of possible future application for making early diagnosis and for clarification of pathogenesis of systemic sclerosis.

2. Materials and Methods

2.1. Clinical assessment and patients' material

Thirty-three Japanese patients who were suspected as having SSc were included in this study. Among them, twenty-one patients (nineteen females and two males) fulfilled ACR/EULAR 2013 classification criteria (*4*). These patients with typical SSc were grouped according to the classification system proposed by LeRoy, *et al.* (*5*). Fifteen patients were limited cutaneous systemic sclerosis (lcSSc), while six patients had diffuse cutaneous systemic sclerosis (dcSSc). Clinical and laboratory data

Table 1. Summary of clinical/serological features in patients with typical systemic sclerosis (n = 21)

Males : Females	2:19
Age at the time of capillaroscopy (mean years)	67.5
Duration of disease (mean months)	113.7
Type (diffuse:limited)	6:15
Clinical features	
Pitting scars	28.6
Ulcers	14.3
Nailfold bleeding	61.9
Telangiectasia	38.1
Contracture of phalanges	42.9
Diffuse pigmentation	14.3
Short SF	42.9
Sicca symptoms	52.4
Organ involvment	
Pulmonary fibrosis	28.6
Mean %VC	87.2
Mean %DLco	78.1
Pulmonary hypertension	14.3
Esophagus	38.1
Heart	14.3
Kidney	0.05
Joint	38.1
ANA Specificity	
Anti-topoisomerase I	23.8
Anti-centromere	76.2

Unless indicated, values are percentages. SF: sublingual frenulum, VC: vital capacity, DLco: diffusion capacity for carbon monooxidase, ANA: antinuclear antibodies, Anti-topoisomerase I: anti-topoisomerase I antibody, Anti-centromere: anti-centromere antibody.

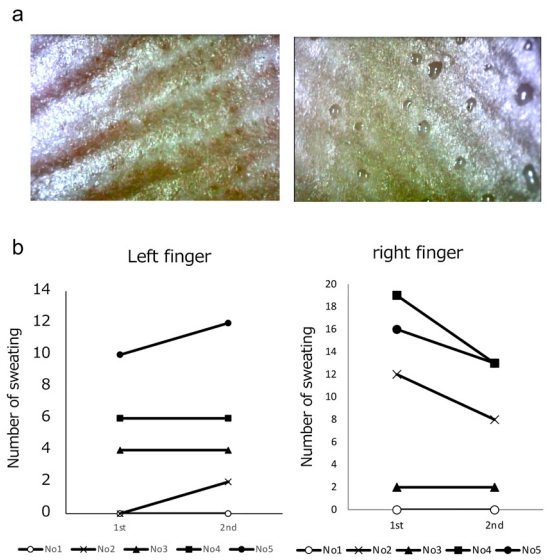

Figure 1. Reproductivity of sweating levels on the finger pads of five healthy subjects. (a) Representative capillaroscopic images of the fourth finger in healthy subjects. Left: image of poor sweating (subject no. 3), right: image of abundant sweating (no. 4). **(b)** Total number of secreting sweat gland on left and right fourth fingers of five healthy subjects (no. 1-5) are shown on the ordinate. The sweating levels were evaluated by capillaroscopy twice (first and second).

were obtained at the time of the evaluation of sweating levels (Table 1). Five healthy subjects (three females and two males) were also included in this study.

This study was approved by the Wakayama Medical University Institutional Review Board (No.2542), and written informed consent were obtained before patients and healthy volunteers were entered into this study, in accordance with the Declaration of Helsinki.

2.2. Measurement of sweating levels

Sweating was evaluated using capillaroscopy (BSCAN-Pro, Toku Corporation, Tokyo, Japan) at 25°C in all patients and healthy subjects (*5*). Number of secreting sweat glands was counted on the three sides (front, left and right sides) of the fourth finger pads for five seconds each, and the total number of sweating was recorded.

2.3. Statistical analysis

Statistical analysis was carried out with Fisher's exact probability test to compare percentages by using Excel 2011 spreadsheet (Microsoft Corp., Redmond, WA) and Statcel4 (OMS, Tokorozawa, Japan). $P < 0.05$ was considered significant.

3. Results

3.1. Reproducibility of sweating levels on finger pads

In this study, capillaroscopy was used according to the protocol of nailfold observation (*6*), and sweating ability was evaluated at 25°C.

The fourth finger was chosen as the site of examination, because many changes characteristic to SSc (*e.g.* round finger pad sign and nailfold capillaroscopic abnormalities) are known to predominantly appear on fourth finger (*7,8*). Representative capillaroscopic video images of fourth fingertip in healthy subjects showed both little (Figure 1a, left) and abundant (Figure 1a, right) sweating levels in each healthy subject, indicating individual differences.

Because this is the first report to evaluate sweating using capillaroscopy, we attempted to prove its reproducibility. Number of secreting sweat glands within a fixed area (width = 1 mm) for total fifteen seconds was counted on the three sides (front, left and right sides) of the fourth finger pads, and the total number of sweating was compared between first evaluation and second evaluation (duration: 1-15 days) in five healthy subjects (No. 1-5, two males and three females with the ages ranging between 34 and 40 years) (Figure 1b).

The difference of finger sweating levels between the two evaluations were < 5 in both the left and right fingers of each individual, indicating the reproducibility of finger sweating levels by our method.

3.2. Comparison of finger sweating levels in patients with typical and pre-clinical stage of SSc

Based on the above results, we measured the finger sweating levels in patients with typical and pre-clinical

stage of SSc (n = 33). Total number of secreting glands of left and right finger sweating levels were recorded.

When the cut-off value was set at 10 secreting glands, in twenty-one patients with typical SSc (male:female = 2:19) who fulfilled ACR/EULAR 2013 classification criteria (criteria score ≥ 9 points), seven had increased amount of sweating (Table 2). On the other hand, among twelve pre-clinical stage patients (all female) that did not fulfil ACR/EULAR 2013 classification criteria (criteria score ≤ 8 points), no patient had increased finger sweating levels. There was statistically significant difference (p = 0.029 by Fisher's exact probability test). Only one typical SSc fulfilled 2016 ACR/EULAR classification criteria for primary Sjögren's syndrome (*9*), but the finger sweating levels of the patient was 20 and not reduced. Our results suggest that finger sweating levels were increased in typical SSc that fulfilled the criteria compared with those in the pre-clinical stage of SSc.

Table 2. Comparison of finger sweating levels between typical and preclinical early stage of systemic sclerosis

	Preclinical stage Criteria score ≤ 8	Typical systemic sclerosis Criteria score ≥ 9
Sweating levels ≤ 9	12	14
Sweating levels ≥10	0	7

Criteria score was calculated based on American College of Rheumatology (ACR)/ European League against Rheumatism (EULAR) 2013 classification criteria. Sweating levels was sum of total number of finger sweating levels.

3.3. Correlation between sweating levels and clinical features in SSc

Lastly, we examined the correlation of finger sweating levels with clinical and serological features in patients with typical SSc who fulfilled ACR/EULAR 2013 criteria (n = 21). Summary of clinical/laboratory features of patients enrolled in this study are shown in Table 1. Mean age was 67.5 years, and patients comprised six dcSSc and 15 lcSSc.

In seven patients with increased sum finger sweating levels, the mean disease duration (between symptom onset and first visit to the hospital) was 72.0 months (Table 3). Meanwhile, in subjects with normal sweating, mean disease duration was 134.6 months. Thus, patients with increased sweating tended to have a shorter disease duration, albeit insignificant. In addition, the ratio of dcSSc was significantly higher in patients with increased sweating levels than in those with the normal sweating levels (dcSSc: lcSSc = 6:1 *vs.* 0:14, p = 0.00013 by Fisher's exact probability test). Furthermore, the positivity of topoisomerase I antibody was statistically higher in patients with increased sweating levels than those without (57.1 *vs.* 7.1%, p = 0.025).

Accordingly, among patients with typical SSc, those with dcSSc and positive for anti-topoisomeraseIantibody

Table 3. Correlation of clinical/serological features and finger sweating levels in typical systemic sclerosis

	Increased sweating (n = 7)	Normal sweating (n = 14)	p value
Males : Females	1:6	1:13	N.S.
Age at the time of capillaroscopy (mean years)	61.1	70.7	N.S.
Duration of disease (mean months)	72.0	134.6	N.S.
Type (diffuse:limited)	6:1	0:14*	p = 0.00013
Clinical features			
Pitting scars	28.6	28.6	N.S.
Ulcers	14.3	14.3	N.S.
Nailfold bleeding	71.4	57.1	N.S.
Telangiectasia	28.6	42.9	N.S.
Contracture of phalanges	57.1	35.7	N.S.
Diffuse pigmentation	14.3	14.3	N.S.
Short SF	57.1	35.7	N.S.
Sicca symptoms	28.6	64.3	N.S.
Organ involvement			
Pulmonary fibrosis	57.1	14.3	N.S.
Mean %VC	76.8	92.5	N.S.
Mean % DLco	64.3	85.0	N.S.
Pulmonary hypertension	0	21.4	N.S.
Esophagus	28.6	42.9	N.S.
Heart	0	21.4	N.S.
Kidney	0	7.1	N.S.
Joint	14.3	50.0	N.S.
ANA Specificity			
Anti-topoisomerase I	57.1	7.1	p = 0.025
Anti-centromere	42.9	92.9	N.S.

Unless indicated, values are percentages. SF: sublingual frenulum, VC: vital capacity, DLco: diffusion capacity for carbon monooxidase, Anti-topoisomerase I: anti-topoisomerase I antibody, Anti-centromere: anti-centromere antibody. *p < 0.05 by Fisher's exact probability test. N.S. : not significant.

tended to have increased finger sweating. Thirteen out of 21 patients with typical SSc were administrated with vasodilators. However, there were no significant association between sweating levels and the use of vasodilators.

4. Discussion

Sclerotic skin lesions of patients with SSc are known to be characterized by histopathologically thickened and increased collagen bundles, which makes sweat glands atrophic or absent (*10*). Sweating of SSc patients is therefore believed to be decreased, and no reports have yet proven abnormal sweating levels in SSc patients.

In this study, we directly measured sweat secretion of SSc fingers using capillaroscopy and present three major findings. Firstly, we proposed a novel mean of evaluating sweating levels. Both qualitative and quantitative techniques have been used to measure sweating levels. For example, qualitative measurements include iodine starch method and Minor's method, whereas weight measurement and ventilation capsule method are used as quantitative measurements (*11,12*). Each of these techniques is either time-consuming or it restricts the subject's physical activity by the firmly-attached measurement probes. Capillaroscopy, meanwhile, is readily and commonly used for the observation of capillary abnormalities in SSc patients, and has the advantage of being a brief and real-time quantification of sweat secretion by use of a small probe. We were able to prove its reproducibility, and our method can be considered as a new option for evaluation of sweat ability.

Second, contrary to expectation, we found patients with typical SSc that fulfilled ACR/EULAR 2013 classification criteria have significantly increased finger sweating levels compared with patients in pre-clinical stage of SSc that did not meet the classification criteria. Considering that the SSc patient group with high sweating levels tended to have a shorter disease duration, there is a possibility that serial measurement of finger sweating levels may help early differentiation of typical SSc from pre-clinical stage of SSc.

Another finding of this study is that, among patients with typical SSc, the ratio of dcSSc was significantly higher in patients with increased sweating levels compared to those with the normal sweating levels. The increased positivity of topoisomerase I antibody in patients with increased sweating levels supported this notion. As described above, sweating of SSc patients has been believed to be impaired because collagen accumulation causes atrophy of the sweat glands. Our unexpected results suggest the possibility that sweating is regulated by the autonomic nervous system (*13,14*), and it may be stimulated for unknown reasons in SSc patients. Alternatively, because skin sclerosis of the finger pads is usually mild, there may be compensatory hyperhidrosis. To prove this hypothesis, the sweating levels of other sites including sclerotic lesions using the same method by capillaroscopy are needed. In our preliminary data, however, we could not obtain reproducible results in sclerotic lesions (data not shown).

The current study has several limitations. First, we did not compare the results on sweating levels detected by the video capillaroscopy to those by any standard methods (*e.g.* iodine-starch test and/or perspiration meter). There are the possibility that the difference of sweating secretion ability among patient groups become clearer by the forced sweating situation such as warm. Next, the data of age/sex-matched healthy subjects was not available, because they rarely visit our hospital as a center in the area. Thus, we could not compare sweating levels of SSc patients with those of healthy control. In addition, the result from healthy subjects was very variable. Although we tried to identify the factor that influenced to sweat secreting, it is still unknown. Furthermore, 13.2% of Japanese SSc patients are reported to accompanied with Sjögren's syndrome (*15*). Because only one typical SSc had been diagnosed with Sjögren's syndrome in this study, ruling out of Sjögren's syndrome might not be enough in some patients. Even if some SSc patients are accompanied with Sjögren's syndrome, however, this does not explain increased sweating levels in typical SSc. Lastly, we did not record skin score and nailfold capillary findings, and these data was not available. The relationship between the clinical disease course (*e.g.* by the changes of skin score) and the changes of finger sweating levels could not be clarified in this manuscript. We will deal with these problems in the future project.

In summary, this pilot study indicated that measurement of finger sweating levels has potential usefulness for early diagnosis and clarification of pathogenesis in SSc. Detailed research with larger number of samples is necessary to prove its usefulness.

Acknowledgements

We acknowledge editing and proofreading by Benjamin Phillis from the Clinical Study Support Center at Wakayama Medical University.

Funding: None.

Conflict of Interest: The authors have no conflicts of interest to disclose.

References

1. Makino K, Jinnin M, Makino T, Kajihara I, Fukushima S, Inoue Y, Ihn H. Serum levels of soluble carbonic anhydrase IX are decreased in patients with diffuse cutaneous systemic sclerosis compared to those with limited cutaneous systemic sclerosis. Biosci Trends. 2014; 8:144-148.

2. Kawashita Y, Jinnin M, Makino T, Kajihara I, Makino K, Honda N, Masuguchi S, Fukushima S, Inoue Y, Ihn H. Circulating miR-29a levels in patients with scleroderma spestrum disorder. J Dermatol Sci. 2011; 61:67-69.
3. Mugii N, Hasegawa M, Hamaguchi Y, Tanaka C, Kaji K, Komura K, Ueda-Hayakawa I, Horie S, Ikuta M, Tachino K, Ogawa F, Sato S, Fujimoto M, Takehara K. Reduced red blood cell velocity in nail-fold capillaries as a sensitive and specific indicator of microcirculation injury in systemic sclerosis. Rheumatology. 2009; 48:696-703.
4. van den Hoogen F, Khanna D, Fransen J, *et al.* 2013 classification criteria for systemic sclerosis: an American college of rheumatology/European league against rheumatism collaborative initiative. Ann Rheum Dis. 2013; 72:1747-1755.
5. LeRoy EC, Black C, Fleischmajer R, Jablonska S, Krieg T, Medsger Jr TA, Rowell N, Wollheim F. Scleroderma (systemic sclerosis): classification, subsets and pathogenesis. J Rheumatol. 1988; 15:202-205.
6. Ichimura Y, Kawaguchi Y, Takagi K, Tochimoto A, Higuchi T, Kataoka S, Katsumata Y, Yamanaka H. Capillary abnormalities observed by nailfold video-capillaroscopy in Japanese patients with systemic sclerosis. Mod Rheumatol. 2018; 28:1066-1068.
7. Mizutani H, Mizutani T, Okada H, Kupper T S, Shimizu M. Round fingerpad sign: An early sign of scleroderma. J Am Acad Dermatol. 1991; 24:67-69.
8. Dinsdale G, Roberts C, Moore T, *et al.* Nailfold capillaroscopy - how many fingers should be examined to detect abnormality? Rheumatology. 2019; 58:284-288.
9. Shiboski CH, Shiboski SC, Seror, Criswell LA, Labetoulle M, Lietman TM, Rasmussen A, Scofield H, Vitali C, Bowman SJ, Mariette X, 2016 American College of Rheumatology/European League Against Rheumatism classification criteria for primary Sjögren's syndrome: A consensus and data-driven methodology involving three international patient cohorts. Ann Rheum Dis. 2017; 76:9-16.
10. Krieg T, Takehara K. Skin disease: a cardinal feature of systemic sclerosis. Rheumatology. 2009; 48:iii14-iii18.
11. Minor V. Ein neues verfahren zu der klinischen unteruchung der shweissabsonderung. Z Neurol. 1927; 101:302-308.
12. Lowe NJ, Yamauchi PS, Lask GP, Patnaik R, Iyer S. Efficacy and safety of botulinum toxin type A in the treatment of palmar hyperhidrosis: A double-blind, randomized, placebo-controlled study. Dermatol Surg. 2002; 28:822-827.
13. Nishiyama T, Sugenoya J, Matsumoto T, Iwase S, Mano T. Irregular activation of individual sweat glands in human sole observed by a videomicroscopy. Auton Neurosci. 2001; 88:117-126.
14. Maeda Y, Nakane S, Higuchi O, Nakamura H, Komori A, Migita K, Mukaino A, Umeda M, Ichinose K, Tamai M, Kawashiri S, Sakai W, Yatsuhashi H, Kawakami A, Matsuo H. Ganglionic acetylcholine receptor autoantibodies in patients with autoimmune diseases including primary biliary cirrhosis. Mod Rheumatol. 2017; 27:664-668.
15. Tsuboi H, Asashima H, Takai C, *et al.* Primary and secondary surveys on epidemiology of Sjögren's syndrome in Japan. Mod Rheumatol. 2014; 24:464-470.

Received November 11, 2020; Revised December 13, 2020; Accepted December 23, 2020.

**Address correspondence to:*
Dr. Masatoshi Jinnin, Department of Dermatology, Wakayama Medical University Graduate School of Medicine, 811-1 Kimiidera, Wakayama, Wakayama, 641-0012, Japan.
E-mail: mjin@wakayama-med.ac.jp

Released online in J-STAGE as advance publication December 30, 2020.

Brief Report

DOI: 10.5582/ddt.2020.03110

Clinical spectrum and predictors of severe *Plasmodium vivax* infections at a tertiary care center in North India

Dinesh Walia[1], Umang Arora[1], Upendra Baitha[1,*], Arvind Kumar[1], Piyush Ranjan[1], Manish Soneja[1], Nishant Verma[2], Maroof Ahmad Khan[3], Praveen Aggarwal[4], Ashutosh Biswas[1], Naveet Wig[1]

[1] Department of Medicine, All India Institute of Medical Sciences, New Delhi, India;
[2] Department of Microbiology, All India Institute of Medical Sciences, New Delhi, India;
[3] Department of Biostatistics, All India Institute of Medical Sciences, New Delhi, India;
[4] Department of Emergency Medicine, All India Institute of Medical Sciences, New Delhi, India.

SUMMARY Traditionally attributed only to *Plasmodium falciparum*, *Plasmodium vivax* has recently been reported to cause a significant burden of complicated malaria cases. The present study aimed to delineate the clinical spectrum and identify predictors for severe disease. This was a prospective observational cohort study conducted at a tertiary care hospital in North India. Patients with acute febrile illness (AFI) aged at least 14 years were included if they were diagnosed with vivax malaria based on rapid kits or peripheral smears. Clinical data and investigations during hospital stay was recorded. 439 cases of acute febrile illness were screened, of whom 50 (11%) were diagnosed with malaria including eight *P. falciparum* infections. Forty-two vivax malaria cases, 22 (52%) of whom were severe, were followed till discharge or death. The median age of the cohort was 24.5 years (Q1-Q3, 19-36 years), including a total of 29 males (69%). Severe malaria was more frequently associated with historical complaints of oliguria or dyspnea, and examination findings of pallor, splenomegaly or altered sensorium. The following five factors were identified to predict severe disease: prolonged illness over 7 days, symptoms of oliguria or dyspnea, examination findings of pallor or crepitations on auscultation. Malaria accounts for 1 in 10 cases of AFI at our North Indian tertiary care center and approximately half of them present with severe disease. Prolonged duration of disease prior to presentation is a modifiable predictor for severe disease and should be targeted for reducing morbidity.

Keywords Malaria, acute febrile illness, disease severity, tropical infections

1. Introduction

Malaria is an endemic, vector-borne, tropical infection caused by the protozoan parasite of the genus *Plasmodium*, of which five species have been identified to infect humans. The clinical spectrum ranges from uncomplicated high-grade fever with headache and rigors to severe disease with the potential for devastating multi-organ dysfunction – cardiovascular, pulmonary, hematological, hepatic, renal, or neurological. *Plasmodium vivax* is classically considered to be benign compared *to Plasmodium falciparum*. In recent years, *P. vivax* has been reported to be the cause of many complicated malaria cases, and even deaths, in countries including Papua New Guinea (*1*), India (*2,3*), Brazil (*4*), and Malaysia (*5*). Factors predisposing to severe *P. vivax* malaria are unclear. Identification of patients at risk of severe disease and close monitoring, with or without hospitalization, can help triage these patients appropriately to improve outcomes.

In observance of the increasing burden of severe *P. vivax* infections and its impact on the community, the present study aimed to identify these patients' clinical spectrum as well as predictors for severe disease.

2. Methodology

2.1. Study setting and design

The present study was a prospective observational cohort study conducted at a tertiary care teaching hospital situated in North India (All India Institute of Medical Sciences, Delhi, India). The recruitment period extends from September 2018 to May 2020, and the study was approved by the institute ethics committee.

2.2. Study population

Patients presenting with acute febrile illness of ≤ 14 days duration were evaluated for malaria infection. Malaria fever was diagnosed by examining a quantitative buffy coat or peripheral smear, or antigen detection by rapid diagnostic kit (Optimal, Bio-Rad, Marnes-la-Coquette, France). The species were identified by antigen detection or peripheral smear examination by microbiologists with at least ten years of experience in the field. Patients aged ≥ 14 years diagnosed with malaria were recruited after informed consent. The patients were excluded if they were infected with more than one malaria species, another cause for the febrile illness was demonstrated, or refused consent. Patients were treated following the national guidelines using oral chloroquine and primaquine if they were diagnosed with non-severe vivax malaria, and with intravenous artesunate therapy in case of severe vivax malaria (*6*).

2.3. Data collection

Information was obtained from the patients' medical records and collected in a uniformly structured questionnaire. Details noted include demographic characteristics, duration between onset of symptoms and diagnosis, duration of fever, headache, and complications, including active bleeding, altered sensorium, decreased urine output, or seizures. The patients were clinically examined daily till discharge or death. Routine blood investigations were performed at baseline and recorded every alternate day to identify the development of severe malaria infection. These included hemogram, renal function tests, liver function tests, blood lactate level, random plasma glucose, and blood gas analysis, including pH value and blood bicarbonate levels.

2.4. Definitions

Severe vivax malaria was defined by the presence of any one of the following World Health Organization (WHO) 2014 epidemiological and research criteria, as described for *P. falciparum* (except parasitemia) (*7*). The criteria include impaired consciousness (Glasgow coma score < 11), acidosis (base deficit of > 8 meq/L or plasma bicarbonate of < 15 mEq/L or venous plasma lactate > 5 mmol/L), hypoglycemia (blood glucose < 40 mg/dL), severe anemia (hemoglobin concentration < 7 gm/dL or hematocrit < 20% in adults, together with a parasite count > 10,000/μL), acute kidney injury (serum creatinine > 3 mg/dL or blood urea > 20 mg/dL), jaundice (serum bilirubin > 3 mg/dl together with a parasite count > 100,000/μL), pulmonary edema (radiologically confirmed, or oxygen saturation < 92% on room air with a respiratory rate > 30/min), significant bleeding (recurrent or prolonged epistaxis, hematemesis or melena), and shock (compensated with capillary filling time ≥ 3 seconds without hypotension or decompensated with systolic blood pressure < 80 mm Hg).

2.5. Statistical analysis

All data were analysed using Stata 14.0 (StataCorp, College Station, Texas, USA). Categorical variables are presented as frequencies and percentages. The chi-square test/Fisher's exact test was used to establish the association between 2 or more groups. Data was tested for normality using the Kolmogorov-Smirnov test. Continuous variables are represented as mean ± standard deviations (SD) or median and interquartile range (IQR). Unpaired *t*-test was used to observe the difference between the groups if normality assumed otherwise Mann-Whitney-*U* test applied. Univariate logistic regression analysis was performed. A step-wise approach was used to estimate the risk and relative 95% confidence interval for each covariate. A value of *p* less than 0.05 was considered to represent statistical significance of the study.

3. Results

Four hundred thirty-nine cases of acute febrile illness were screened, of whom fifty (11%) were diagnosed with malaria and recruited (Figure 1). After excluding eight *P. falciparum* infections, forty-two *P. vivax* malaria cases were identified and followed up till discharge or death. Twenty-two of these (52%) were classified as severe. The median age of the cohort was 24.5 years (Q1-Q3, 19-36 years), including a total of 29 males (69%). Ten patients (38%) with severe malaria had associated comorbidities.

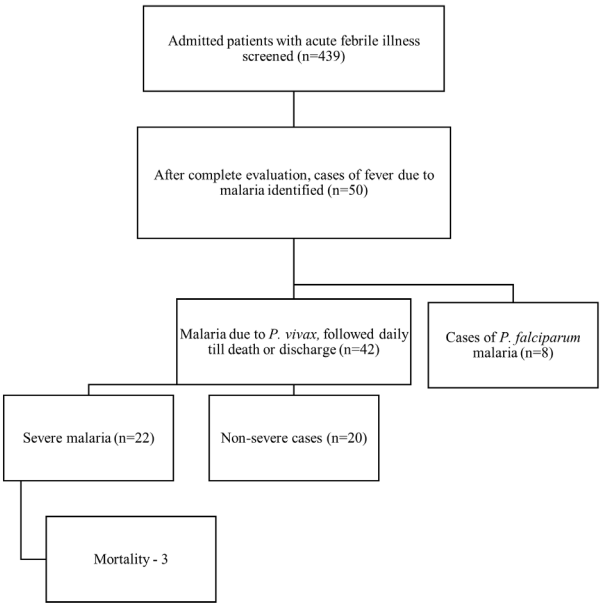

Figure 1. Study flow chart.

Table 1. Clinical profile of severe and non-severe vivax malaria (*n* = 42)

Clinical feature	Severe vivax *n* = 22	Non-severe vivax *n* = 20	*p*-value (chi-square or fischers' exact test, as appropriate)
Symptoms			
Fever	22 (100%)	20 (90.9%)	-
Headache	22 (100%)	19 (86.4%)	0.47
Prostration	19 (86.4%)	19 (86.4%)	0.60
Altered sensorium	2 (9.1%)	0 (0%)	0.48
Decreased urine output	9 (40.9%)	2 (9.1%)	0.035
Shortness of breath	9 (40.9%)	1 (4.5%)	0.009
Nausea/Vomiting	11 (50%)	5 (22.7%)	0.12
Pain abdomen	5 (22.7%)	1 (4.5%)	0.19
Examination			
Altered sensorium (Glasgow coma score < 11/15)	4 (18.2%)	0 (0%)	0.1
Hypotension (systolic blood pressure <80 mmHg)	3 (13.6%)	0 (0%)	0.23
Tachycardia (Heart rate > 100/min)	14 (63.6%)	5 (22.7%)	0.016
Tachypnea (Respiratory rate > 30/min)	6 (27.3%)	1 (4.5%)	0.09
Pallor	18 (81.8%)	10 (45.5%)	0.02
Icterus	12 (54.5%)	2 (9.1%)	0.002
Edema	4 (18.2%)	1 (4.5%)	0.34
Skin rash	7 (31.8%)	3 (13.6%)	0.28
Facial swelling	3 (13.6%)	0 (0%)	0.23
Active bleed	3 (13.6%)	0 (0%)	0.23
Hematuria	1 (4.5%)	0 (0%)	1
Epistaxis	2 (9.1%)	0 (0%)	1
Mechanically ventilated	5 (22.7%)	0 (0%)	0.02
Hepatomegaly	3 (13.6%)	1 (4.5%)	0.6
Splenomegaly	8 (36.4%)	2 (9.1%)	0.07
Ascites	5 (22.7%)	0 (0%)	0.04
Right upper quadrant tenderness	4 (18.2%)	0 (0%)	0.1
Lung crepitations	6 (27.3%)	1 (4.5%)	0.09
Bronchial breathing	3 (13.6%)	0 (0%)	0.23
Chest X-ray (CXR)			
Infiltrates on CXR	7 (31.8%)	1 (4.5%)	0.04
Effusion on CXR	6 (27.3%)	0 (0%)	0.02

3.1. Demographic characteristics and clinical presentation

Patients with severe and non-severe vivax infections had a similar median age at presentation (29 *vs.* 22 years, $p = 0.15$), sex distribution (73% *vs.* 65% males, $p = 0.74$) and mean duration of fever at presentation (8 ± 3.8 *vs.* 6.7 ± 3.2 days, $p = 0.2$). Patients in the severe vivax group were more likely to complain of decreased urine output (40% *vs.* 10%, $p = 0.035$) and shortness of breath (40% *vs.* 5%, $p = 0.009$). The duration of decreased urine output was over 2 days in severe vivax and up to 1 day in non-severe vivax infections. Majority of patients with severe vivax on examination demonstrated pallor ($n = 18$, 81%) and icterus ($n = 12$, 54%), splenomegaly ($n = 8$, 36%), ascites ($n = 5$, 22.7%) and altered sensorium with Glasgow Coma Score (GCS) < 11 ($n = 4$, 18%) (Table 1).

3.2. Biochemical parameters

The mean hemoglobin concentration was lower in the severe vivax group but did not reach statistical significance. Investigations that were used to classify patients were expectedly deranged in the severe vivax group: elevated leukocyte count, serum urea, creatine, total bilirubin, and lactate levels, and lower hematocrit and bicarbonate levels (Table 2). Time trends for the measured parameters were plotted and the recovery in platelet counts was faster in the non-severe group, shown in Figure 2. There were three mortalities in the severe vivax group, all of whom developed acute kidney injury, and pulmonary infiltrates on chest X-ray and required mechanical ventilation. Those who died had decreased hemoglobin values (7.2 *vs.* 10 gm/dL, $p = 0.004$) and bicarbonate levels (13 *vs.* 22 mEq/L, $p = 0.02$), and elevated serum urea (136 *vs.* 55 mg/dL, $p = 0.03$) and creatinine levels (4.6 *vs.* 1, $p = 0.02$), compared to survivors.

3.3. Predicting severe malaria

Univariate logistic regression was used to find factors which could predict the diagnosis of severe malaria prior to the application of the diagnostic criteria (Table 3). The following findings were associated with the final diagnosis of severe vivax malaria: prolonged illness over 7 days, symptoms of decreased urine output or dyspnea, examination findings of pallor or crepitations on chest auscultation. Other findings such as icterus, elevated serum urea, lactate and bilirubin levels, and infiltrates on chest-X ray are used to diagnose as severe malaria and hence not truly predictive.

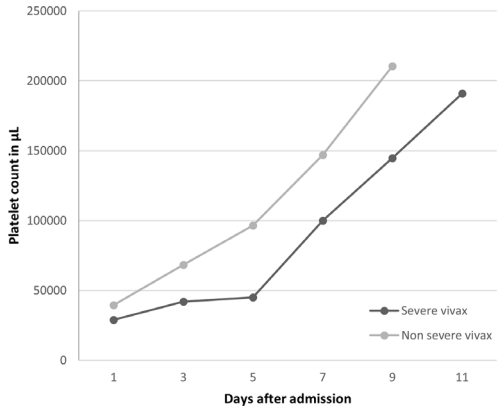

Figure 2. Trend of mean platelet count between severe and non-severe vivax groups.

4. Discussion

According to the WHO malaria report, most malaria cases in 2018 belonged to the African region (213 million, 93%), followed by the South-East Asian region (7.9 million, 3.4%) (*8*). The WHO South-East Asia region reports 53% of the *P. vivax* burden, with the most significant contributor being India (47%). *P. vivax* accounts for a third of all malaria cases in India, with around 380,000 confirmed cases in 2014 (*9*). Two-thirds of these arise in only five states: Jharkhand, Madhya Pradesh, Odisha, Uttar Pradesh, and Gujarat.

Prospective studies have shown that severe disease occurs in approximately 23% to 42% of vivax malaria infections (*10,11*). Thrombocytopenia is the most

Table 2. Laboratory investigations in the severe and non-severe vivax groups

	Severe vivax Median (Q1-Q3) $n = 22$	Non-severe vivax Median (Q1-Q3) $n = 20$	*p* Value
Hemoglobin (g/dL)	8.3 (6.7 - 11.8)	11.2 (8.9 - 12.9)	0.08
Hematocrit (%)	23.7 (20.225 - 29)	28.75 (24.15 - 36.525)	0.02
Platelet count (/µL)	29,000 (12,750 - 47,500)	39,500 (13,750 - 50,000)	0.69
Leukocyte count (/µL)	6,495 (4,290 - 9,550)	4,559.5 (3,425 - 6,095)	0.04
Urea (mg/dL)	95.5 (59.5 - 134.25)	32 (19 - 57.75)	0.0001
Creatine (mg/dL)	1.6 (1.05 - 4.575)	0.8 (0.675 - 1)	0.0006
Alanine aminotransferase (ALT, IU/mL)	34 (25.25 - 67.5)	26 (20.75 - 34.75)	0.04
Aspartate aminotransferase (AST, IU/mL)	47.5 (35 - 85.75)	36 (25.5 - 48)	0.03
Sodium (mEq/L)	136.5 (134.25 - 140.75)	138 (136 - 141)	0.75
Potassium (mEq/L)	4.85 (4.175 - 4.975)	4.15 (3.875 - 4.375)	0.004
Total Bilirubin (mg/dL)	2.8 (1.15 - 5.075)	1.05 (0.75 - 1.6)	0.007
Conjugated bilirubin (mg/dL)	2 (1.1 - 3.65)	0.8 (0.45 - 1.075)	0.1
Bicarbonate (mEq/L)	16.55 (13.325 - 20.85)	22.8 (21.925 - 23)	0.0001
Lactate (mmol/L)	1.95 (1.125 - 2.9)	1.2 (0.875 - 1.475)	0.01
International Normalized Ratio (INR)	1.2 (1.115 - 1.4)	1.18 (1.0925 - 1.285)	0.34

Table 3. Univariate logistic regression analysis to identify predictive factors for severe *P. vivax* infection

Parameter	OR	95% CI	*P*-Value
Clinico-Demographic details			
Female sex	0.67	0.16 - 2.73	0.58
Age > 29 years	2.78	0.77 - 10.04	0.11
Duration of illness > 7 days	4.33	1.15 - 16.32	0.02
Duration of hospitalization > 7 days	1.88	0.53 - 6.68	0.32
Signs and symptoms			
Decreased urine output	5.2	0.94 - 28.90	0.03
Shortness of breath	13.5	1.50 - 120.78	0.003
Pallor	4.72	1.14 - 19.40	0.02
Icterus*	9.35	1.71 - 51.03	0.003
Splenomegaly	4.25	0.75 - 23.81	0.07
Creptitations on auscultation	7.2	0.77 - 66.63	0.04
Investigations			
Infiltrates (on chest X-ray)*	9	0.98 - 81.92	0.01
Oxygen saturation < 92%*	1.89	0.15 - 22.75	0.6
Hemoglobin < 7g/dL*	13.5	1.50 - 120.78	0.003
Urea > 50mg/dL*	16.28	2.88 - 91.83	0.0002
Alanine aminotransferase (ALT) > 45 IU/L*	1.87	0.44 - 7.82	0.4
Bilirubin > 3 mg/dL*	15.8	1.79 - 139	0.001
Lactate > 2 mmol/L*	5.6	1.42 - 21.94	0.009

*These parameters are part of the WHO classification criteria and thus cannot be considered predictive.

common "severe" manifestation of vivax infection (*12*). A prolonged history of fever, dyspnea, and oliguria were more frequent in severe vivax infections in the present study. Serum bilirubin and urea levels have been shown to carry good discriminatory performance for severe vivax malaria (*11*), and the mean duration of fever and tachycardia at presentation predict poor outcome (*13*).

Patients with severe vivax malaria had significantly higher serum urea and creatinine level indicating that patients with early renal impairment had a more severe course and poor outcome than those without renal impairment. Renal impairment is multifactorial, can be prerenal or intrinsic renal damage. Renal biopsy in vivax-associated acute kidney injury (AKI) shows patchy cortical necrosis, acute tubular necrosis (*14*), or thrombotic microangiopathy have also been reported (*15*). Icterus, splenomegaly, crepitations on auscultation, consolidation on chest X-ray, and hospitalization duration over 7 days predicted severity in vivax patients in our cohort. Similarly, tachypnea, elevated bilirubin and creatinine, and falling hemoglobin have been shown to be independent predictors of disease severity (*16*). Even though elevations in urea over 50 mg/dL and severe anemia (hemoglobin below 7 gm/dL) were associated with severity, these were used to classify the infection as severe and cannot be used as predictors. Mortality occurred in 7% of vivax infections, much higher than reported estimates of 0.3% to 1.3% (*10,11*).

Severe anemia occurs at comparable rates among *P. vivax* and *P. falciparum*, despite lower rates of parasitemia in vivax (*17*). This is attributable to increased destruction of non-parasitized red blood cells because of increased fragility, and a toxic effect on erythroblasts precursors (*18*). Parasite load is frequently unavailable, owing to low parasite density, prior treatment, or slide techniques.

The present study comprehensively assessed the clinical spectrum and risk factors associated with severity in *P. vivax* infections. However, our study's limitations include referral bias- the higher rates of severity may be attributed to the study being performed in a tertiary referral center. Since premorbid baseline investigations are not available for most patients, biochemical parameters associated with severe disease may be affected by comorbidities resulting in confounding. The parasite load could not be detected for most patients, possibly due to empirical treatment. We could not perform polymerase chain reaction (PCR) to establish mono-infection due to non-availability.

In conclusion, severe disease is predicted by delayed presentation (beyond one week) and findings of icterus, dyspnea, oliguria, and infiltrates on chest X-ray. Faster access to healthcare and education about early initiation of therapy may help prevent delayed presentation and subsequently severe vivax malaria.

Funding: None.

Conflict of Interest: The authors have no conflicts of interest to disclose.

References

1. Genton B, D'Acremont V, Rare L, Baea K, Reeder JC, Alpers MP, Müller I. *Plasmodium vivax* and mixed infections are associated with severe malaria in children: a prospective cohort study from Papua New Guinea. PLoS Med. 2008; 5:e127.
2. Kochar D, Das A, Kochar S, Saxena V, Sirohi P, Garg S, Kochar A, Khatri M, Gupta V. Severe *Plasmodium vivax* malaria: A report on serial cases from Bikaner in Northwestern India. Am J Trop Med Hyg. 2009; 80:194-198.
3. Yadav D, Chandra J, Aneja S, Kumar V, Kumar P, Dutta AK. Changing profile of severe malaria in north Indian children. Indian J Pediatr. 2012; 79:483-487.
4. Lacerda MVG, Mourão MPG, Alexandre MAA, Siqueira AM, Magalhães BML, Martinez-Espinosa FE, Filho FSS, Brasil P, Ventura AMRS, Tada MS, Couto VSCD, Silva AR, Silva RSU, Alecrim MGC. Understanding the clinical spectrum of complicated *Plasmodium vivax* malaria: a systematic review on the contributions of the Brazilian literature. Malar J. 2012; 11:12.
5. Barber BE, William T, Grigg MJ, Menon J, Auburn S, Marfurt J, Anstey NM, Yeo TW. A prospective comparative study of knowlesi, falciparum, and vivax malaria in Sabah, Malaysia: high proportion with severe disease from *Plasmodium knowlesi* and *Plasmodium vivax* but no mortality with early referral and artesunate therapy. Clin Infect Dis. 2013; 56:383-397.
6. Directorate of National Vector Borne Disease Control Programme. Diagnosis and Treatment of Malaria. Ministry of health and family welfare, Government of India; 2013.
7. Severe Malaria. Trop Med Int Health. 2014; 19:7-131.
8. World Health Organization. World Malaria Report 2019. World Health Organization. 2019.
9. Anvikar AR, Shah N, Dhariwal AC, Sonal GS, Pradhan MM, Ghosh SK, Valecha N. Epidemiology of *Plasmodium vivax* malaria in India. Am J Trop Med Hyg. 2016; 95:108-120.
10. Kumar R, Saravu K. Severe vivax malaria: a prospective exploration at a tertiary healthcare centre in Southwestern India. Pathog Glob Health. 2017; 111:148-160.
11. Mathews SE, Bhagwati MM, Agnihotri V. Clinical spectrum of *Plasmodium vivax* infection, from benign to severe malaria: A tertiary care prospective study in adults from Delhi, India. Trop Parasitol. 2019; 9:88.
12. Rahimi BA, Thakkinstian A, White NJ, Sirivichayakul C, Dondorp AM, Chokejindachai W. Severe vivax malaria: a systematic review and meta-analysis of clinical studies since 1900. Malar J. 2014; 13:481.
13. Kotepui M, Kotepui KU, Milanez GDJ, Masangkay FR. Prevalence and risk factors related to poor outcome of patients with severe *Plasmodium vivax* infection: a systematic review, meta-analysis, and analysis of case reports. BMC Infect Dis. 2020; 20:363.
14. Kute VB, Trivedi HL, Vanikar AV, Shah PR, Gumber MR, Patel HV, Goswami JG, Kanodia KV. *Plasmodium vivax* malaria-associated acute kidney injury, India, 2010-2011. Emerg Infect Dis. 2012; 18:842-845.

15. Sinha A, Singh G, Bhat AS, Mohapatra S, Gulati A, Hari P, Samantaray JC, Dinda AK, Agarwal SK, Bagga A. Thrombotic microangiopathy and acute kidney injury following vivax malaria. Clin Exp Nephrol. 2013; 17:66-72.
16. Sypniewska P, Duda JF, Locatelli I, Althaus CR, Althaus F, Genton B. Clinical and laboratory predictors of death in African children with features of severe malaria: a systematic review and meta-analysis. BMC Med. 2017; 15:147.
17. Douglas NM, Anstey NM, Buffet PA, Poespoprodjo JR, Yeo TW, White NJ, Price RN. The anaemia of *Plasmodium vivax* malaria. Malar J. 2012; 11:135.
18. Wickramasinghe SN, Looareesuwan S, Nagachinta B, White NJ. Dyserythropoiesis and ineffective erythropoiesis in *Plasmodium vivax* malaria. Br J Haematol. 1989; 72:91-99.

Received November 25, 2020; Revised December 20, 2020; Accepted December 27, 2020.

**Address correspondence to:*
Upendra Baitha, Department of Medicine, All India Institute of Medical Sciences, New Delhi, India.
E-mail: drupendraraj14@gmail.com

Released online in J-STAGE as advance publication December 31, 2020.

DD&T
Drug Discoveries & Therapeutics

Guide for Authors

1. Scope of Articles

Drug Discoveries & Therapeutics (Print ISSN 1881-7831, Online ISSN 1881-784X) welcomes contributions in all fields of pharmaceutical and therapeutic research such as medicinal chemistry, pharmacology, pharmaceutical analysis, pharmaceutics, pharmaceutical administration, and experimental and clinical studies of effects, mechanisms, or uses of various treatments. Studies in drug-related fields such as biology, biochemistry, physiology, microbiology, and immunology are also within the scope of this journal.

2. Submission Types

Original Articles should be well-documented, novel, and significant to the field as a whole. An Original Article should be arranged into the following sections: Title page, Abstract, Introduction, Materials and Methods, Results, Discussion, Acknowledgments, and References. Original articles should not exceed 5,000 words in length (excluding references) and should be limited to a maximum of 50 references. Articles may contain a maximum of 10 figures and/or tables. Supplementary Data are permitted but should be limited to information that is not essential to the general understanding of the research presented in the main text, such as unaltered blots and source data as well as other file types.

Brief Reports definitively documenting either experimental results or informative clinical observations will be considered for publication in this category. Brief Reports are not intended for publication of incomplete or preliminary findings. Brief Reports should not exceed 3,000 words in length (excluding references) and should be limited to a maximum of 4 figures and/or tables and 30 references. A Brief Report contains the same sections as an Original Article, but the Results and Discussion sections should be combined.

Reviews should present a full and up-to-date account of recent developments within an area of research. Normally, reviews should not exceed 8,000 words in length (excluding references) and should be limited to a maximum of 10 figures and/or tables and 100 references. Mini reviews are also accepted, which should not exceed 4,000 words in length (excluding references) and should be limited to a maximum of 5 figures and/or tables and 50 references.

Policy Forum articles discuss research and policy issues in areas related to life science such as public health, the medical care system, and social science and may address governmental issues at district, national, and international levels of discourse. Policy Forum articles should not exceed 3,000 words in length (excluding references) and should be limited to a maximum of 5 figures and/or tables and 30 references.

Case Reports should be detailed reports of the symptoms, signs, diagnosis, treatment, and follow-up of an individual patient. Case reports may contain a demographic profile of the patient but usually describe an unusual or novel occurrence. Unreported or unusual side effects or adverse interactions involving medications will also be considered. Case Reports should not exceed 3,000 words in length (excluding references).

Communications are short, timely pieces that spotlight new research findings or policy issues of interest to the field of global health and medical practice that are of immediate importance. Depending on their content, Communications will be published as "Comments" or "Correspondence". Communications should not exceed 1,500 words in length (excluding references) and should be limited to a maximum of 2 figures and/or tables and 20 references.

Editorials are short, invited opinion pieces that discuss an issue of immediate importance to the fields of global health, medical practice, and basic science oriented for clinical application. Editorials should not exceed 1,000 words in length (excluding references) and should be limited to a maximum of 10 references. Editorials may contain one figure or table.

News articles should report the latest events in health sciences and medical research from around the world. News should not exceed 500 words in length.

Letters should present considered opinions in response to articles published in *Drug Discoveries & Therapeutics* in the last 6 months or issues of general interest. Letters should not exceed 800 words in length and may contain a maximum of 10 references. Letters may contain one figure or table.

3. Editorial Policies

For publishing and ethical standards, *Drug Discoveries & Therapeutics* follows the Recommendations for the Conduct, Reporting, Editing, and Publication of Scholarly Work in Medical Journals (*http://www.icmje.org/recommendations*) issued by the International Committee of Medical Journal Editors (ICMJE), and the Principles of Transparency and Best Practice in Scholarly Publishing (*https://doaj.org/bestpractice*) jointly issued by the Committee on Publication Ethics (COPE), the Directory of Open Access Journals (DOAJ), the Open Access Scholarly Publishers Association (OASPA), and the World Association of Medical Editors (WAME).

Drug Discoveries & Therapeutics will perform an especially prompt review to encourage innovative work. All original research will be subjected to a rigorous standard of peer review and will be edited by experienced copy editors to the highest standards.

Ethics: *Drug Discoveries & Therapeutics* requires that authors of reports of investigations in humans or animals indicate that those studies were formally approved by a relevant ethics committee or review board. For research involving human experiments, a statement that the participants gave informed consent before taking part (or a statement that it was not required and why) should be indicated. Authors should also state that the study conformed to the provisions of the Declaration of Helsinki (as revised in 2013). When reporting experiments on animals, authors should indicate whether the institutional and national guide for the care and use of laboratory animals was followed.

Conflict of Interest: All authors are required to disclose any actual or potential conflict of interest including financial

interests or relationships with other people or organizations that might raise questions of bias in the work reported. If no conflict of interest exists for each author, please state "There is no conflict of interest to disclose".

Submission Declaration: When a manuscript is considered for submission to *Drug Discoveries & Therapeutics*, the authors should confirm that 1) no part of this manuscript is currently under consideration for publication elsewhere; 2) this manuscript does not contain the same information in whole or in part as manuscripts that have been published, accepted, or are under review elsewhere, except in the form of an abstract, a letter to the editor, or part of a published lecture or academic thesis; 3) authorization for publication has been obtained from the authors' employer or institution; and 4) all contributing authors have agreed to submit this manuscript.

Cover Letter: The manuscript must be accompanied by a cover letter prepared by the corresponding author on behalf of all authors. The letter should indicate the basic findings of the work and their significance. The letter should also include a statement affirming that all authors concur with the submission and that the material submitted for publication has not been published previously or is not under consideration for publication elsewhere. The cover letter should be submitted in PDF format. For example of Cover Letter, please visit: Download Centre (*https://www.ddtjournal.com/downcentre)*.

Copyright: When a manuscript is accepted for publication in *Drug Discoveries & Therapeutics*, the transfer of copyright is necessary. A JOURNAL PUBLISHING AGREEMENT (JPA) form will be e-mailed to the authors by the Editorial Office and must be returned by the authors as a scan. Only forms with a hand-written signature are accepted. This copyright will ensure the widest possible dissemination of information. Please note that your manuscript will not proceed to the next step in publication until the JPA form is received. In addition, if excerpts from other copyrighted works are included, the author(s) must obtain written permission from the copyright owners and credit the source(s) in the article.

Peer Review: *Drug Discoveries & Therapeutics* uses single-blind peer review, which means that reviewers know the names of the authors, but the authors do not know who reviewed their manuscript. The external peer review is performed for research articles by at least two reviewers, and sometimes the opinions of more reviewers are sought. Manuscripts sent out for peer review are evaluated by independent reviewers. Peer reviewers are selected based on their expertise and ability to provide high quality, constructive, and fair reviews. For research manuscripts, the editors may, in addition, seek the opinion of a statistical reviewer. Consideration for publication is based on the article's originality, novelty, and scientific soundness, and the appropriateness of its analysis.

Suggested Reviewers: A list of up to 3 reviewers who are qualified to assess the scientific merit of the study is welcomed. Reviewer information including names, affiliations, addresses, and e-mail should be provided at the same time the manuscript is submitted online. Please do not suggest reviewers with known conflicts of interest, including participants or anyone with a stake in the proposed research; anyone from the same institution; former students, advisors, or research collaborators (within the last three years); or close personal contacts. Please note that the Editor-in-Chief may accept one or more of the proposed reviewers or may request a review by other qualified persons.

Language Editing: Manuscripts prepared by authors whose native language is not English should have their work proofread by a native English speaker before submission. If not, this might delay the publication of your manuscript in *Drug Discoveries & Therapeutics*.

The Editing Support Organization can provide English proofreading, Japanese-English translation, and Chinese-English translation services to authors who want to publish in *Drug Discoveries & Therapeutics* and need assistance before submitting a manuscript. Authors can visit this organization directly at *http://www.iacmhr.com/iac-eso/support.php?lang=en.* IAC-ESO was established to facilitate manuscript preparation by researchers whose native language is not English and to help edit works intended for international academic journals.

4. Manuscript Preparation

Manuscripts are suggested to be prepared in accordance with the "Recommendations for the Conduct, Reporting, Editing, and Publication of Scholarly Work in Medical Journals", as presented at *http://www.ICMJE.org*.

Manuscripts should be written in clear, grammatically correct English and submitted as a Microsoft Word file in a single-column format. Manuscripts must be paginated and typed in 12-point Times New Roman font with 24-point line spacing. Please do not embed figures in the text. Abbreviations should be used as little as possible and should be explained at first mention unless the term is a well-known abbreviation (*e.g.* DNA). Single words should not be abbreviated.

Title page: The title page must include 1) the title of the paper (Please note the title should be short, informative, and contain the major key words); 2) full name(s) and affiliation(s) of the author(s), 3) abbreviated names of the author(s), 4) full name, mailing address, telephone/fax numbers, and e-mail address of the corresponding author; and 5) conflicts of interest (if you have an actual or potential conflict of interest to disclose, it must be included as a footnote on the title page of the manuscript; if no conflict of interest exists for each author, please state "There is no conflict of interest to disclose"). Please visit Download Centre and refer to the title page of the manuscript sample.

Abstract: The abstract should briefly state the purpose of the study, methods, main findings, and conclusions. For article types including Original Article, Brief Report, Review, Policy Forum, and Case Report, a one-paragraph abstract consisting of no more than 250 words must be included in the manuscript. For Communications, Editorials, News, or Letters, a brief summary of main content in 150 words or fewer should be included in the manuscript. Abbreviations must be kept to a minimum and non-standard abbreviations explained in brackets at first mention. References should be avoided in the abstract. Three to six key words or phrases that do not occur in the title should be included in the Abstract page.

Introduction: The introduction should be a concise statement of the basis for the study and its scientific context.

Materials and Methods: The description should be brief but with sufficient detail to enable others to reproduce the experiments. Procedures that have been published previously should not be described in detail but appropriate references should simply be cited. Only new and significant modifications of previously published procedures require complete description. Names of products and manufacturers with their locations (city and state/country) should be given and sources of animals and cell lines should always be indicated. All clinical investigations must have been conducted in accordance with Declaration of Helsinki principles. All human and animal studies must have been approved by the appropriate institutional review board(s) and a specific declaration of approval must be made within this section.

Results: The description of the experimental results should be succinct but in sufficient detail to allow the experiments to be analyzed and interpreted by an independent reader. If necessary, subheadings may be used for an orderly presentation. All figures and tables must be referred to in the text.

Discussion: The data should be interpreted concisely without repeating material already presented in the Results section. Speculation is permissible, but it must be well-founded, and discussion of the wider implications of the findings is encouraged. Conclusions derived from the study should be included in this section.

Acknowledgments: All funding sources should be credited in the Acknowledgments section. In addition, people who contributed to the work but who do not meet the criteria for authors should be listed along with their contributions.

References: References should be numbered in the order in which they appear in the text. Citing of unpublished results, personal communications, conference abstracts, and theses in the reference list is not recommended but these sources may be mentioned in the text. In the reference list, cite the names of all authors when there are fifteen or fewer authors; if there are sixteen or more authors, list the first three followed by *et al*. Names of journals should be abbreviated in the style used in PubMed. Authors are responsible for the accuracy of the references. The EndNote Style of *Drug Discoveries & Therapeutics* could be downloaded at **EndNote** (*https://www.ddtjournal.com/examples/Drug_Discoveries_Therapeutics.ens*).

Examples are given below:

Example 1 (Sample journal reference):

Nakata M, Tang W. Japan-China Joint Medical Workshop on Drug Discoveries and Therapeutics 2008: The need of Asian pharmaceutical researchers' cooperation. Drug Discov Ther. 2008; 2:262-263.

Example 2 (Sample journal reference with more than 15 authors):

Darby S, Hill D, Auvinen A, *et al*. Radon in homes and risk of lung cancer: Collaborative analysis of individual data from 13 European case-control studies. BMJ. 2005; 330:223.

Example 3 (Sample book reference):

Shalev AY. Post-traumatic stress disorder: Diagnosis, history and life course. In: Post-traumatic Stress Disorder, Diagnosis, Management and Treatment (Nutt DJ, Davidson JR, Zohar J, eds.). Martin Dunitz, London, UK, 2000; pp. 1-15.

Example 4 (Sample web page reference):

World Health Organization. The World Health Report 2008 – primary health care: Now more than ever. *http://www.who.int/whr/2008/whr08_en.pdf* (accessed September 23, 2010).

Tables: All tables should be prepared in Microsoft Word or Excel and should be arranged at the end of the manuscript after the References section. Please note that tables should not in image format. All tables should have a concise title and should be numbered consecutively with Arabic numerals. If necessary, additional information should be given below the table.

Figure Legend: The figure legend should be typed on a separate page of the main manuscript and should include a short title and explanation. The legend should be concise but comprehensive and should be understood without referring to the text. Symbols used in figures must be explained. Any individually labeled figure parts or panels (A, B, *etc*.) should be specifically described by part name within the legend.

Figure Preparation: All figures should be clear and cited in numerical order in the text. Figures must fit a one- or two-column format on the journal page: 8.3 cm (3.3 in.) wide for a single column, 17.3 cm (6.8 in.) wide for a double column; maximum height: 24.0 cm (9.5 in.). Please make sure that artwork files are in an acceptable format (TIFF or JPEG) at minimum resolution (600 dpi for illustrations, graphs, and annotated artwork, and 300 dpi for micrographs and photographs). Please provide all figures as separate files. Please note that low-resolution images are one of the leading causes of article resubmission and schedule delays.

Units and Symbols: Units and symbols conforming to the International System of Units (SI) should be used for physicochemical quantities. Solidus notation (*e.g*. mg/kg, mg/mL, mol/mm^2/min) should be used. Please refer to the SI Guide *www.bipm.org/en/si/* for standard units.

Supplemental data: Supplemental data might be useful for supporting and enhancing your scientific research and *Drug Discoveries & Therapeutics* accepts the submission of these materials which will be only published online alongside the electronic version of your article. Supplemental files (figures, tables, and other text materials) should be prepared according to the above guidelines, numbered in Arabic numerals (*e.g*., Figure S1, Figure S2, and Table S1, Table S2) and referred to in the text. All figures and tables should have titles and legends. All figure legends, tables and supplemental text materials should be placed at the end of the paper. Please note all of these supplemental data should be provided at the time of initial submission and note that the editors reserve the right to limit the size and length of Supplemental Data.

5. Submission Checklist

The Submission Checklist will be useful during the final checking of a manuscript prior to sending it to *Drug Discoveries & Therapeutics* for review. Please visit Download Centre and download the Submission Checklist file.

6. Online Submission

Manuscripts should be submitted to *Drug Discoveries & Therapeutics* online at *https://www.ddtjournal.com*. The manuscript file should be smaller than 5 MB in size. If for any reason you are unable to submit a file online, please contact the Editorial Office by e-mail at *office@ddtjournal.com*.

7. Accepted Manuscripts

Proofs: Galley proofs in PDF format will be sent to the corresponding author *via* e-mail. Corrections must be returned to the editor (*proof-editing@ddtjournal.com*) within 3 working days.

Offprints: Authors will be provided with electronic offprints of their article. Paper offprints can be ordered at prices quoted on the order form that accompanies the proofs.

Page Charge: Page charges will be levied on all manuscripts accepted for publication in *Drug Discoveries & Therapeutics* ($140 per page for black white pages; $340 per page for color pages). Under exceptional circumstances, the author(s) may apply to the editorial office for a waiver of the publication charges at the time of submission.

Misconduct: *Drug Discoveries & Therapeutics* takes seriously all allegations of potential misconduct and adhere to the ICMJE Guideline (*http://www.icmje.org/recommendations*) and COPE Guideline (*http://publicationethics.org/files/Code_of_conduct_for_journal_editors.pdf*). In cases of suspected research or publication misconduct, it may be necessary for the Editor or Publisher to contact and share submission details with third parties including authors' institutions and ethics committees. The corrections, retractions, or editorial expressions of concern will be performed in line with above guidelines.

(As of June 2020)

Drug Discoveries & Therapeutics
Editorial and Head Office
Pearl City Koishikawa 603,
2-4-5 Kasuga, Bunkyo-ku,
Tokyo 112-0003, Japan.
E-mail: office@ddtjournal.com